

AD-A090 017

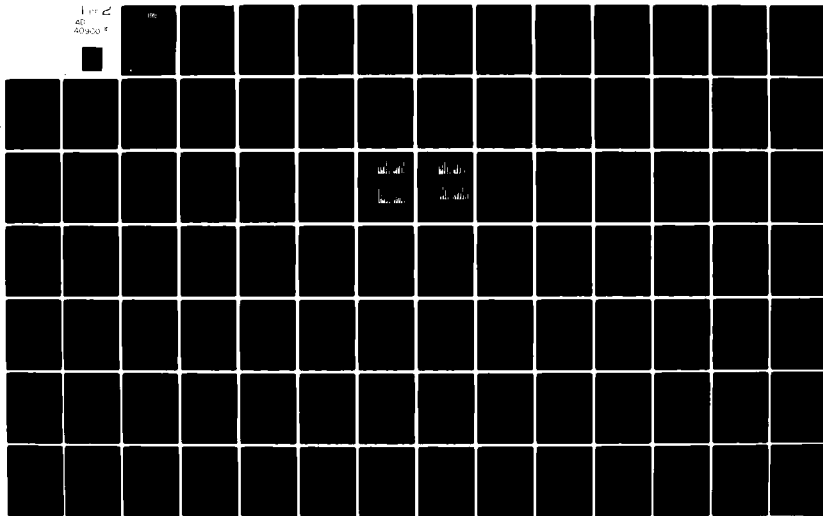
BOSTON COLL CHESTNUT HILL MA DEPT OF PHYSICS F/6 8/14
PHENOMENOLOGICAL AND THEORETICAL STUDIES ON MAGNETIC INDICATORS--ETC(U)
MAR 80 R L CAROVILLANO, R E SHEEHAN F19628-77-C-0085

UNCLASSIFIED

AF6L-TR-80-0094

NL

1 of 2
40
40900 4



AFGL-TR-80-0094

LEVEL III

P

PHENOMENOLOGICAL AND THEORETICAL STUDIES ON
MAGNETIC INDICATORS OF SUBSTORM ACTIVITY

Robert L. Carovillano
Department of Physics, Boston College
Chestnut Hill, Massachusetts 02167
March 21, 1980

**DTIC
SELECTED
OCT 7 1980**

Final Report
March 21, 1980

Period Covered: December 3, 1976 - September 30, 1979

Approved for public release; distribution unlimited

Prepared for

Air Force Geophysics Laboratory
Air Force Systems Command
United States Air Force
Hanscom Air Force Base, Massachusetts 01731

DDC FILE COPY.

AD A090017

80 10 7 070

Qualified requestors may obtain additional copies from the Defense Documentation Center. All others should apply to the National Technical Information Service.

7. AUTHORS (con't.)
R.H. Eather, W.J. Burke

19. KEY WORDS (con't.)

ionospheric electric fields	auroral boundary
ionospheric tensor conductivity	injection boundary
successive relaxations	particle precipitation
Fukushima-Vasyliunas Theorem	ring current
shielding currents	polar cap
low latitude asymmetry	scaling relations
DMSP satellite	

20. ABSTRACT (con't.)

exceeds 200 γ , and less sensitivity for dayside detection. The AFGL magnetometer chain would give improved detection capability and reliability, in real time. A literature review is given on micropulsations as indicators of geomagnetic activity, and recommendations made for utilizing the AFGL chain in this regard. Field aligned currents drive ionospheric current systems on a global scale. A model is developed to describe this process for quiet and disturbed conditions. Determination of the ground magnetic signature from an ionospheric current distribution is not unique and requires specification of image currents and ionospheric closure currents. This process is discussed and estimates are developed for the relative contributions of Pederson and Hall currents to the ground magnetic signature that would apply for a realistic circumstance. DMSP images have been used to determine the location of the equatorward and poleward boundary of the aurora as a function of magnetic activity. A model is developed that shows the ring current to be an important factor, but not the only one operative, in determining the size of the polar cap.

Unclassified

AUTHORS

The scientists who contributed to the research reported in this document are:

1. Robert L. Carovillano, Principal Investigator
2. Joseph N. Barfield
3. William J. Burke
4. Nancy U. Crooker
5. Robert H. Eather
6. Michael Heinemann
7. Richard W. Nopper, Jr.
8. M.S. Gussenhoven-Shea
9. Robert E. Sheehan
10. George L. Siscoe

Author credits for Chapters 2 - 7 of this report are:

2. Sheehan, Carovillano, Eather
3. Barfield, Crooker, Carovillano
4. Nopper, Carovillano, Heinemann, Burke
5. Siscoe, Crooker, Carovillano
6. Sheehan, Carovillano, Shea
7. Siscoe

Accession Form	<input checked="" type="checkbox"/>
NCIS - GMAIL	<input type="checkbox"/>
DUIC FAX	<input type="checkbox"/>
Unassigned	<input type="checkbox"/>
Justified	<input type="checkbox"/>
By _____	
Distribution/	
Availability/	
Date _____	
Initials _____	
A	

TABLE OF CONTENTS

DD Form 1473.....	i
Authors.....	iii
Table of Contents.....	iv
List of Figures.....	vi
List of Tables.....	xi
1. Introduction.....	1
2. Mid Latitude Indicators of Substorm Activity.....	4
A. Introduction.....	4
B. The Relationship between Auroral and Mid Latitude Magnetic Signatures.....	7
C. Correlations between Mid Latitude Activity and AE.....	14
D. Description and Examples of Mid Latitude Variation Procedure.....	25
E. Comparison of Short Time Scale AFGL Data with Auroral Zone Magnetograms.....	35
F. Summary and Estimate of Reliability.....	51
References.....	56
3. Micropulsations as Indicators of Geomagnetic Activity.....	58
A. Introduction.....	58
B. General Background.....	60
C. Recent Results.....	61
D. Summary and Recommendations.....	67
References.....	70
4. Ionospheric Electric Fields and Currents Driven by Birkeland Currents.....	72
A. Introduction.....	72
B. Definition of the Model.....	73
C. Application of the Model.....	74
D. Reprinted Publications (Papers I, II, and III).....	78
E. Refinements of the Model.....	100
F. Magnetic Ground Signatures.....	103
References.....	107

5. Simple Estimate of the Ground Magnetic Signature of the Birkeland-Ionospheric Current System at Low Latitudes.....	111
A. Introduction.....	111
B. Ionospheric Shielding Effects.....	112
C. Model Results at Low Latitudes.....	115
D. Recommended Approach.....	123
References.....	124
6. Auroral Boundary Locations.....	126
Reprints.....	131
References.....	138
7. Magnetospheric Determinants of the Global Distribution of Particle Precipitation.....	139
A. Introduction.....	139
B. Quasi-Self-Consistent Ring Current Model.....	140
C. Ring Current Effects on Polar Cap Size.....	142
D. Polar Cap Off-Set.....	146
E. Two-Parameter Scaling Relations.....	149
References.....	153

LIST OF FIGURES

- Figure 2.1. Northern hemisphere map showing locations of stations used in this report. Circles defined by ticks are 10° intervals of Corrected Geomagnetic Latitude; tick marks at one hour intervals of local time..... 9
- Figure 2.2. Stacked H component magnetograms (X component at FC and BL) from 9 auroral zone stations on December 9, 1976. Bars indicate 200γ deflections up is positive. Dots under each trace mark local midnight. Solid and dashed vertical lines are major and minor events discussed in the text.....11
- Figure 2.3. Stacked magnetograms from 5 AFGL chain stations (MA, MI, WI, SD, and WA) on Dec. 9, 1976 (0000-1200UT). X components above, Y components below. Dots under each trace at local midnight. Solid vertical lines correspond to events in Figure 2.2. Amplitude bar is 50γ for X components; for Y components, amplitude bar is 50γ at MA, 70γ at MI, 80γ at WI and WA, and 120γ at SD.....12
- Figure 2.4. Same as Figure 2.3 for 1200 - 2400 UT on December 9, 1976. Amplitude bar for X components: 30γ at MA, MI, and WA, 40γ at WI, and SD; for Y components: 30γ at MI, WI, and SD, 40γ at WA, and 60γ at MA. The Y component at MA may be unreliable.....13
- Figure 2.5. AE plot for October 9 - 16, 1972. Events described in the text are marked by arrows with peak AE values (in hundreds of gammas) indicated above.....16
- Figure 2.6. H component magnetograms from Fredericksburg, October 9 - 16, 1972. Events marked by arrows correspond to those in Figure 2.5, with the peak AE value (in hundreds of gammas) indicated above. Solid triangle on UT scale indicates local noon at Fredericksburg.....17
- Figure 2.7. Distribution of 806 AE events, identified during October, 1972 - January, 1973, according to strength (left histogram) in 200γ intervals of AE, and UT of occurrence (right histogram), in 8 three-hour intervals of UT and CGLT at FB and BD. Midpoint between FB and BD defines the CGLT interval. Intervals span the beginning of the first hour to the beginning of the second (00 - 03 UT = 0000 - 0300 UT).....19
- Figure 2.8. Breakdown of mid latitude responses to AE events occurring in October 1972 - January 1973. Each 3-bar cluster gives the number of weak (W), moderate (M) and strong (S) responses to AE events, defined in the text, occurring in the indicated 200γ strength interval (Figure 2.7) and CGLT interval of FB and BD. Dayside mid latitude responses shown in this figure.....20

Figure 2.9.	Breakdown of nightside mid latitude responses. Same format as Figure 2.8.....	21
Figure 2.10.	Histograms showing the proportion of strong responses (top panels), relative to moderate and weak, accompanying AE enhancements in intervals of increasing strength (defined in Figure 2.7). Dayside local time sectors in the first row, nightside in the second. Bottom panel, in the same format as the top, combines strong and moderate responses.....	23
Figure 2.11.	Comparison of AFGL chain data (upper two panels) with a modified AE index and K_p index on December 9-10, 1976. Crosses connected by solid lines in the ΔX and ΔY panels indicate the average of the hourly variations from the chain (procedure described in the text). Dots above and below each cross indicate the maximum and minimum hourly variation from the chain. Crosses in the lower panel give an hourly "AE" value, described in the text. K_p values shown by dots.....	26
Figure 2.12.	Same format as Figure 2.11 for December 12-13, 1976.....	27
Figure 2.13.	Same format as Figure 2.11 for December 29-30, 1976.....	28
Figure 2.14a.	Hourly H component variations at Fredericksburg (dots) and Boulder (crosses) plotted in the top panels; 2.5 minute average AE index in the bottom panels. Time period Dec. 1-8, 1972..	31
Figure 2.14b.	Hourly H component variations at Fredericksburg (dots) and Boulder (crosses) plotted in the top panels; 2.5 minute average AE index in the bottom panels. Time period is Dec. 9-16... 1972.	32
Figure 2.14c.	Hourly H component variations at Fredericksburg (dots) and Boulder (crosses) plotted in the top panels; 2.5 minute average AE index in the bottom panels. Time period Dec. 17-24, 1972.....	33
Figure 2.14d.	Hourly H component variations at Fredericksburg (dots) and Boulder (crosses) plotted in the top panels; 2.5 minute average AE index in the bottom panels. Time period Dec. 25-31, 1972.....	34
Figure 2.15a.	Station averaged X component variations (dots) and extreme values (top and bottom of bar) computed every 10 minutes from June 2, (0610 UT) to June 6 (0030 UT), 1978. Average, maximum and minimum ΔX based on 5 values in a 10 minute interval, one from each AFGL station (WA, SD, WI, MI, and MA). Same format applies in Figure 2.15 b-e.....	36
Figure 2.15b.	37
Figure 2.15c.	38
Figure 2.15d.	39
Figure 2.15e.	40

Figure 2.16.	Same format as Figure 2.15. 1 hour time intervals (June 2 (0600 UT) - June 3 (2100 UT), 1978).....	41
Figure 2.17a.	Same format as Figure 2.15. $\frac{1}{2}$ hour time intervals (June 2 (0600 UT) - June 3 (2100 UT), 1978).....	42
Figure 2.17b.	Same format as Figure 2.17a.....	43
Figure 2.18.	Maximum AE achieved in each hour, June 2 (0500 UT) - June 3 (2100 UT), 1978. Four auroral zone stations employed, Tixie, Dixon, Great Whale River, and Fort Churchill.....	44
Figure 2.19a.	H component magnetograms from Tixie Bay on June 2-3, 1978.....	46
Figure 2.19b.	H component magnetograms from Tixie Bay on June 3-5, 1978.....	47
Figure 2.19c.	X component magnetograms from Great Whale River on June 2-3, 1978.....	48
Figure 2.19d.	X component magnetograms from Great Whale River on June 3-4, 1978.....	49
Figure 2.19e.	X component magnetograms from Great Whale River on June 4-5, 1978.....	50
Figure 2.20.	Example showing the calculation of ΔX at a chain station. X component magnetograms at Wisconsin (WI) on December 9 and 12, 1976 appear in the top panels. Variations over 1 hour time interval, indicated by dotted boxes in magnetograms, plotted in bottom panels.....	52
Figure 3.1.	From <u>Plyasova-Bakunina</u> (1972): Occurrence frequency of pulsations for intervals of angle γ measured in the solar wind at Imp 3,4. γ is the projection onto the ecliptic plane of the angle between the IMF and sun-earth line.....	59
Figure 3.2.	From <u>Troitskaya</u> (1967); Dependence of Pc 2-4 periods on Kp at Borok.....	61
Figure 3.3.	Spectra and cross-spectral coherence of the radial and aximuthal magnetic fields obtained by the three space craft during a typical local morning pulsation. From <u>Hughes et al.</u> (1978).....	63
Figure 3.4.	The variation of the azimuthal wave number (m) as a function of time. Mean local noon is computed at the midpoint between ATS 6 and SMS 1. From <u>Hughes et al.</u> (1978)...	64
Figure 3.5.	Diagrammatical summary of joint δB versus $\cos\theta_{xB}$ and V_{sw} correlations. From <u>Greenstadt et al.</u> (1979).....	65
Figure 3.6.	Time dependence of distributions of the autospectra of each magnetic field component measured at ATS-6. From <u>Arthur et al.</u> (1978).....	66

- Figure 3.7. Average power spectra for the five regions, interplanetary, magnetosheath, magnetopause, synchronous orbit, and ground. From Arthur et al. (1978).....67
- Figure 4.1. Schematic representation of the distribution of ionospheric conductivity used in the model. Conductivity is proportional to density of stippling. Features shown include the solar-zenith (i.e., day-night) variation, and enhanced conductivity in the auroral ovals.....75
- Figure 4.2. The orientation of the model electric field at the north pole, measured counterclockwise from noon, as a function of the ratio of total Region 1 current to total Region 2 current.....79
- Figure 4.3. Illustration of northern hemisphere structure of observed field-aligned currents and correlative high-latitude phenomena for IMF B_y positive (left) and negative (right). The top panels show interplanetary magnetic and electric field components and observed Region 2, 1, and cusp currents. The bottom panels indicate Heppner's (1972) convection velocities in the polar cap, and the DPY equivalent currents (Friis-Christensen and Wilhjelm, 1978) and ΔB of McDiarmid, et al. (1978) in the cusp region..... 102
- Figure 5.1. Simple representation of Birkeland currents corresponding to Region 1 (quiet time) and Region 2 (active) configurations..... 120
- Figure 6.1. Average corrected geomagnetic latitude of the equatorward auroral boundary at 0100 CGLT as a function of K_p . Error bars demark one standard deviations. From Sheehan and Carovillano (1978)..... 127
- Figure 6.2. Data of Figure 6.1 along with the McIlwain injection boundary mapped to the auroral zone. Two field models shown, dipole (solid line), and empirical Mead-Fairfield (MF73). From Sheehan and Carovillano, 1978..... 128
- Figure 6.3. Average latitude of the poleward and equatorward auroral boundaries, determined from DMSP images, in the 23-01 local time sector as a function of $-D_{st}$. Number of poleward and equatorward cases in each D_{st} interval shown in the upper and lower boxes, respectively. Bars indicate one standard deviation. From Gussenhoven et al. (1978)..... 129
- Figure 6.4. Average latitude of the poleward and equatorward auroral boundaries, determined from DMSP images, in the 04-06 local time sector as a function of $-D_{st}$. Number of poleward and equatorward cases in each D_{st} interval shown in the upper and lower boxes, respectively. Bars indicate one standard deviation. From Gussenhoven et al. (1978)..... 130

- Figure 7.1. The dependence of the ring current disturbance field at earth (H) on the distance to the inner edge of the ring current (R) for different "entropy" plasmas characterized by k , the distance at which the beta of the plasma is unity..... 141
- Figure 7.2. The magnetic moment of the ring current (M_{RC}) in units of the geomagnetic dipole moment (M_E) as a function of the disturbance field (H) for different values of k 141
- Figure 7.3. A comparison between the model-predicted ($R = 4$, $k = 8$) disturbance field profile and storm-time disturbance field data from the S3-A satellite for the storm of 17 December, 1971 (Cahill, 1973)..... 141
- Figure 7.4. The dependence of the latitudinal shift of the poleward border of the auroral oval on the magnetic moment of the ring current, M_R (measured here in units of the geomagnetic dipole moment, M_E).
- The two cases shown correspond to initial ($M_R = 0$) locations of the border at $\lambda_p^* = 60^\circ$ and 70° geomagnetic latitudes..... 144
- Figure 7.5. The dependence of the latitudinal shift of the poleward border of the auroral oval on the ring current magnetic field ($Dst \sim 1.5 H$), as determined from the $\lambda_p^* = 70^\circ$ curve of Fig. 7.4 and the previous derived relation between M_R and H (Siscoe, 1979a) in Fig. 7.2..... 144
- Figure 7.6. Geometry of the polar cap in terms of an auroral circle of size θ_p and offset angle, δ , from the magnetic pole (m.p.). p_{st} is the solar wind dynamic pressure, starred quantities are reference values..... 147

LIST OF TABLES

Table 2.1.	List of stations used in this report. Symbols appear at station locations in Figure 2.1. Corrected Geomagnetic Coordinates are North Latitude and East Longitude. AFGL station symbols indicate the state in which the installation is located.....	10
Table 2.2.	Summary of procedures and interpretations discussed in Chapter 2.....	55
Table 5.1.	Parameters used to evaluate antipodal magnetic disturbances at the equator.....	119

1. INTRODUCTION

The magnetospheric substorm is a natural phenomenon associated with splendid visual effects and complex scientific descriptions. The substorm concept came from Akasofu who attempted to organize a wealth of all-sky camera data into a single cohesive picture. Today, Akasofu's original auroral substorm concept is known to be manifest in many complementary data sets (magnetic bay phenomena, polar magnetic substorms, ionospheric substorms, proton aurora, VLF emissions, etc.), and it has become apparent that a full understanding of the substorm process will require a very comprehensive knowledge of the magnetosphere, including its coupling mechanisms to the solar wind and ionosphere.

The substorm is a major event characterized by time dependence, vast spatial scales, and probably non linear physical processes. For these reasons, a complete observational definition of a substorm is not yet available. In this research, we addressed certain aspects of substorm behavior using specific data sources and well defined models.

In chapter 2, we report on a study made of the feasibility of substorm detection at subauroral latitudes that would utilize the AFGL magnetometer network. High latitude magnetic disturbances and gradients are very large during substorms and are often associated essentially with overhead auroras and currents. In contrast, mid latitude magnetic signatures are smaller but distributed more widely geographically than at high latitudes. We have studied the amplitude and longitudinal extent of mid latitude signatures to serve as indicators of substorm occurrence. The reliability of this approach, evaluated for available data samples, depends upon such factors as the longitudinal wedge of the mid latitude station coverage, the local time of this wedge during a substorm event and the intensity and duration of the substorm. From our study, a mid latitude magnetic index is defined and an operational scheme developed for substorm detection.

In Chapter 3, a review is given of micropulsations as indicators of geomagnetic activity. The AFGL sub auroral chain has a digital data base and is well suited to be used in a procedure to formulate and calibrate a micropulsation index of geomagnetic activity level.

Chapters 4 and 5 deal with the global ionospheric distribution of currents driven by field aligned currents, and the properties of the ground magnetic signature associated with such currents. The model developed to determine global ionospheric distributions uses input variables that are known to calculate selected output variables quantitatively. The input variables are the driving currents distributed in the auroral zone and the ionospheric conductivity. These input variables are defined by observational evidence. The calculated output variables are the ionospheric electric field, potential, and currents. Model limitations and desirable generalizations are discussed in detail.

Determination of the ground magnetic signature from a configuration of currents is, in principle, a straight-forward matter if all the currents are known. In our case, however, we have a firm handle only on the ionospheric portion of the currents. The crucial missing parts of the current network are induced earth currents and the upwards (three dimensional) extension and closure of the field aligned currents in the magnetosphere. The comparative roles of Pederson and Hall currents, the shielding effects of the ionosphere, and other physical considerations necessary for a reliable determination of the ground magnetic signature are discussed in context.

Chapters 6 and 7 relate to studies made on auroral boundary locations. Observational information is given in Chapter 6 on: the location of the equatorward auroral boundary as a function of K_p and AE; and the location of the poleward boundary as a function of Dst. Boundary locations were determined from DMSP images. In Chapter 7 a model is developed that relates properties of the ring current to the size of the polar cap. Through parametric representation, the

axially symmetric ring current evolves into a storm time configuration with an associated growth in Dst. Ring current parameters are the inner edge location and the distance where the beta of the plasma is unity. The ring current is shown to contribute substantially to the change in polar cap size (taken to be determined by the poleward auroral boundary) during magnetic storms.

2. MID LATITUDE INDICATORS OF SUBSTORM ACTIVITY

A. Introduction

Magnetospheric substorms influence magnetic fields on the earth's surface at places far removed from the site of spectacular auroral displays and ionospheric disruptions. Magnetic bays at sub auroral, mid, and low latitudes have been attributed to ionospheric return currents from auroral electrojets (Rostoker, 1966), or to an asymmetric partial ring current closing in the magnetosphere (Cummings, 1966; Akasofu and Meng, 1969; Crooker and McPherron 1972; Fukunishi and Kamide, 1973). In a study of coordinated satellite and ground based data, McPherron (1973) used mid latitude positive H bays near local midnight as a prime indicator of substorm onset. He noted that midlatitude magnetic signatures were simpler than auroral zone records which are commonly affected by intense, rapidly changing overhead currents. Other magnetic phenomena which have been connected with substorms are bursts of Pi 2 pulsations (Saito et al., 1976) and long period oscillations (Wang et al., 1977).

The purpose of this study is to explore the utilization of the AFGL sub-auroral, five station magnetometer network to detect the occurrence and strength of magnetospheric substorms. These AFGL stations operate automatically to provide high time resolution, 3 component magnetic data (Knecht and Pazich, 1976), and are located in Washington, South Dakota, Wisconsin, Michigan, and Massachusetts (Figure 2.1). The station network spans about 4 hours of local time (60° of longitude) at 55° CGL (Corrected Geomagnetic Latitude). (Two additional stations in California and Florida are now operational but are not used in this study.) Lincoln (1967) and Rostoker (1972) have reviewed and

appraised the more common geomagnetic indices. Details of the most familiar indices, K_p and AE (Auroral Electrojet), are given by Mayaud (1967), Davis and Sugiura (1966), and Allen and Kroehl (1975). An implicit requirement for the quality of any geomagnetic index is reasonably complete longitudinal coverage, a property that the AFGL network does not offer. Given this limitation, we must focus on the local time dependence of magnetic effects accompanying substorms.

Contour maps of mid latitude magnetic variations in local time vs. universal time were constructed by Clauer and McPherron (1974) to describe the time development of substorms as seen by stations at low latitudes. They emphasize that mid latitude signatures are highly dependent on location relative to the substorm's central meridian. For example, an idealized magnetospheric-ionospheric current system centered on local midnight produces positive H variations about local midnight and smaller negative H changes on the dayside tending to zero near local noon. Caan et al. (1978) and Kokubun and Iijima (1975) employed superposed epoch methods to depict the statistical local time behavior of midlatitude signatures accompanying selected substorms. The selection criteria in Caan et al. were limited to mid latitude bays within 5 hours of local midnight to avoid contamination by si events. World wide magnetic changes caused by an si could be misinterpreted as indication of a substorm if only one local time sector is considered. Substorm triggering by an si or ssc has been analyzed by Kokubun et al. (1977), who found that high AE ($> 100\gamma$) and southward B_z were necessary preconditions before the solar wind event. They suggested that a favorable tail configuration allowed triggering.

Substorms are usually more complicated than a simple process of expansion and recovery. In their study of multiple onset substorms, Pytte et al. (1976) stated that Pi 2 bursts seemed to accompany each brightening of an equatorward

auroral arc, while sub auroral and mid latitude magnetic activity signaled westward travelling surges. However, when substorm expansion begins during the recovery of an earlier substorm in the same local time sector, mid latitude positive H bays near local midnight may not clearly distinguish the two events (Kamide et al., 1977). Thus, it is not a simple matter to identify unequivocally every substorm on the basis of mid latitude magnetic bays, especially during extended periods of magnetic conditions which favor continuous substorm activity.

A simple current system designed to explain high and low latitude magnetic disturbances during substorm expansion was discussed in a detailed analysis of a single event (McPherron et al., 1973). Rostoker (1974) suggested a modification of this system featuring field aligned currents which feed the east and west electrojets at dawn and dusk, and has an upward field aligned current at the Harang discontinuity connecting to the tail current. More recent treatments of current systems seek to explain conditions during moderate activity (Hughes and Rostoker, 1977), the dynamics of dayside auroral and cusp movements (Yashuhara et al., 1975; Eather et al., 1979), and seasonal asymmetries between northern and southern hemispheres (Gizler et al., 1976). Finally, there is a class of events reported by Pytte et al. (1978) which they call "convection substorms". These events produce sustained negative bays in the auroral zone but exhibit hardly any mid latitude indications of field aligned currents originating in the tail. Instead of impulsive releases of stored energy symptomatic of ordinary substorms, it appears that a steady transfer of energy from the solar wind to the ionosphere may power the process.

Park and Meng (1973) found that mid latitude magnetic activity did not correlate well with ionospheric electric fields deduced from F layer disturbances, and concluded that the currents responsible for the mid latitude activity instead must flow in the magnetosphere. Model studies by Yashuhara et al. (1975) with

field aligned currents into a conducting ionosphere also showed remarkably little current spreading to mid and low latitudes.

Additional studies of the way field aligned currents distribute globally in the ionosphere have been conducted quantitatively by Nopper and Carovillano (1978), Nisbet et al. (1978), and Kamide and Matsushita (1979). These authors use field aligned current patterns as inputs, like those derived from satellite data by Iijima and Potema (1978), and solve for the ionospheric electric field using tensor conductivity models and Ohm's law. (This topic is the subject of chapter 4 of this report.) One result of this work is that effects traditionally credited to equivalent ionospheric currents at mid latitudes, which represent return currents from the auroral electrojets, are a consequence of the field aligned current systems.

This brief introduction should serve to highlight some of the complexities and uncertainties surrounding the topic of substorm current systems. The current effort is phenomenological in approach and concentrates on the statistical relationship between changes in the midlatitude H component (X components in the AFGL chain) and the intensity of the AE index. The procedure we develop has limitations, but it also has the virtues of simplicity and objectivity. In addition, our method should be applicable even when all data is interrupted momentarily, or when one or more stations is lost for an extended period.

B. The Relationship Between Auroral and Mid Latitude Magnetic Signatures

In this section the relationship between auroral zone and mid latitude magnetic activity is examined qualitatively. The AFGL magnetometer chain is our main source of information on mid latitude activity; magnetograms from Fredericksburg (FB) and Boulder (BD) supply additional data in the local time sector of the AFGL chain. Auroral zone activity indicating substorms is selected from H component magnetograms recorded at 9 high latitude stations of the AE network. A map

showing the stations used in this study appears in Figure 2.1. Table 2.1 lists the station names, symbols, and Corrected Geomagnetic coordinates. Figure 2.2 displays 5 cases of magnetic bay onsets, designated by vertical lines, which occurred on December 9, 1976 in the high latitude network. As expected from the extensive literature on substorm studies, bay onsets usually are observed first by stations located near local midnight. Thus, from 00-12 UT, onsets generally are seen in the Canadian sector, while from 12-24 UT it is the Russian sector that is affected the most. The vertical dashed lines in Figure 2.2 correspond to those in Figure 2.3, which shows X and Y components from the AFGL chain on the same day, December 9, 1976. First, we note that in Figure 2.2 significant changes in the average slope of the X and Y components at mid latitude coincide with high latitude magnetic bay onsets (solid lines). These changes occur at most or all of the AFGL stations and are roughly simultaneous with the bay onsets (within about 20 minutes). On this particular day, it appears that for the event at 1520 UT the Y component gives a somewhat better indication of substorm onset, although less distinct but perceptible changes in the X components did take place about 20 minutes earlier.

In addition to the activity in Figures 2.3 and 2.4 accompanying auroral zone bay onsets, there are gross patterns at other times which also indicate some degree of high latitude disturbances. This "class" of events typically is described at mid latitude by sharper changes in the Y component than in the X component; such cases are marked by dashed vertical lines in both Figures 2.3 and 2.4. Referring again to the high latitude magnetograms in Figure 2.2, we notice that the solid lines (by definition) indicate onsets of major magnetic bays, while the dashed lines, selected on the basis of mid latitude magnetic activity, occur with less pronounced bays taking place both before and after major onsets.

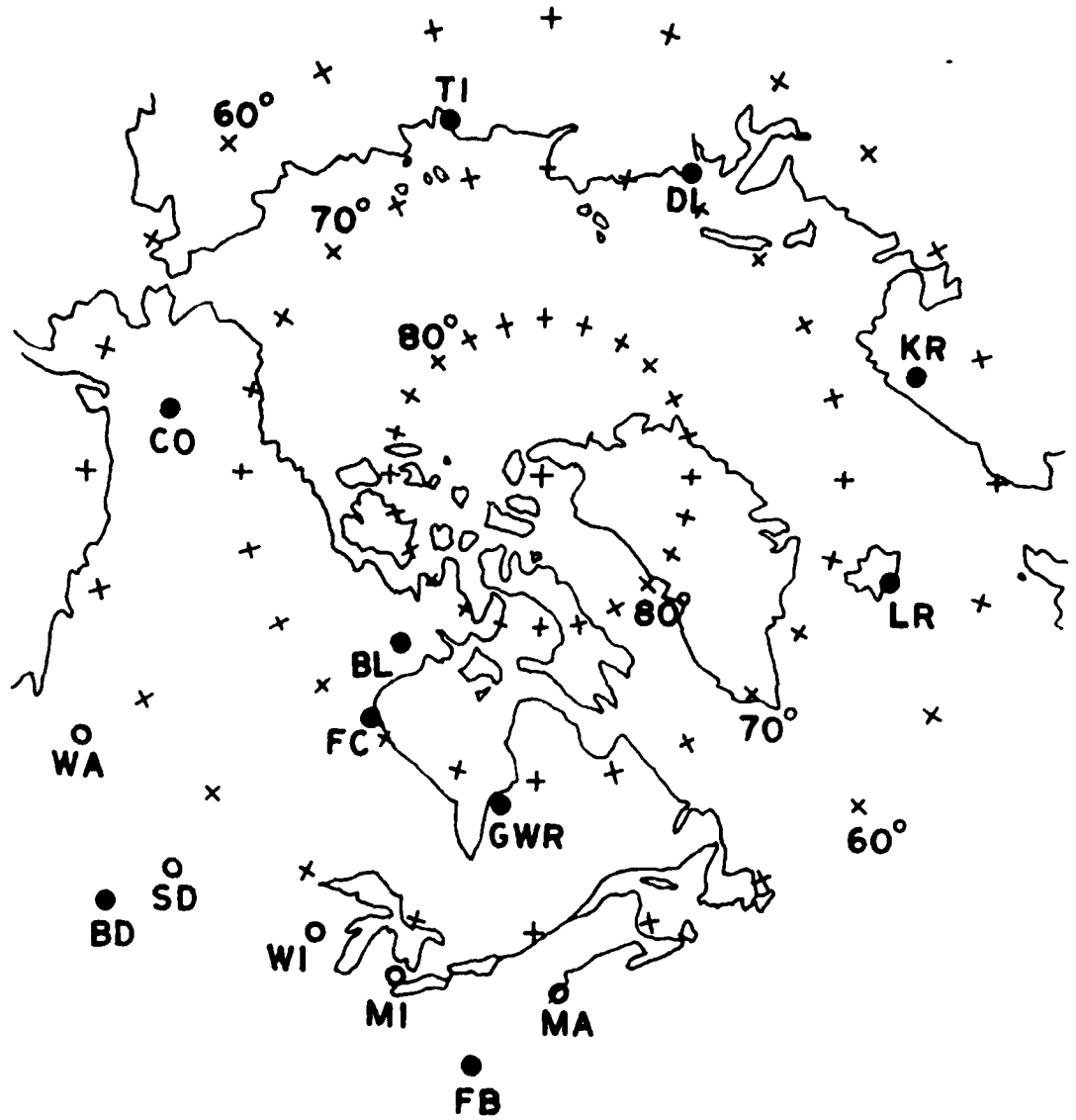


Figure 2.1 Northern hemisphere map showing locations of stations used in this report. Circles defined by ticks are 10° intervals of Corrected Geomagnetic Latitude; tick marks at one hour intervals of local time.

<u>Station</u>	<u>Symbol</u>	<u>CG Latitude (N)</u>	<u>CG Longitude (E)</u>
Tixie Bay	TI	65.6	195.1
Dixon Island	DI	67.9	154.7
Kiruna	KR	64.3	104.8
Leirvogur	LR	66.6	71.1
Great Whale R	GRW	68.2	353.7
Fort Churchill	FC	70.3	325.9
Baker Lake	BL	75.1	320.4
College	CO	64.9	260.3
Fredericksburg	FB	50	352
Boulder	BD	50	315
<u>AFGL Chain</u>			
Sudbury	MA	55.8	1.9
Mt. Clemens	MI	55.8	344.8
Camp Douglas	WI	56.3	334.2
Rapid City	SD	54.1	317.3
Newport	WA	55.2	299.6

Table 2.1 List of stations used in this report. Symbols appear at station locations in Figure 2.1. Corrected Geomagnetic Coordinates are North Latitude and East Longitude. AFGL station symbols indicate the state in which the installation is located.

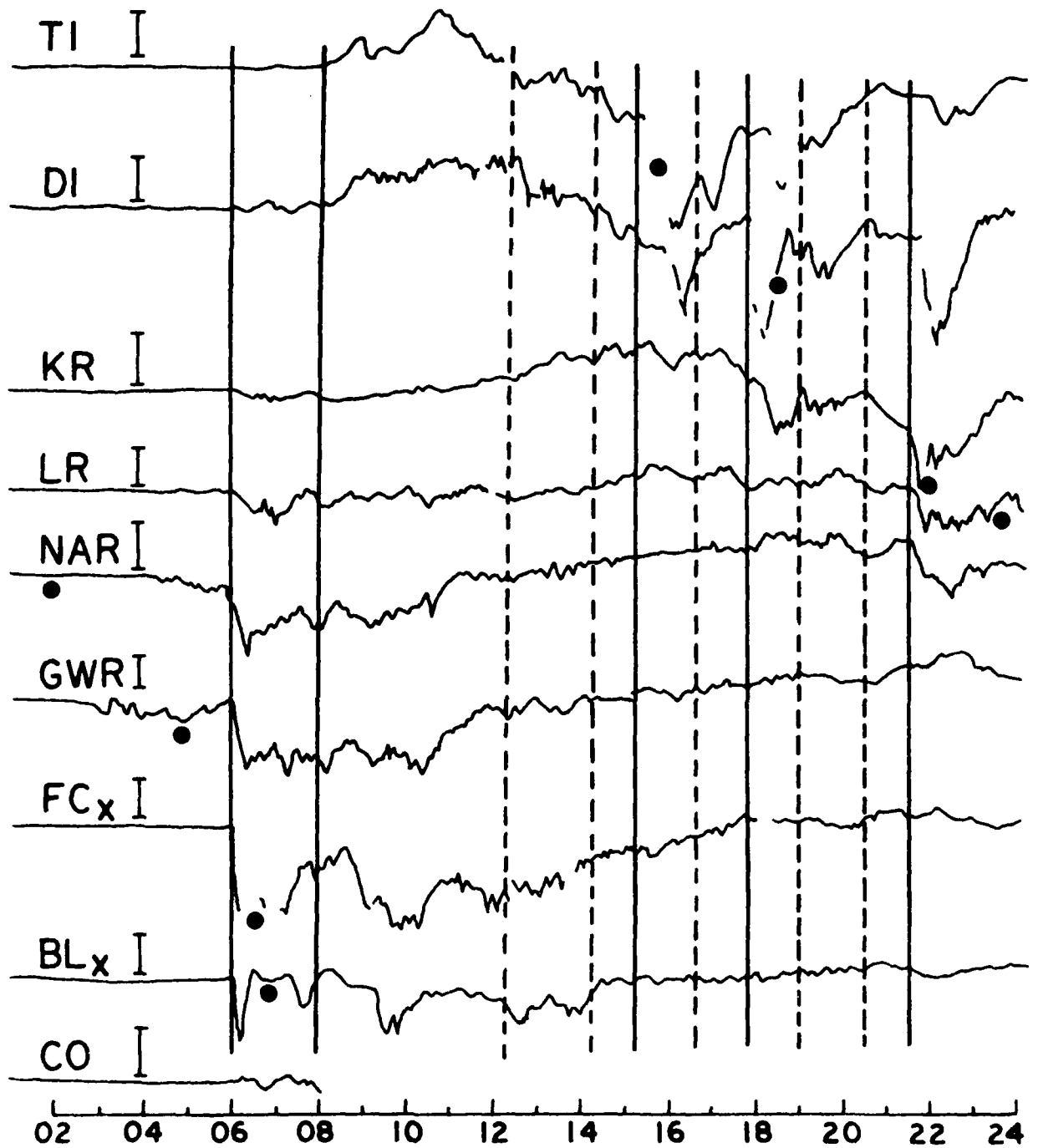


Figure 2.2 Stacked H component magnetograms (X component at FC and BL) from 9 auroral zone stations on December 9, 1976. Bars indicate 200 γ deflections; up is positive. Dots under each trace mark local midnight. Solid and dashed vertical lines are major and minor events discussed in the text.

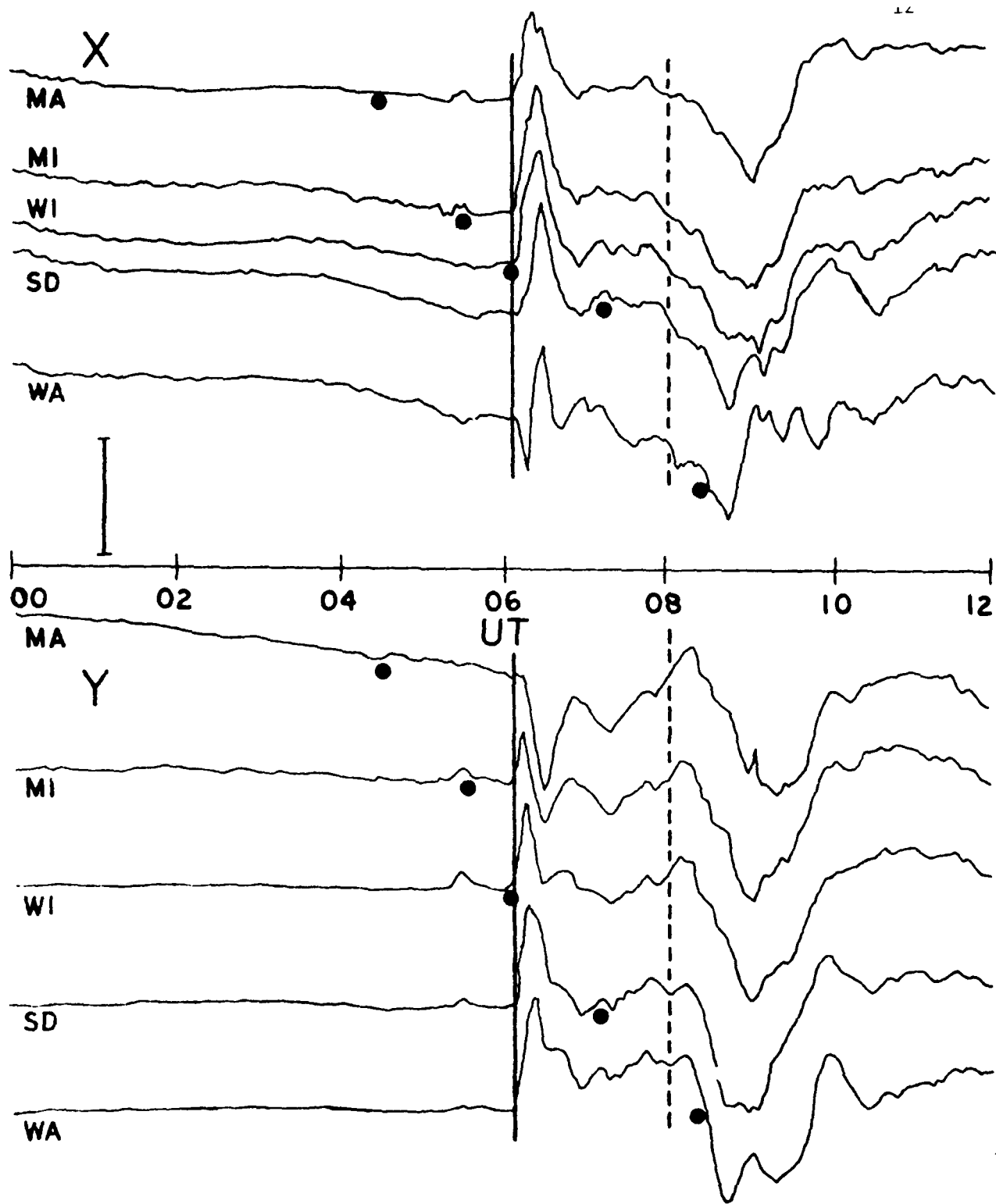


Figure 2.3 Stacked magnetograms from 5 AFGL chain stations (MA, MI, WI, SD, and WA) on Dec. 9, 1976 (0000-1200UT). X components above, Y components below. Dots under each trace at local midnight. Solid vertical lines correspond to events in Figure 2.2. Amplitude bar is 50γ for X components; for Y components, amplitude bar is 50γ at MA, 70γ at MI, 80γ at WI and WA, and 120γ at SD.

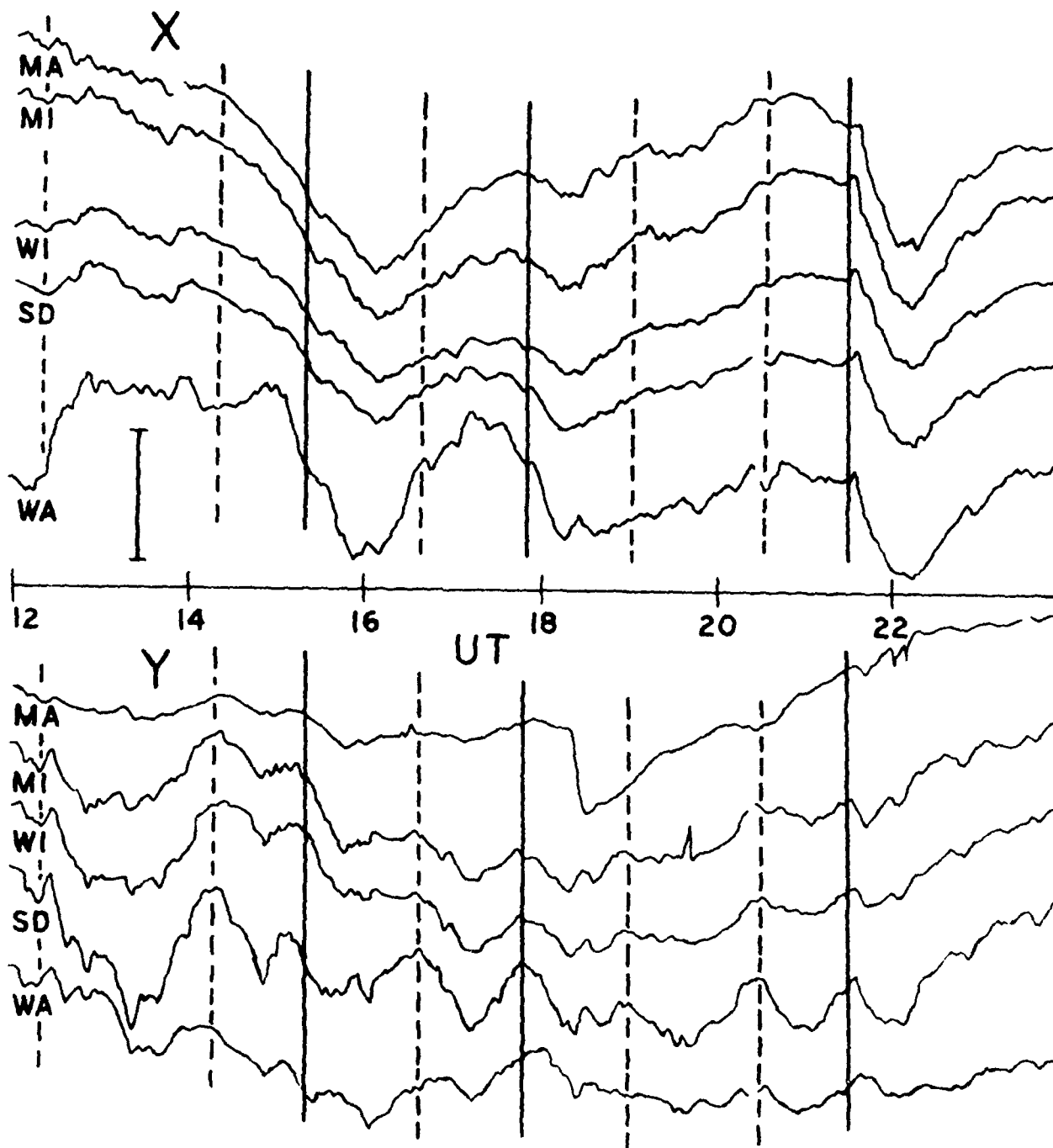


Figure 2.4 Same as Figure 2.3 for 1200 - 2400 UT on December 9, 1976. Amplitude bar for X components: 30 γ at MA, MI, and WA, 40 γ at WI, and SD; for Y components: 30 γ at MI, WI, and SD, 40 γ at WA, and 60 γ at MA. The Y component at MA may be unreliable.

The purpose of this discussion is to demonstrate the range of possible inferences to be drawn from a mid latitude magnetic data set spanning 4 hours of local time. A reasonable conclusion from the rather complicated example in Figures 2.3 and 2.4 is this:

A sustained, rapid change in the X and Y components occurring almost simultaneously at more than one midlatitude station indicates that significant magnetic bay activity has commenced at auroral zone latitudes; definite changes mainly in the Y components at mid latitudes suggest less important high latitude activity occurring before or after major onsets.

Different interpretations are possible in the single example cited in the figures. For example, it could be argued in Figure 2.4 that the activity at 1420 UT is seen also in the X components at MA and MI, or that the major high latitude bay beginning at 1520 UT is not reflected clearly in the midlatitude X component data. In the next section we try to remove or reduce such ambiguities and uncertainties. This is done by making detailed comparisons of mid latitude data from Fredericksburg and Boulder (used to substitute for unavailable AFGL chain data at the time of this study) with AE index data representing auroral zone magnetic activity. Finally, a simple quantitative scheme using AFGL chain data is proposed and examples of its application given.

C. Correlations between Mid Latitude Activity and AE

To assess the applicability of mid latitude magnetic activity occurring at various local times, we analyzed 4 months of magnetograms from Fredericksburg (FB) and Boulder (BD). The magnetic activity at these two stations were compared with the level of auroral zone disturbance depicted in plots of 2.5 minute averaged Auroral Electrojet (AE) index values. Auroral zone events, defined here as significant enhancements in AE discernible by eye, were collected into 200 γ

intervals of increasing strength. The peak value of AE determined both the time and strength of an event. Examples of AE events occurring in an 8 day period (October 9-16, 1972) appear in Figure 2.5. The peak values, in hundreds of gammas, are given above each enhancement. H component magnetograms from FB over the same time period are shown in Figure 2.6; AE enhancements and their strength are indicated at appropriate times above each trace in the same manner as Figure 2.5. It is obvious that there is a wide range of mid latitude activity accompanying auroral zone events, but that, in a rough way, activity at FB is stronger with larger AE events.

In order to uncover a more definite relationship between auroral zone and mid latitude magnetic behavior, a better characterization of mid latitude activity is needed. After a survey of FB and BD magnetograms it was decided that three descriptive levels of activity would be adequate; these levels are:

- (1) Strong: a definite, sudden change in the average slope of the H or D component;
- (2) Moderate: distinct irregular activity in the range of 5-20 γ amplitude;
- (3) Weak: little or no apparent activity.

The strong level corresponds to the mid latitude indication of auroral zone bay onset given in Figures 2.3 and 2.4. The moderate level includes lesser activity which is nonetheless obvious, like that mentioned in Figures 2.3 and 2.4.

In our procedure, the activity level at FB and BD is assigned by the above criteria at the time of each AE event. This yields 4 separate activity estimates for an event, one from each component (H and D) at both stations. Then the 4 estimates are "superposed" so that the most active station component characterizes each event. Such a procedure is similar to creating AE indices, where the most highly disturbed station contributes solely to the index. But, unlike the entire circle of local time coverage provided by the AE network, FB and BD span less than

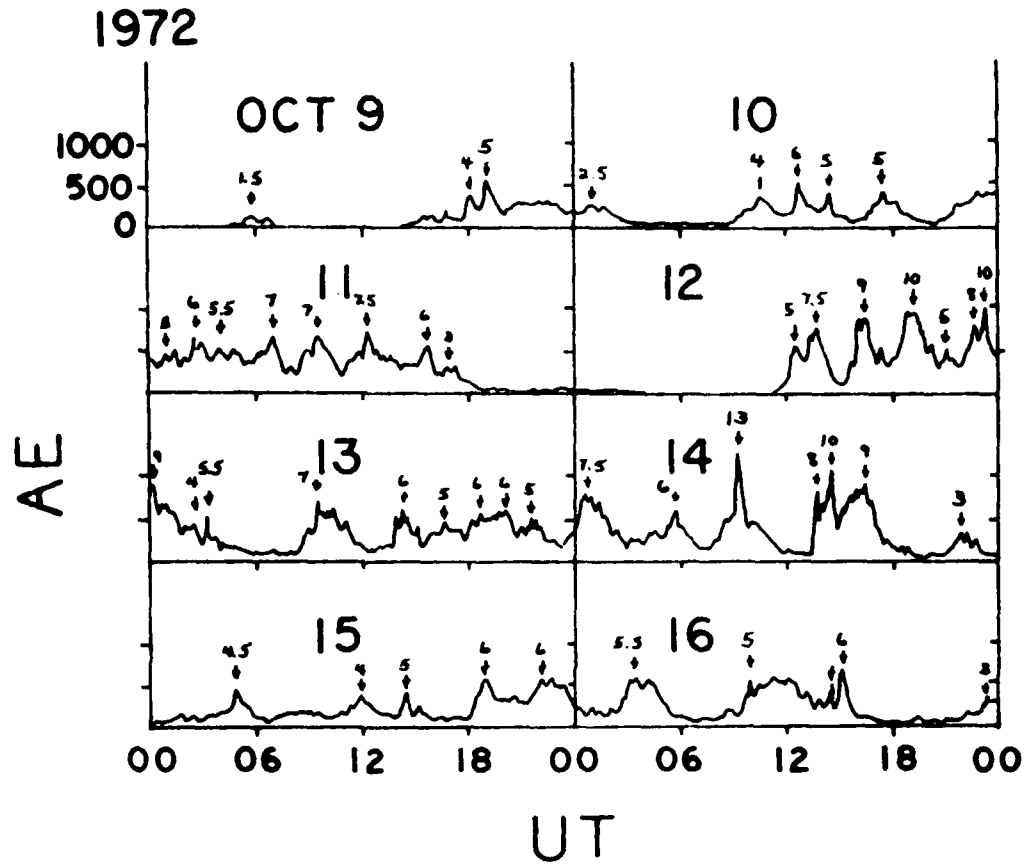


Figure 2.5 AE plot for October 9 - 16, 1972. Events described in the text are marked by arrows with peak AE values (in hundreds of gammas) indicated above.

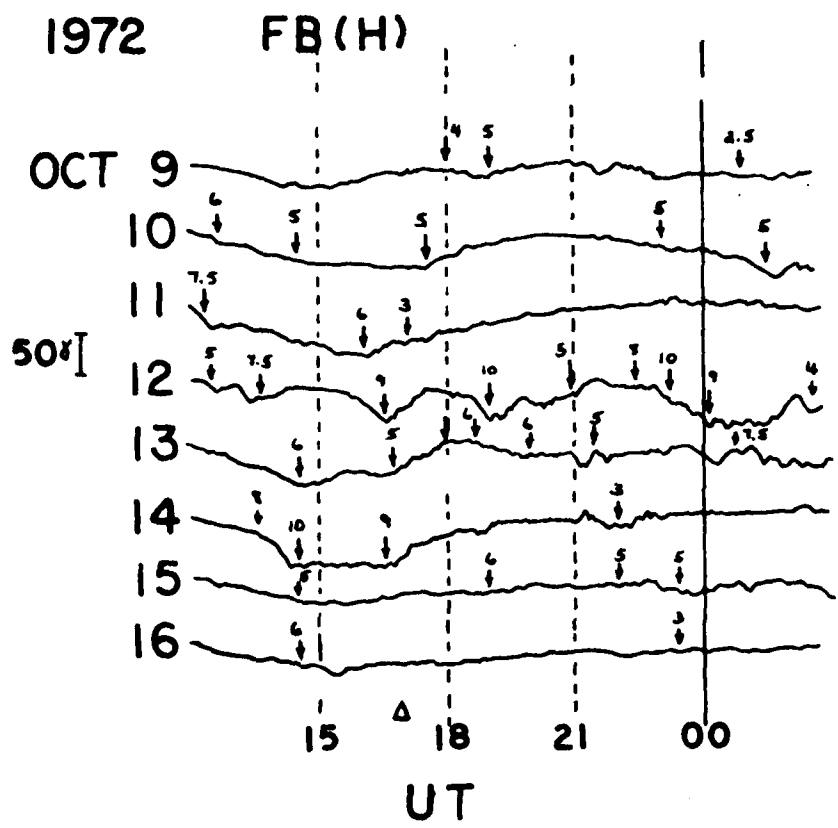


Figure 2.6 H component magnetograms from Fredericksburg, October 9 - 16, 1972. Events marked by arrows correspond to those in Figure 2.5, with the peak AE value (in hundreds of gammas) indicated above. Solid triangle on UT scale indicates local noon at Fredericksburg.

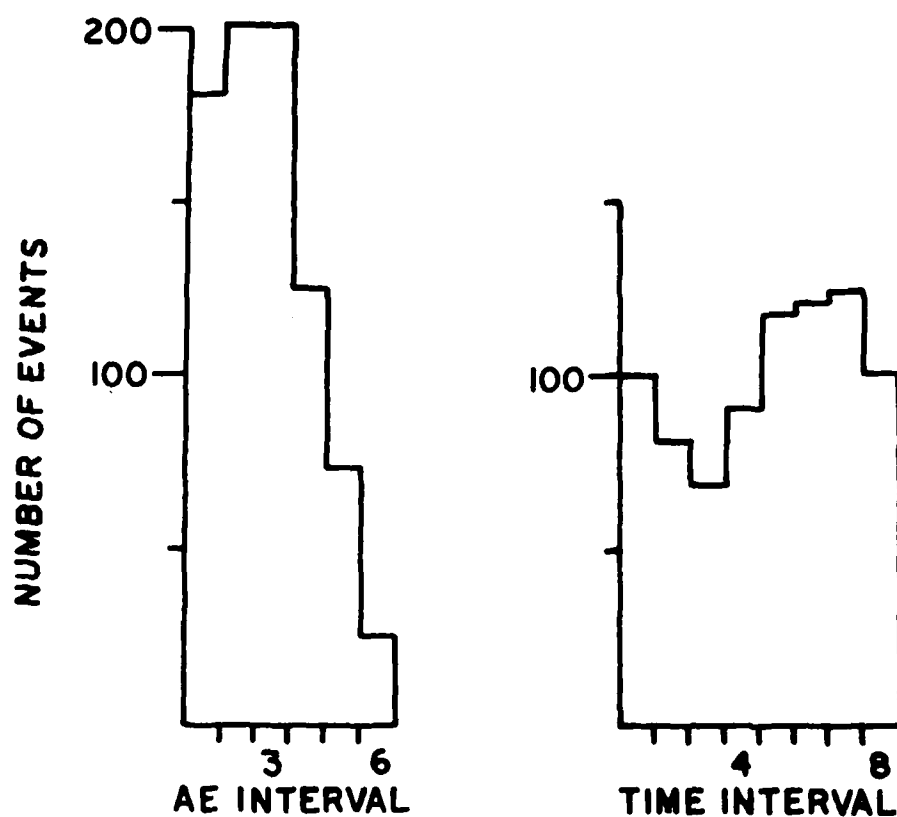
3 hours of local time.

Figure 2.7 shows how 806 AE events occurring from October 2, 1972 through January, 1973 were distributed in strength and time. The first histogram gives the number of events in each 200 γ interval of increasing AE. AE ranges for each interval are listed in the figures. The second histogram shows the diurnal occurrence of events, regardless of strength, collected in 3 hour intervals of UT. Corresponding to each UT interval there is a local time in Figure 2.7 which gives the sector that FB and BD occupied at the time of each event. The midpoint between the two stations defines the local time sector.

The distribution of events by strength shows that almost two-thirds of all events are less than 600 γ in amplitude. Above 600 γ the numbers decrease smoothly and rapidly to about 25 cases (3%) above 1000 γ . The diurnal variation is less regular; occurrences peak markedly during 18-21 UT and decrease by about 45% at 06-09 UT.

All 806 AE events are categorized by the three level (qualitative) description of mid latitude activity defined earlier. Using clusters of 3-bar histograms, Figures 2.8 and 2.9 display actual numbers of events falling into any combination of AE strength, local time sector, and mid latitude activity. The first, second, and third bars in each 3-bar histogram cluster enumerate cases of weak (W), moderate (M), and strong (S) midlatitude activity, respectively. The 3-bar histograms are grouped by intervals of increasing AE strength into 8 histograms distinguished by the local time sector in which mid latitude activity was recorded. This somewhat complicated format gives the actual numbers used below in determining conditional probabilities; in addition, it reveals general trends and permits an appraisal of statistical significance which would be lost if ratios were taken immediately.

Considering one example in detail, the upper left histogram in Figure 2.8 includes all AE events that occurred when FB and BD were in the 07-10 CGLT



<u>INT.</u>	<u>RANGE (I)</u>	<u>INT.</u>	<u>UT</u>	<u>CGLT</u>
1	0-200	1	00-03	19-22
2	200-400	2	03-06	22-01
3	400-600	3	06-09	01-04
4	600-800	4	09-12	04-07
5	800-1000	5	12-15	07-10
6	>1000	6	15-18	10-13
		7	18-21	13-16
		8	21-00	16-19

Figure 2.7 Distribution of 806 AE events, identified during October 1972 - January 1973, according to strength (left histogram) in 200 γ intervals of AE, and UT of occurrence (right histogram), in 8 three-hour intervals of UT and CGLT at FB and BD. Midpoint between FB and BD defines the CGLT interval. Intervals span the beginning of the first hour to the beginning of the second (00 - 03 UT = 0000 - 0300 UT).

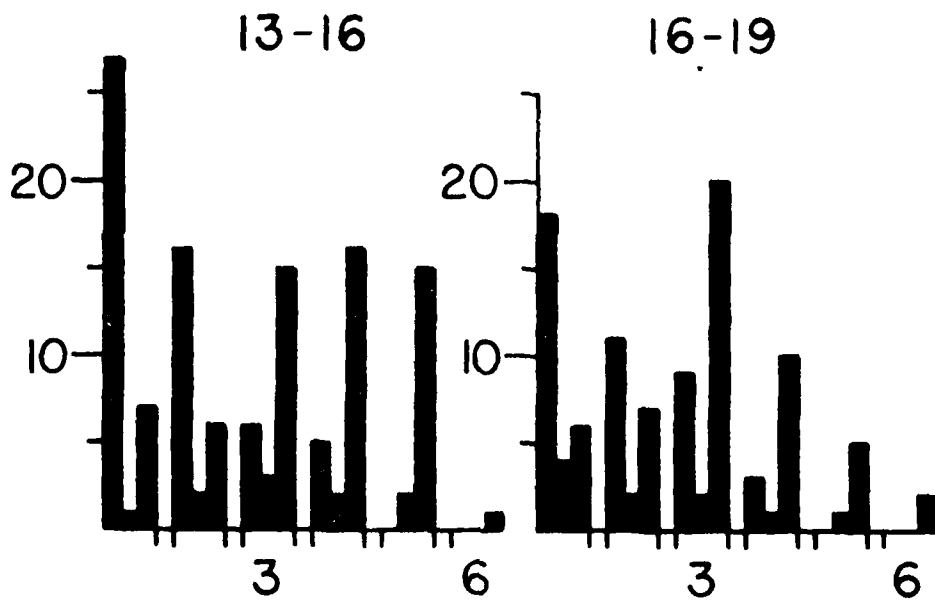
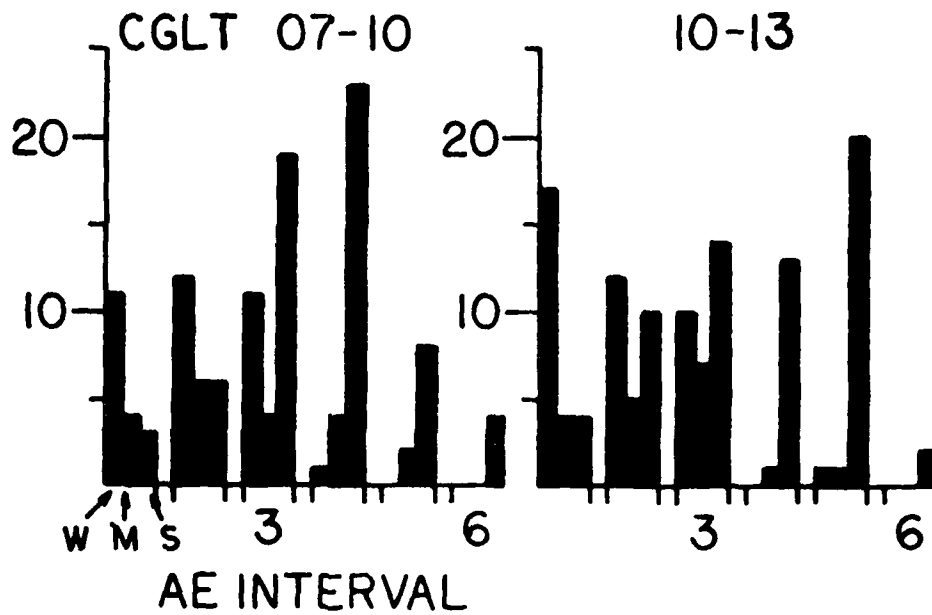


Figure 2.8 Breakdown of mid latitude responses to AE events occurring in October 1972 - January 1973. Each 3-bar cluster gives the number of weak (W), moderate (M) and strong (S) responses to AE events, defined in the text, occurring in the indicated 200 μ strength interval (Figure 2.7) and CGLT interval of FB and BO. Dayside mid latitude responses shown in this figure.

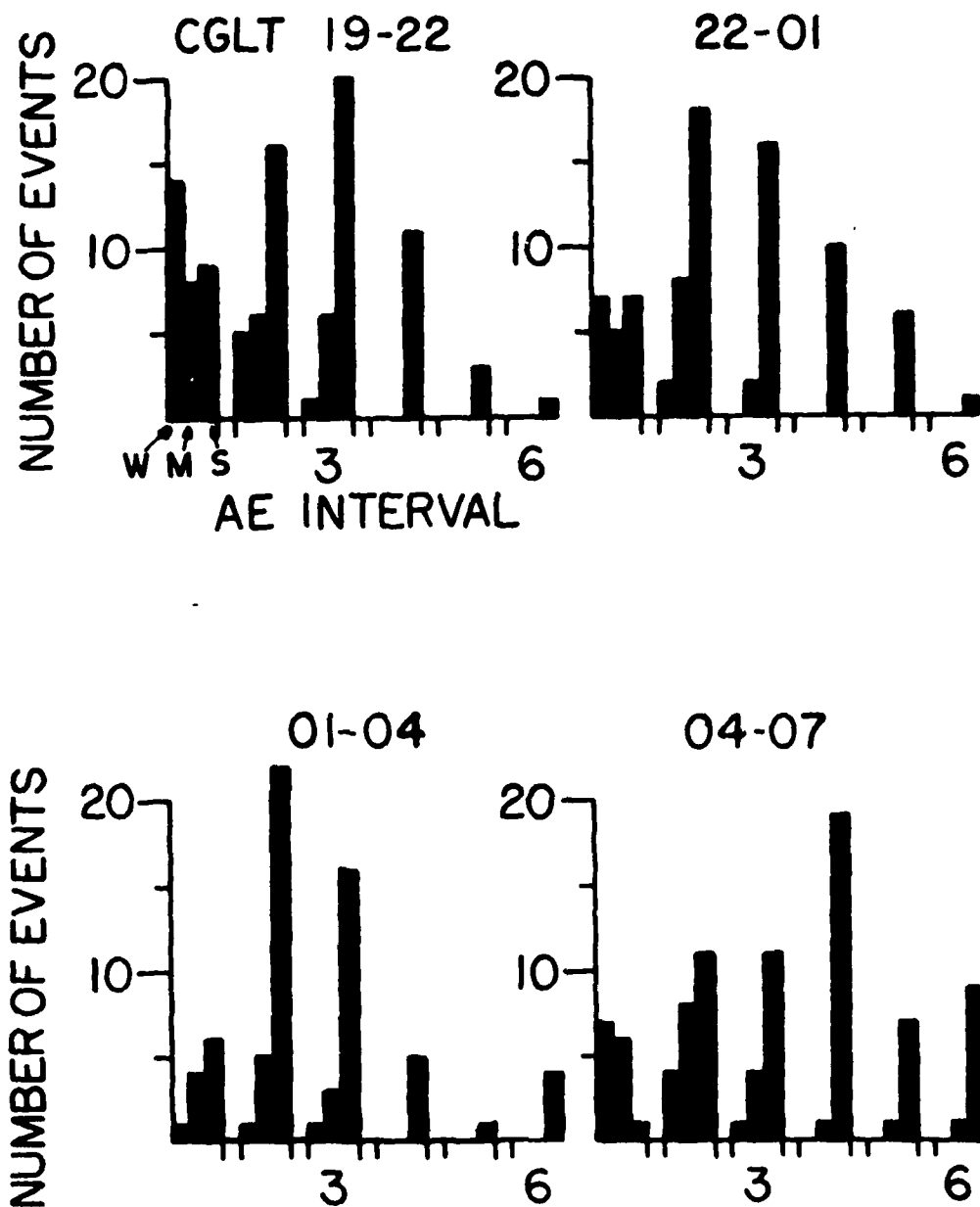


Figure 2.9 Breakdown of nightside mid latitude responses. Same format as Figure 2.8.

(Corrected Geomagnetic Local Time) sector. Weak mid latitude activity dominated for events in the two lowest strength intervals ($AE < 400\gamma$). Strong mid latitude activity prevailed when the AE of an event was greater than 400γ . For all day-side sectors (Figure 2.8) the majority condition at mid latitudes changes from weak to strong activity with $AE = 400-600\gamma$. When FB and BD were on the night-side (Figure 2.9) the same change to strong mid latitude activity occurs with weaker substorm events ($AE = 200-400\gamma$).

Percentages for mid latitude magnetic activity calculated from Figures 2.8 and 2.9 are presented in Figure 2.10. Again, each histogram in Figure 2.10 represents all events that occurred while FB and BD were in the indicated local time sector. Percentages are plotted vs. AE intervals with the same ranges as in Figures 2.7-2.9. The set labeled strong shows relative percentages of strong activity, compared with moderate and weak, for increasing levels of AE strength. The set labeled "strong and moderate" combines events with strong or moderate mid latitude activity.

Figure 2.10 depicts the data in Figures 2.8 and 2.9 compactly and quantifies the properties of the three level activity index described above. For example, approximately 50% of the mid latitude responses in 10-13 CGLT sector are strong for an AE enhancement of $400-600\gamma$ (interval 3). The percentage increases to nearly 70% in that local time sector for the same AE category when moderate responses are added (lower set of histograms). A careful comparison of the upper two rows of histograms reveals that strong responses reach or exceed 50% (48% at 10-13 CGLT) when AE is $400-600\gamma$ or more for daytime local sectors, plotted in the top row. In the second row containing nighttime sectors, 50% is reached when AE is only $200-400\gamma$ (interval 2).

In general, the occurrence of strong activity at mid latitudes suggests different probabilities of high latitude activity, depending on whether the observation is made on the day or night side of the earth. On the day side,

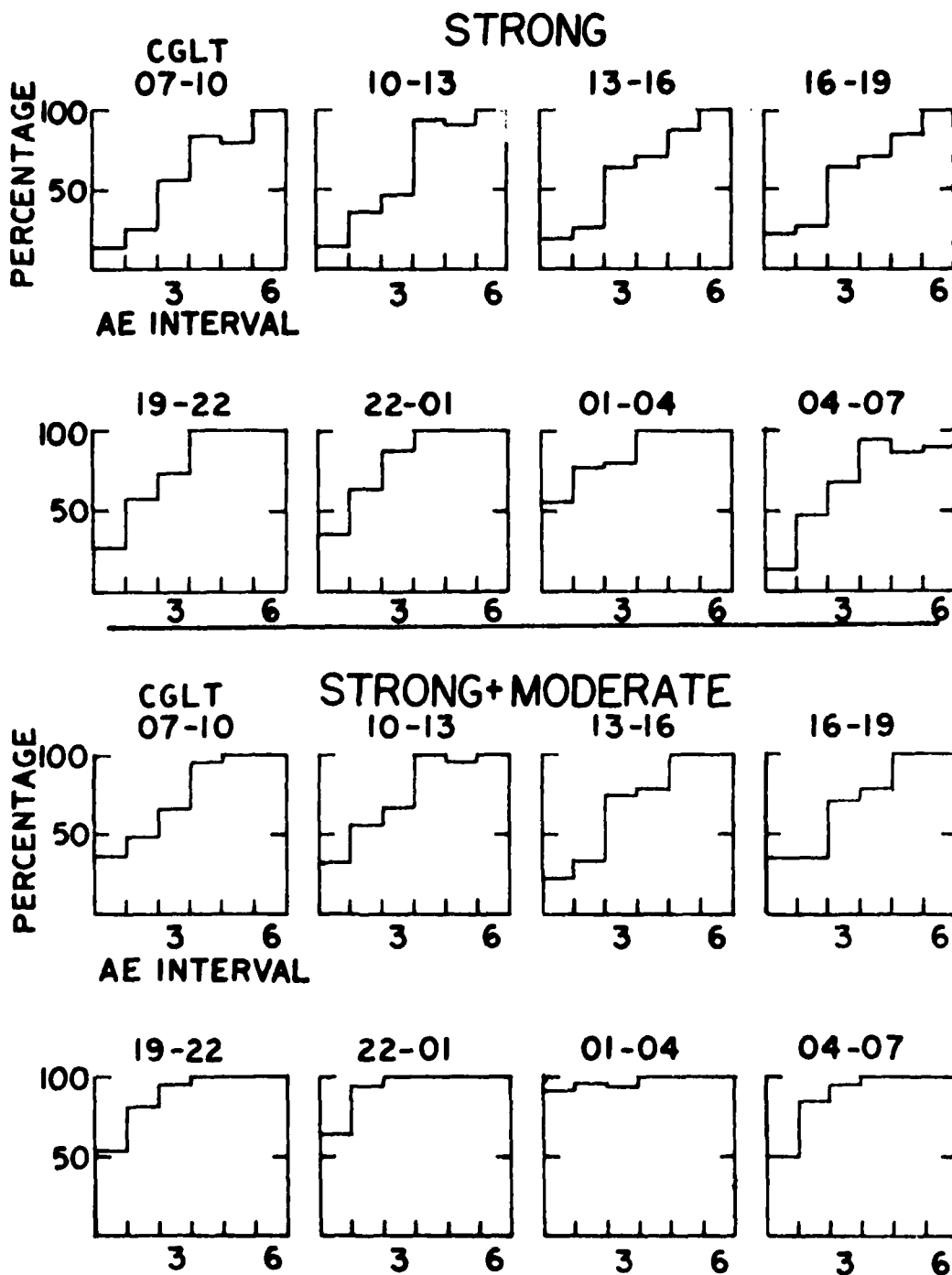


Figure 2.10 Histograms showing the proportion of strong responses (top panel), relative to moderate and weak, accompanying AE enhancements in intervals of increasing strength (defined in Figure 2.7). Dayside local time sectors in the first row, nightside in the second. Bottom panel, in the same format as the top, combines strong and moderate responses.

discrimination between relatively weak and strong AE activity is quite good. That is, strong responses are rather infrequent until AE exceeds 400γ . On the night side discrimination is poorer because weaker AE enhancements elicit a large share of strong responses, but the reliability is greater because almost all very large AE enhancements are detected; all responses are strong for AE greater than 600γ in the 19-04 CGLT sector, and nearly 100% in the 04-07 CGLT sector.

There are two exceptions to the general day and night behavior. First, in the lowest AE interval of the 04-07 CGLT sector, strong responses occur proportionately less compared with the other nighttime sectors. Second, and more interestingly, the noon sector (10-13 CGLT) behaves more like the night sectors in that strong responses exceed 90% during large AE enhancements ($> 600\gamma$). This reverses the trend beginning in the dawn sector (04-07 CGLT) of decreased sensitivity to large AE events. After noon (13-19 CGLT) the proportion of strong responses decreases again until a sharp recovery occurs after dusk (19-22 CGLT).

In summary, two general statements can be made concerning the effectiveness of strong mid latitude magnetic response, defined earlier in this section, as an indicator of high latitude magnetic activity characterized by the AE index.

(1) At stations located in the night sectors, strong responses accompany over 50% of AE enhancements in the 200-400 γ range. With AE $> 600\gamma$ the percentage is almost always 100%.

(2) Stations in the day sectors have 50% strong responses when AE is 400-600 γ . When AE exceeds 600 γ , the proportion of strong responses occurring in pre noon sectors is above 80%. After noontime, the proportion is somewhat lower, 70%, for AE in the 600-800 γ interval.

Combining strong and moderate responses (lower panel in Figure 2.10) does not alter these results appreciably. It assures the detection of extremely large AE enhancements ($> 800\gamma$) at all local times, but greatly reduces the ability to discriminate between large and small enhancements in the night sectors. As a

practical tool it appears that a strong response is the least ambiguous to determine and the cleanest to interpret. In the next section, a more quantitative approach is adopted from the start. Although the technique is more refined, the overall results are similar to those already stated above.

D. Description and Examples of Mid Latitude Variation Procedure

One direct indicator of magnetic activity is the incremental change in a magnetic component over a specified time period. In this section, we apply a simple, quantitative procedure to AFGL chain data that is based on the qualitative descriptions of mid latitude activity presented earlier. Our procedure may be likened to the production of Kp indices but omits elaborate corrections and scaling devices, and, in particular, uses shorter time scales. Our time scales are 1 hour or less compared to 3 hours for Kp indices, a factor which should eliminate much of the need for quiet time corrections. For instance, a typical substorm variation at 55° CGL is about 30γ in 1 hour, while a diurnal variation may amount to $10-20\gamma$ occurring smoothly over 3 hours. During a 3 hour time interval, the substorm contributes only $10-20\gamma$ above the diurnal variation; in contrast, over a 1 hour interval, the substorm variation would again amount to about 30γ , but the quiet time change only to about $3-7\gamma$.

Examples of AFGL chain data are given in the remainder of this section. Seven days of data recorded in December, 1976 were scaled, averaged, and plotted along with a provisional AE index, as shown in Figures 2.11-2.13. X and Y component data from the AFGL chain appear in the upper two panels. Three quantities per component are plotted in each hour: the hourly variation averaged across the chain, plus the maximum and minimum hourly variations. An

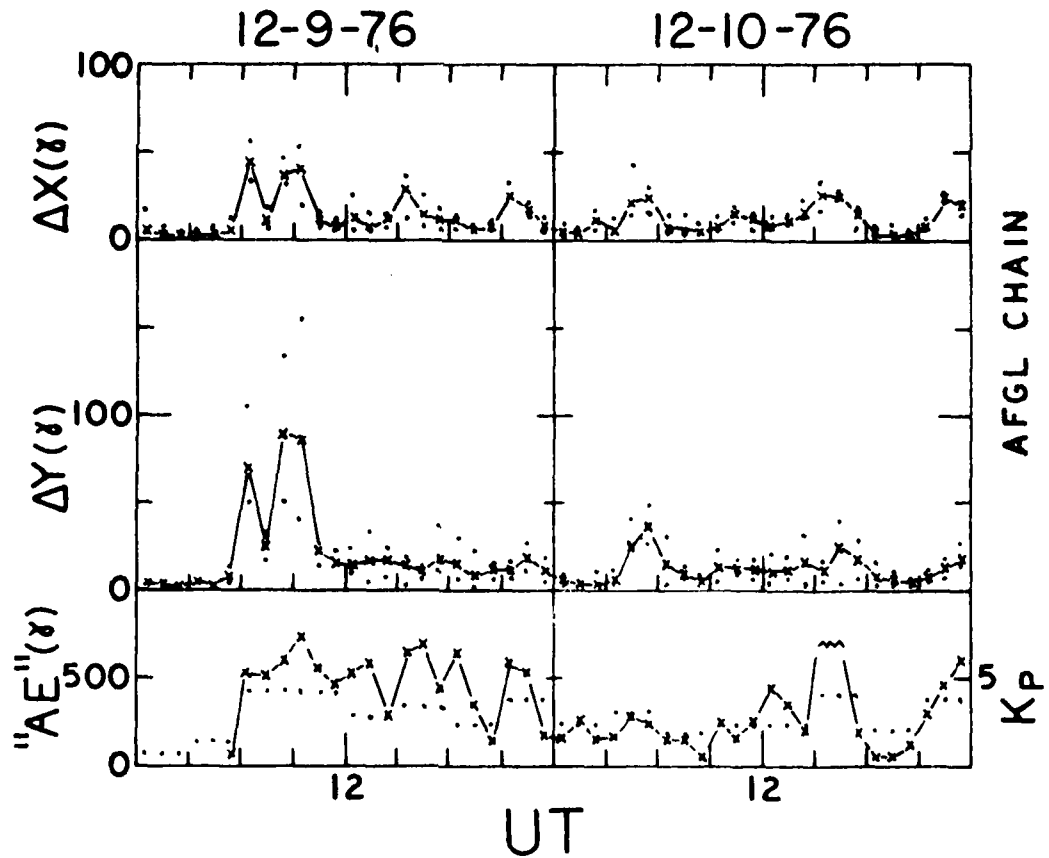


Figure 2.11 Comparison of AFGL chain data (upper two panels) with a modified AE index and K_p index on December 9-10, 1976. Crosses connected by solid lines in the ΔX and ΔY panels indicate the average of the hourly variations from the chain (procedure described in the text). Dots above and below each cross indicate the maximum and minimum hourly variation from the chain. Crosses in the lower panel give an hourly "AE" value, described in the text. K_p values shown by dots.

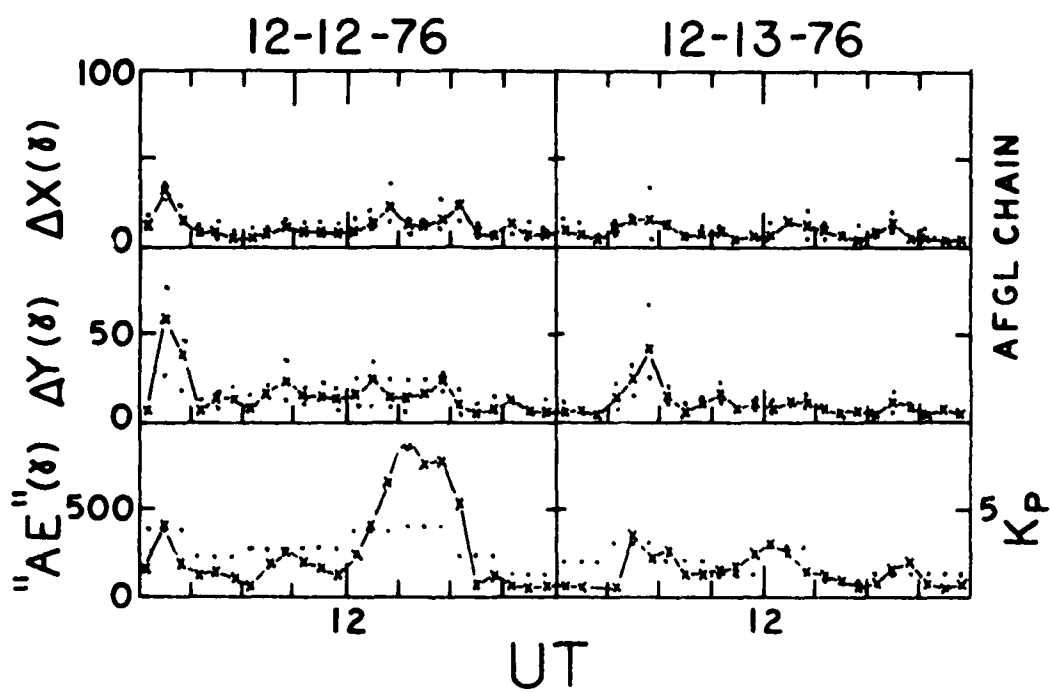


Figure 2.12 Same format as Figure 2.11 for December 12-13, 1976.

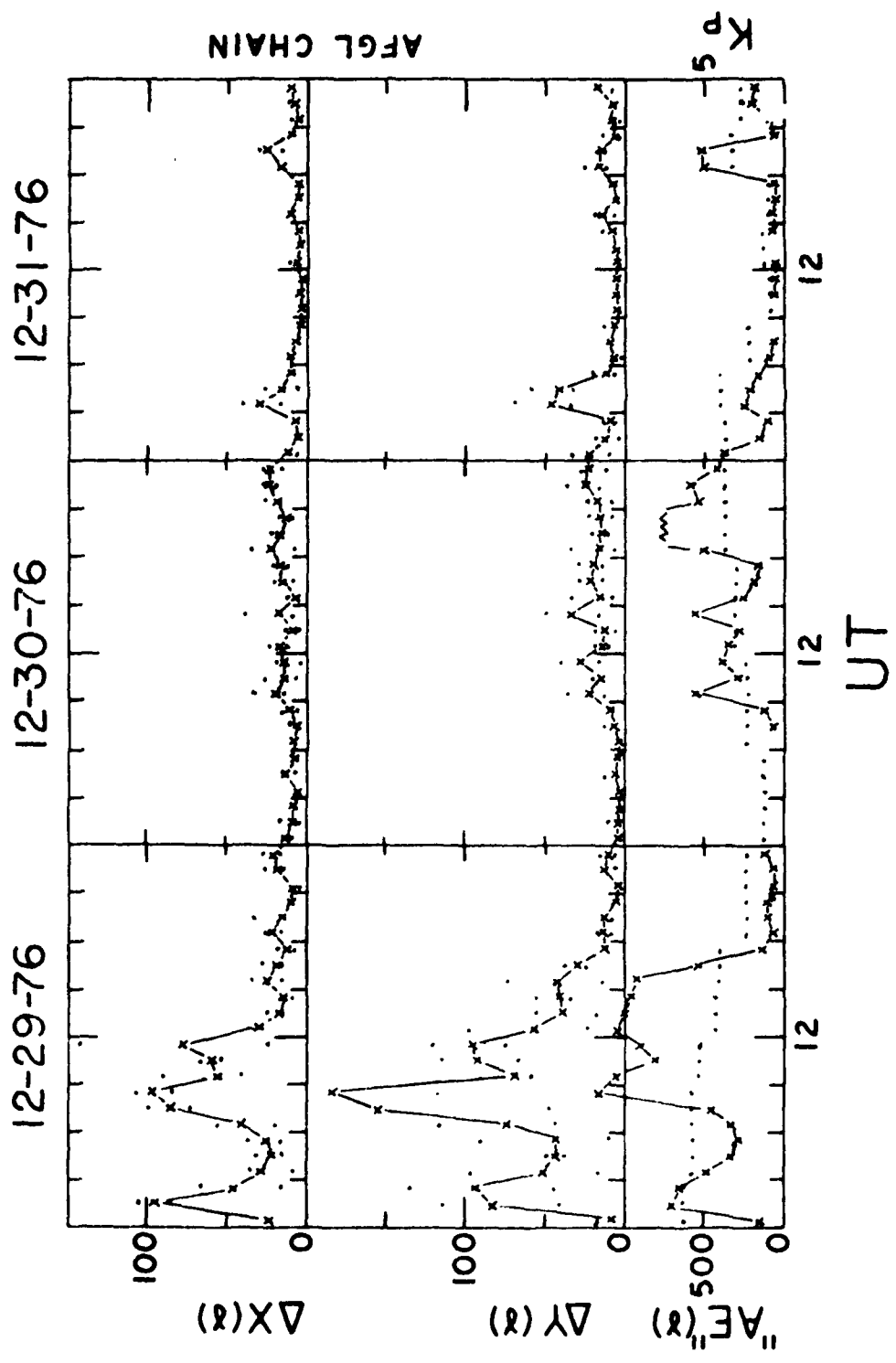


Figure 2.13 Same format as Figure 2.11 for December 29-30, 1976.

hourly variation is defined as the difference between the maximum and minimum values attained during an hour at a station. A cross depicts the chain averaged variation, and a bar indicates the range of variations measured across the chain during 1 hour. The range tells how uniform activity was in the chain sector.

To gauge the effectiveness of this procedure, we constructed an hourly index similar to the AE index. The longitudinal coverage provided by 9 auroral zone stations (see Figure 2.1 for locations) is not ideal but should permit adequate detection of most high latitude activity. First, the maximum hourly deviation of the H component from an estimated baseline was determined at each station. Then, out of the 9 hourly deviations generated every hour, the largest was selected as an appropriate value, an adaptation of the envelope of superposed magnetograms used in true AE determinations.

The general behavior of the mid latitude components in Figures 2.11-2.13 is quite similar, except for somewhat greater variability in the Y component during disturbed periods. Also, mid latitude variations during the night (00-12 UT) are clearly different than those during the day (12-24 UT). The midpoint of the chain, near WI, passes local midnight at approximately 06 UT and local noon around 18 UT. A quiet level of X component variations appears to lie near 5-10 γ . Large auroral zone disturbances (>400 γ) tend to produce X variations of 40 γ or more when the chain sector is at night; in the day sector, X variations are smaller but still noticeable.

Although a general correlation obviously exists between mid latitude variations and high latitude magnetic activity, there is some disagreement in the examples given. Particularly outstanding is the rapid decrease in mid latitude variations after 12 UT on December 29 (Figure 2.13). Also, the high

latitude event at 09 UT on December 30 is reflected poorly in the AFGL variations, while a smaller event one day later at 03 UT is marked by distinct mid latitude variations. Such discrepancies underscore the fact that the quantities plotted here do not provide unambiguous descriptions of simultaneous auroral zone and mid latitude magnetic activity. Improved descriptions might result from more complicated considerations, such as use of more complex functions involving X and Y components, different time scales, or analysis of frequency spectra. At this stage, however, the natural next step is to explore the effectiveness of using shorter time intervals.

Before investigating finer time scales, we present data from FB and BD which was treated in the same way as the AFGL data in Figures 2.11-2.13. Hourly H component variations from FB and BD are shown in Figures 2.14 a-d (upper panels) along with 2.5 minute AE plots for the entire month of December, 1972. During periods of prolonged, extremely low AE, the hourly variations were generally less than 10γ and often less than 5γ (Dec. 5-6, 10, 12, 25, 27-28). However, even with 1 hour time intervals, variations also resulted from smooth changes associated with the Sq focus fixed near local noon. Clear cases are seen around 18 UT on December 1, 6, 21, and 27. A characteristic double wave appearance is evident as first FB and then BD rotated through the H component depression. At the other extreme, periods when AE was above 500γ are reflected clearly by mid latitude variations. There were no cases of very high AE when one or both mid latitude variations were under 10γ . Intervals of sustained AE activity produced the greatest mid latitude activity, as seen on December 13, 15-16, and 22-24. AE episodes reaching $700-1000\gamma$ generally were accompanied by variations of 20γ or more, regardless of the local time sector being monitored at mid latitudes. Marked variations in the day sector occurred with activity

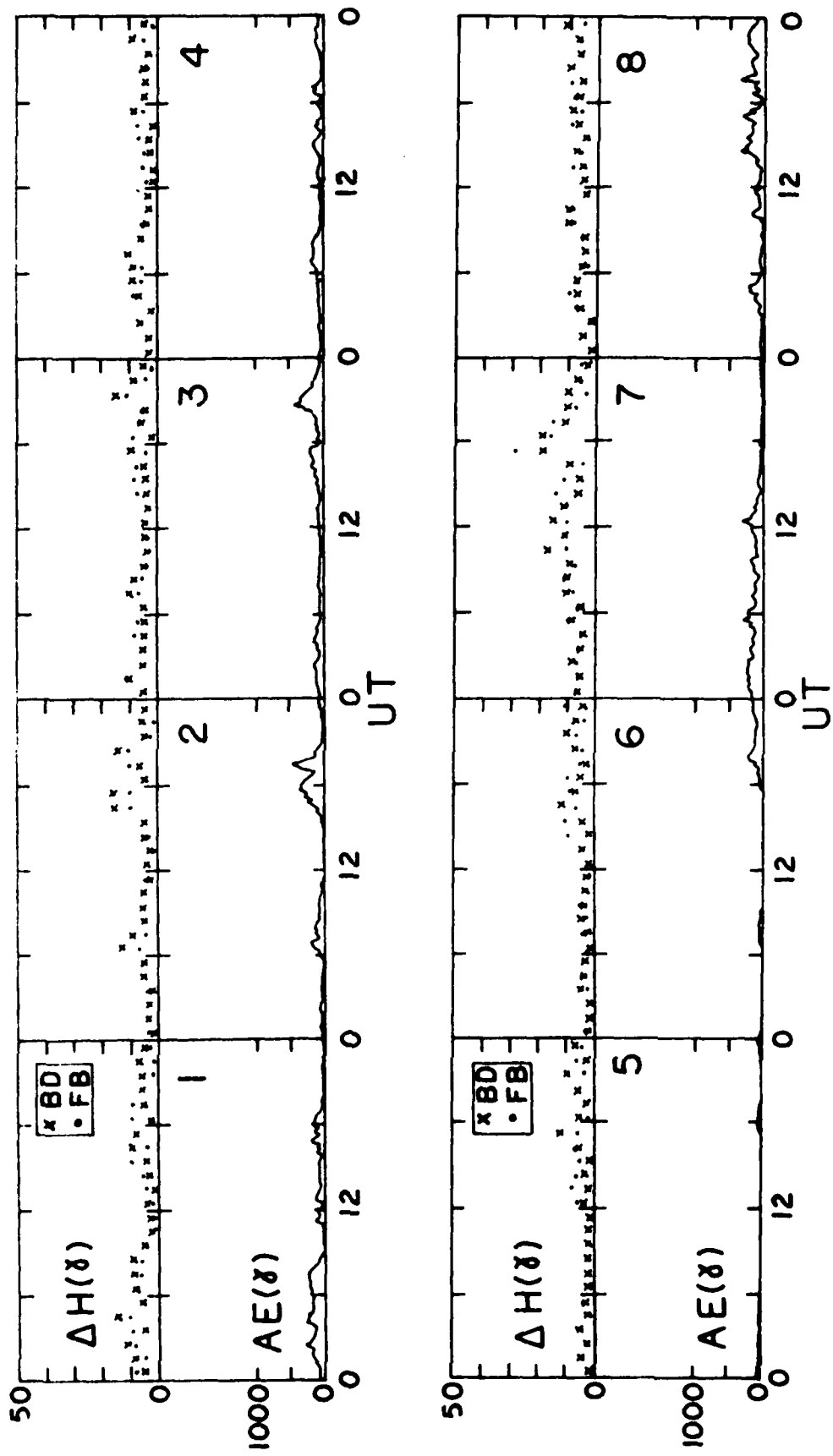


Figure 2.14a. Hourly H component variations at Fredericksburg (dots) and Boulder (crosses) plotted in the top panels; 2.5 minute average AE index in the bottom panels. Time period Dec. 1-8, 1972.

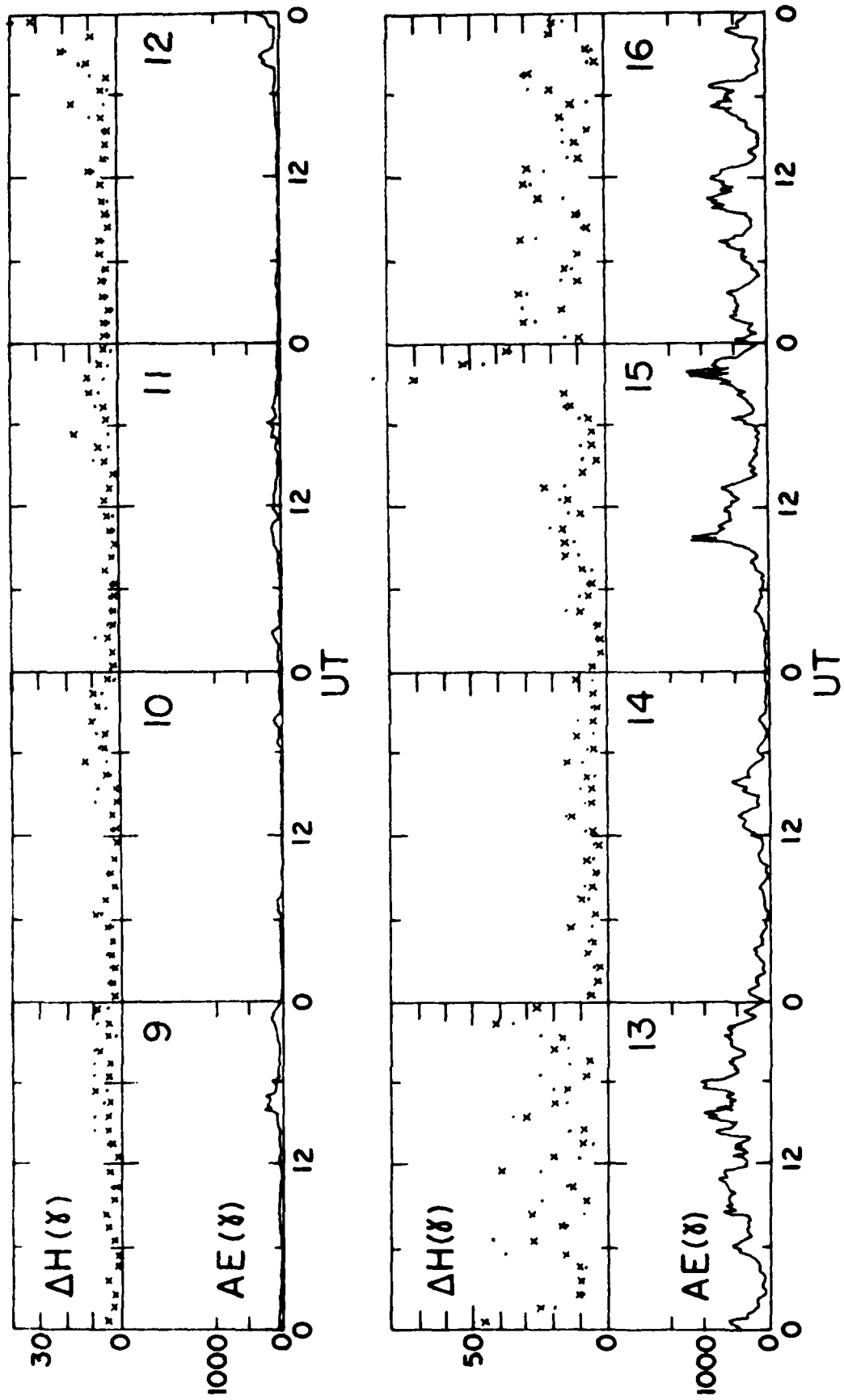


Figure 2.145. Hourly H component variations at Fredericksburg (dots) and Boulder (crosses) plotted in the top panels; 2.5 minute average AE index in the bottom panels. Time period is Dec. 9-16, 1972.

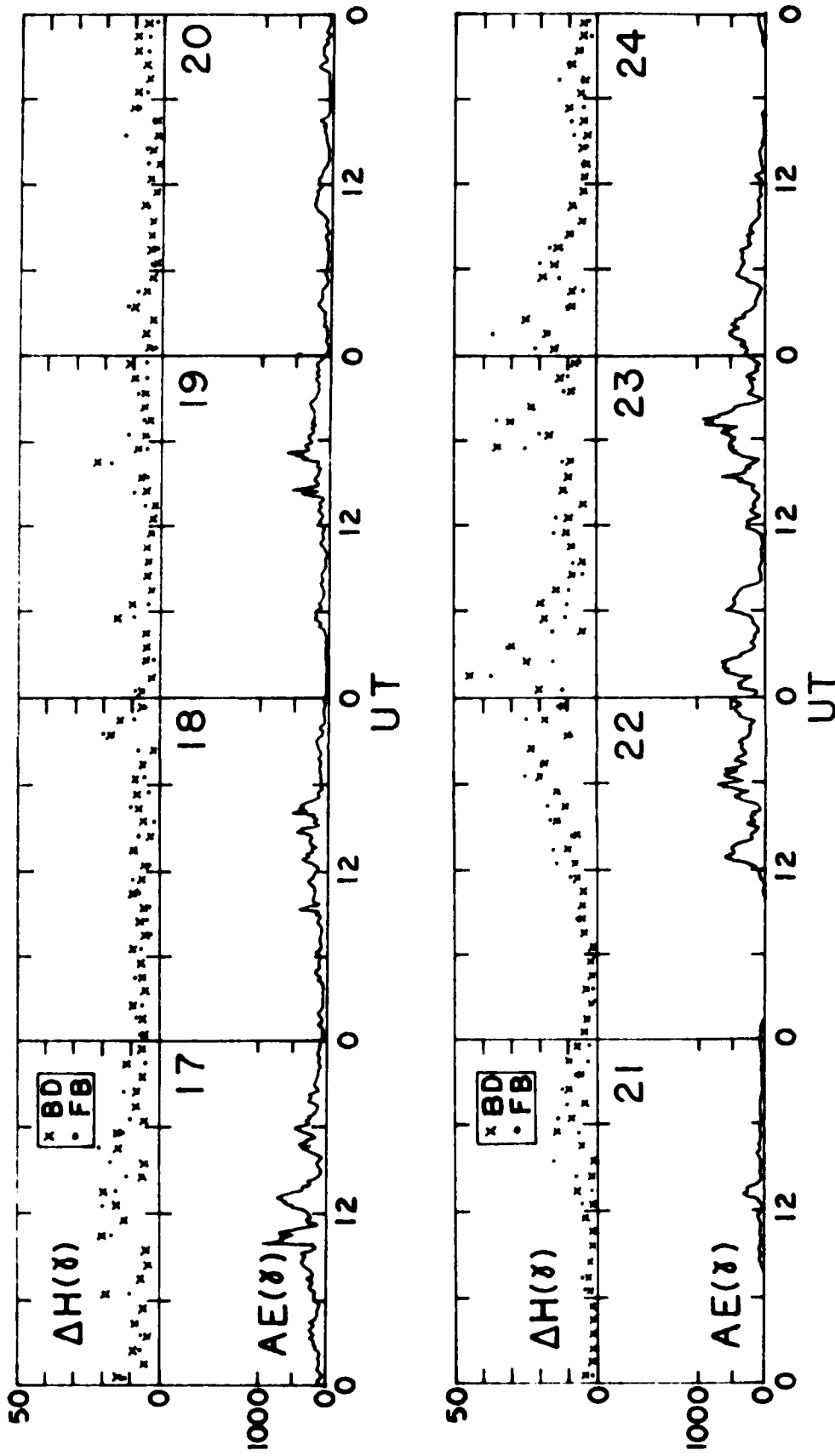


Figure 1.1-c. Hourly H component variations at Fredericksburg (dots) and Boulder (crosses) plotted in the top panels; 2.5 minute average AE index in the bottom panels. Time period Dec. 17-24, 1972. 33

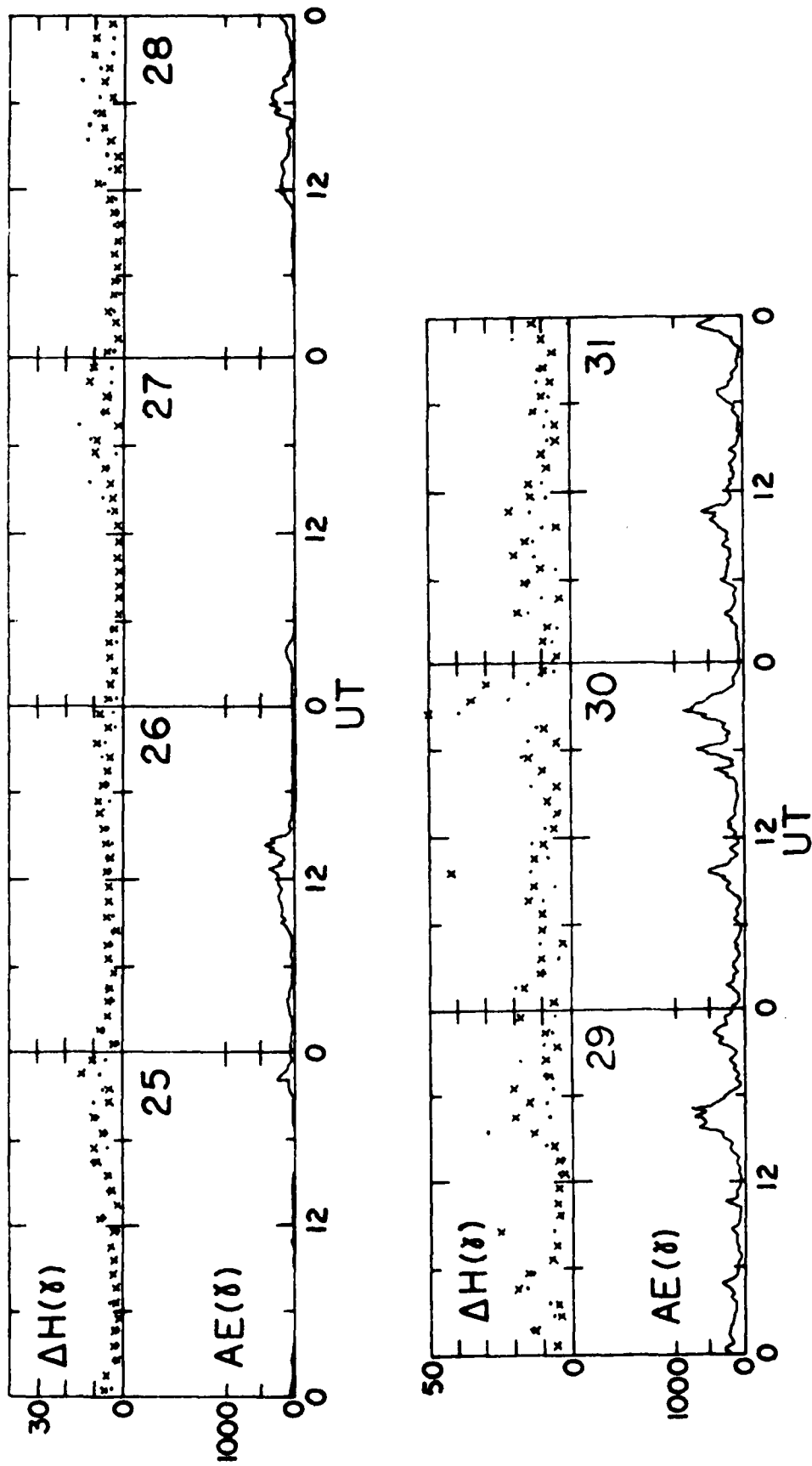


Figure 2.14d. Hourly H component variations at Fredericksburg (dots) and Boulder (crosses) plotted in the top panels; 2.5 minute average AE index in the bottom panels. Time period Dec. 25-31, 1972.

during the latter half of the UT day on December 13, 15-16, 22-23, and 30. Finally, just as our qualitative studies suggested, AE events of lesser magnitude ($<500\gamma$) are not always detectable in the mid latitude day sector. A comparison between data on December 5 and December 18 reveals similar looking mid latitude variations occurring between 12 and 24 UT, in spite of the very dissimilar auroral zone conditions on the two days.

E. Comparison of Short Time Scale AFGL Data with Auroral Zone Magnetograms

AFGL data is now readily accessible in digital form on a two-minute averaged time scale. These data can be used to calculate magnetic variations over any longer time scale desired. Although 1 hour intervals were sufficient for preliminary work with plotted data and normal magnetograms, such a time scale is too coarse to exploit the full potential of good quality AFGL data. To move toward a finer time scale, we show in figures 2.15 a-e the X component variations every 10 minutes during June 2-5, 1978. Except for the finer time scale, variations are calculated in exactly the same way as those appearing in Figures 2.11-2.13. It is interesting to observe the improvement in time resolution if one compares Figures 2.15 a-e with Figures 2.16 and 2.17 a, b which treat the data on June 2-3, 1978, with 1 hour and $\frac{1}{2}$ hour intervals, respectively.

Auroral zone magnetic activity during June 2-3 is shown in Figure 2.18. A provisional AE index gives the maximum value achieved in each hour and is derived from 4 stations, TI, DI, GWR and FC. As seen earlier in this study, agreement between peak hourly AE and hourly mid latitude variations (Figure 2.16) is fairly good. Note the correspondence between peaks in Figures 2.16 and 2.18 near 10, 14 and 19 UT on June 2 and near 00 UT on June 3. A large AE enhancement at 19 UT on June 3 is clearly registered in Figure 2.16 with smaller variations

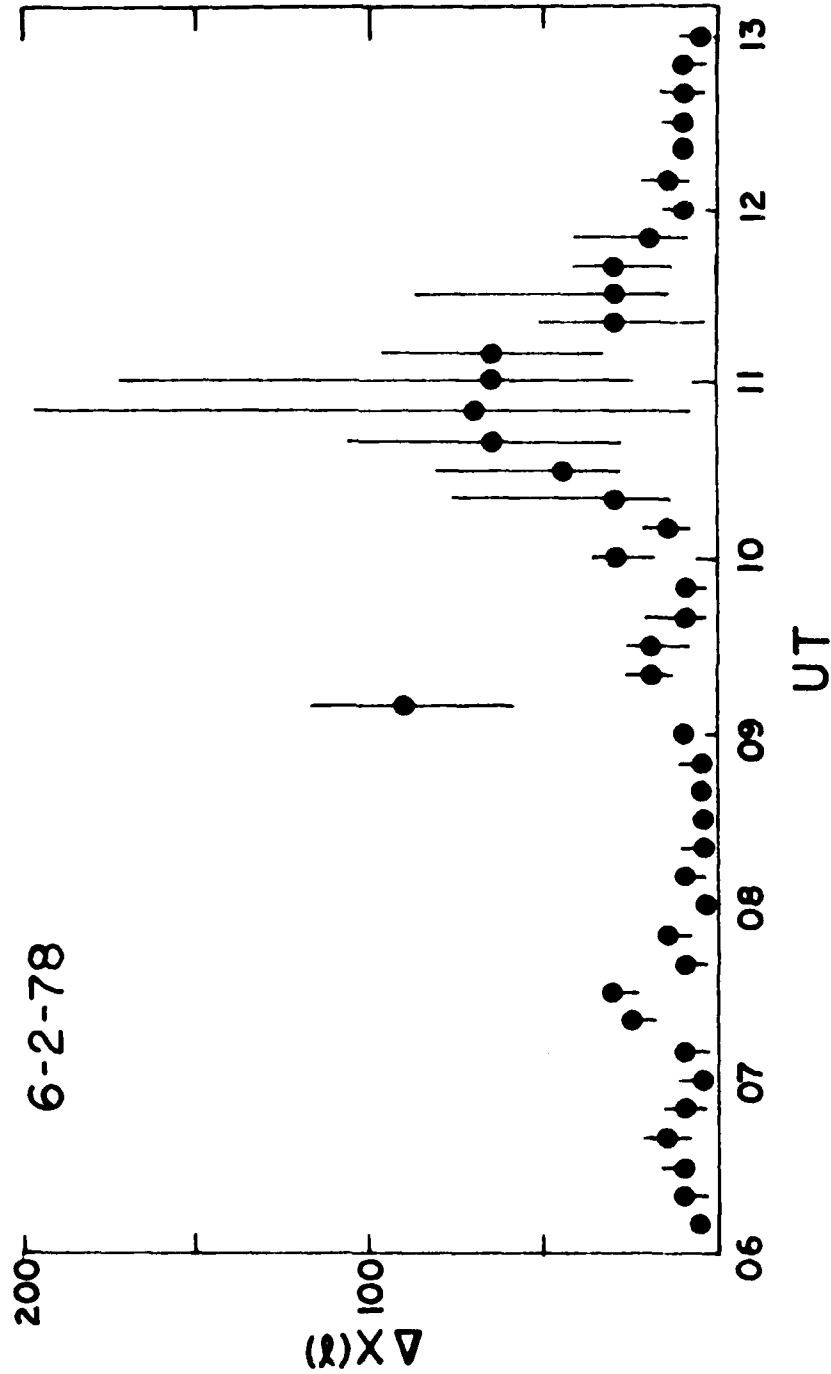


Figure 2.15a Station averaged X component variations (dots) and extreme values (top and bottom of bar) computed every 10 minutes from June 2 (0610 UT) to June 6 (0030 UT), 1978. Average, maximum and minimum ΔX based on 5 values in a 10 minute interval, one (top only) AFGL station (WA, SD, WI, MI, and NA). Same format applies in Figures 2.15 b-e.

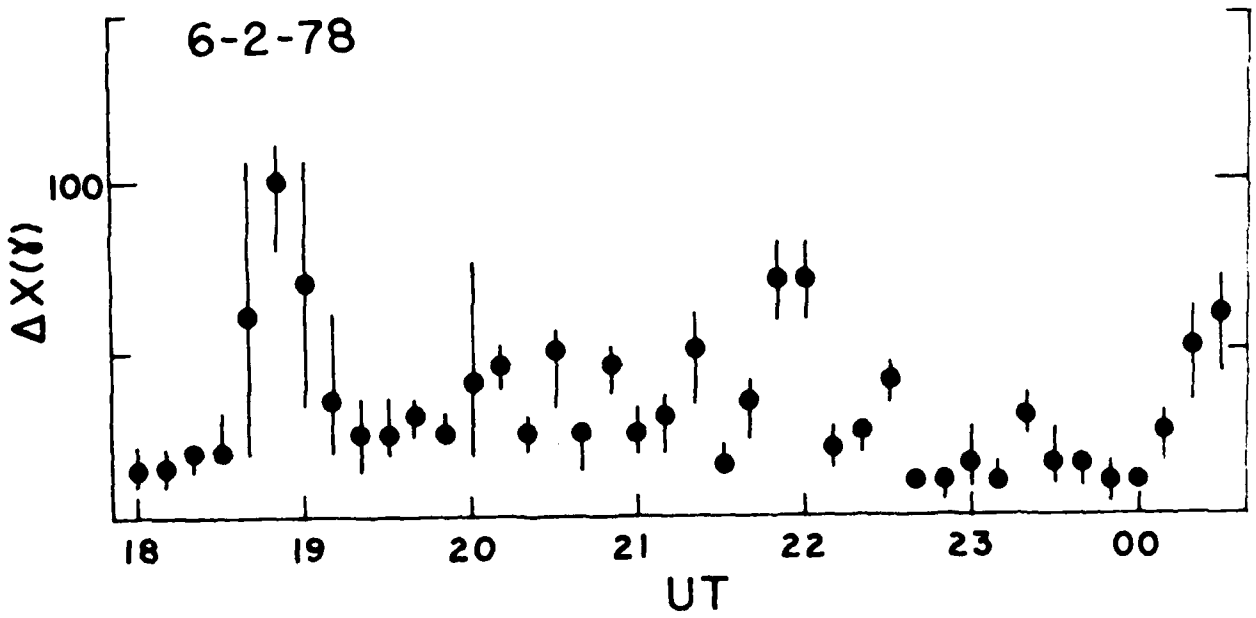
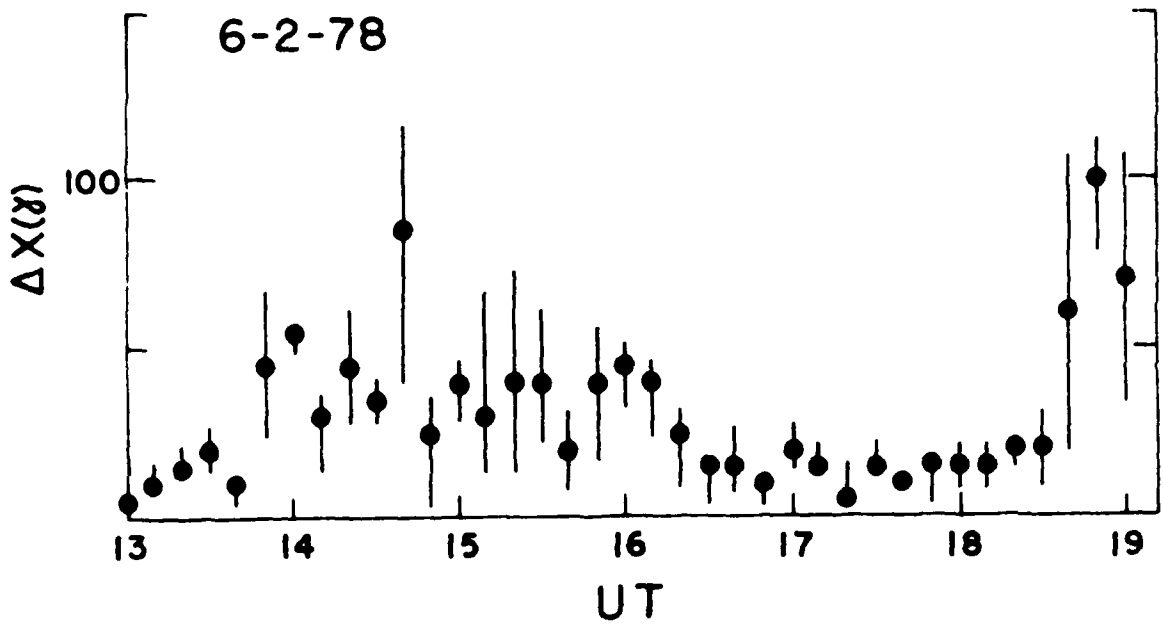


Figure 2.15b

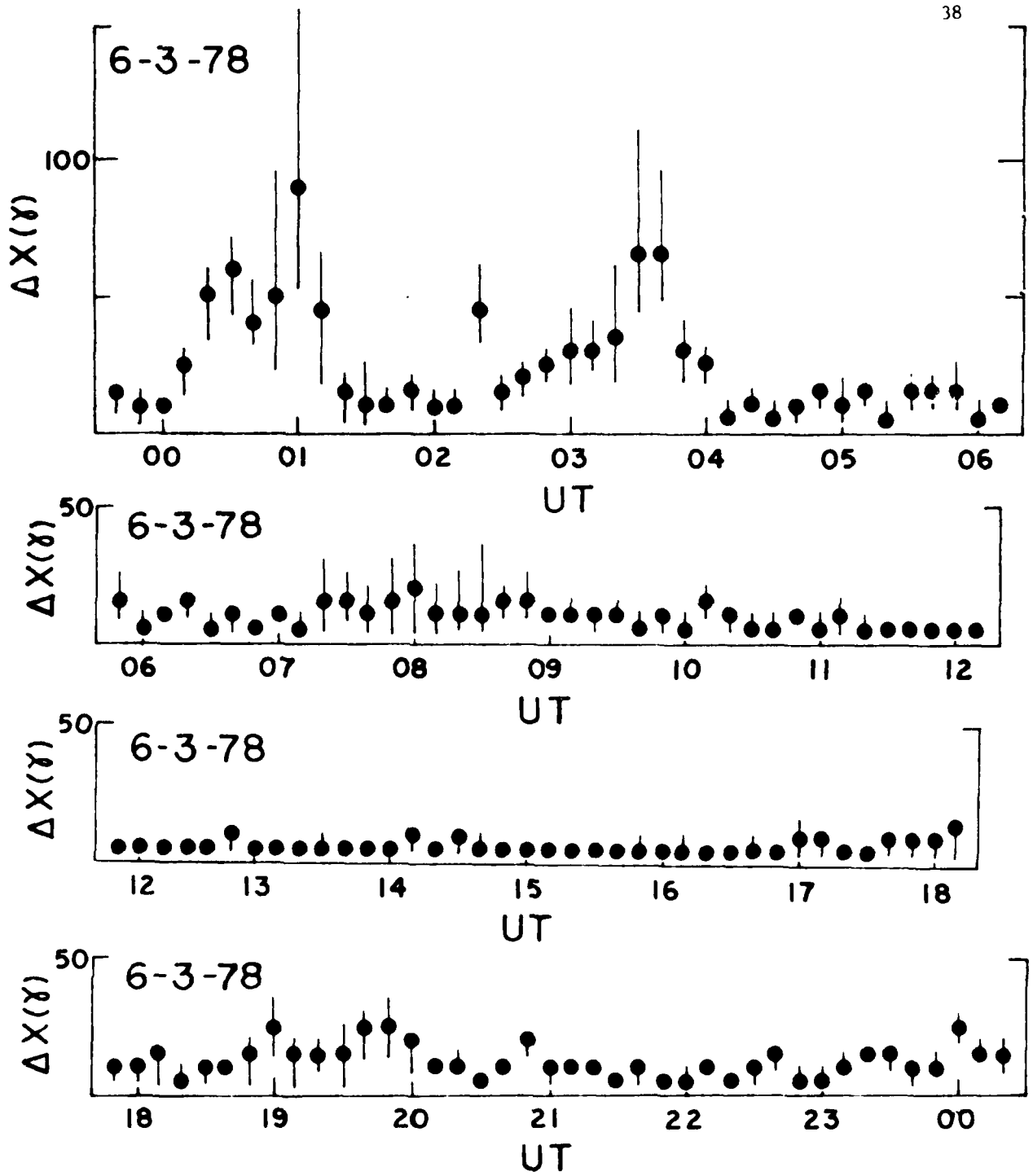


Figure 2.15

[Handwritten signature]

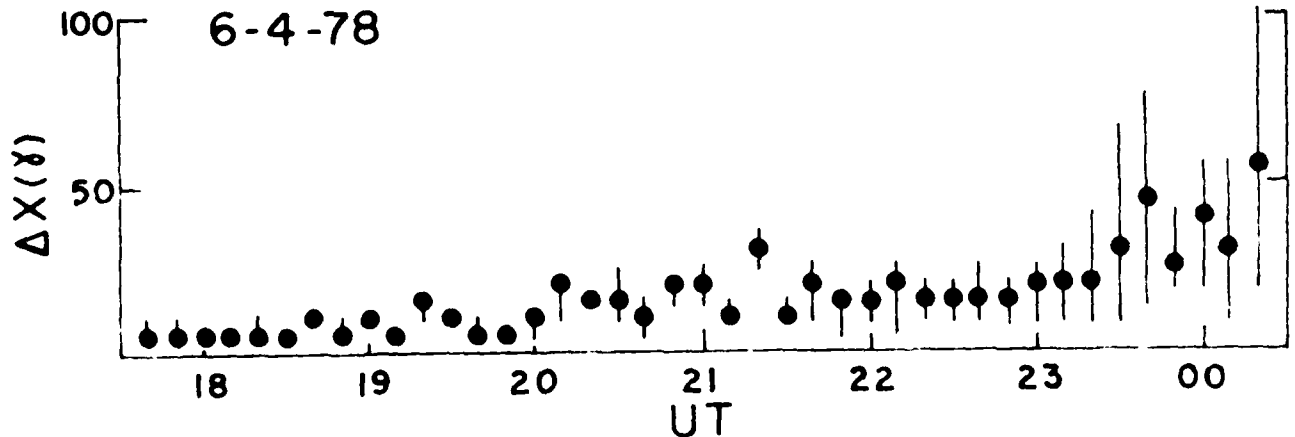
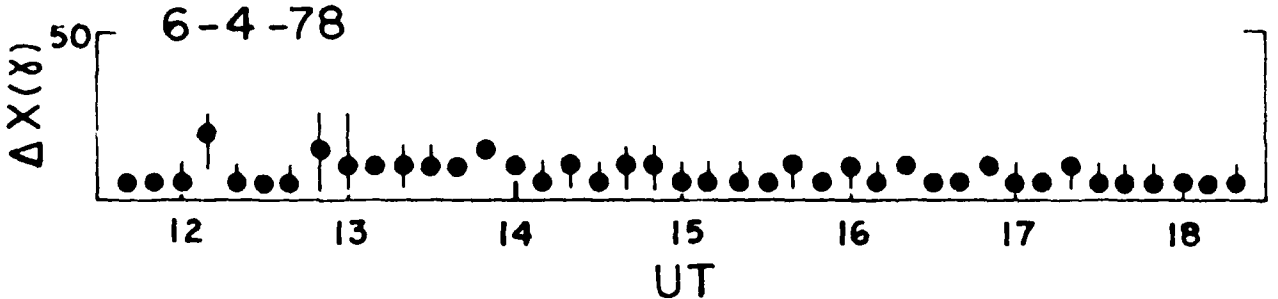
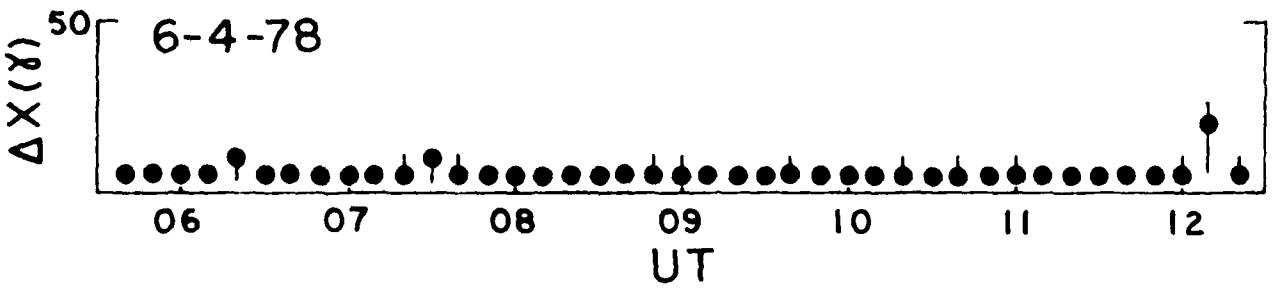
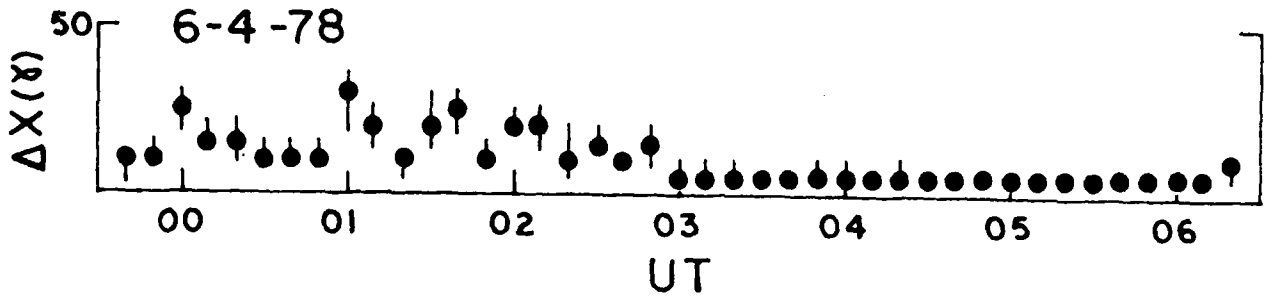


Figure 2.15d

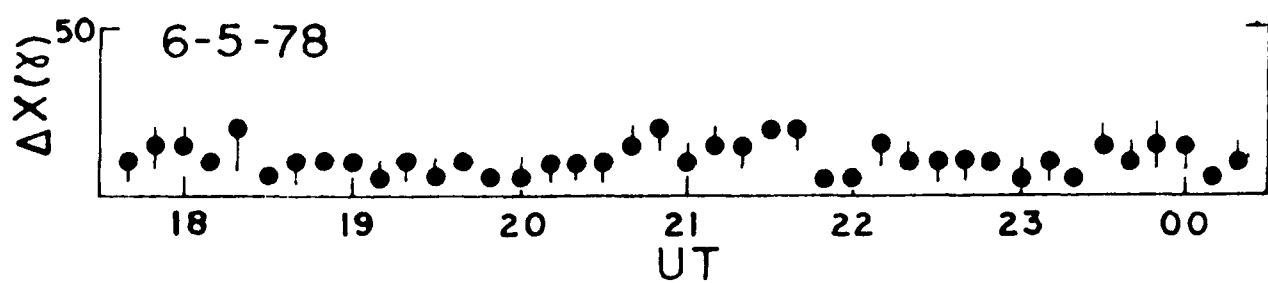
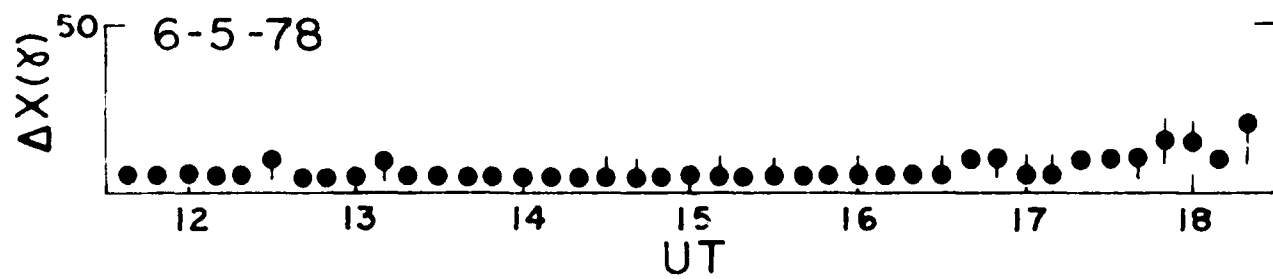
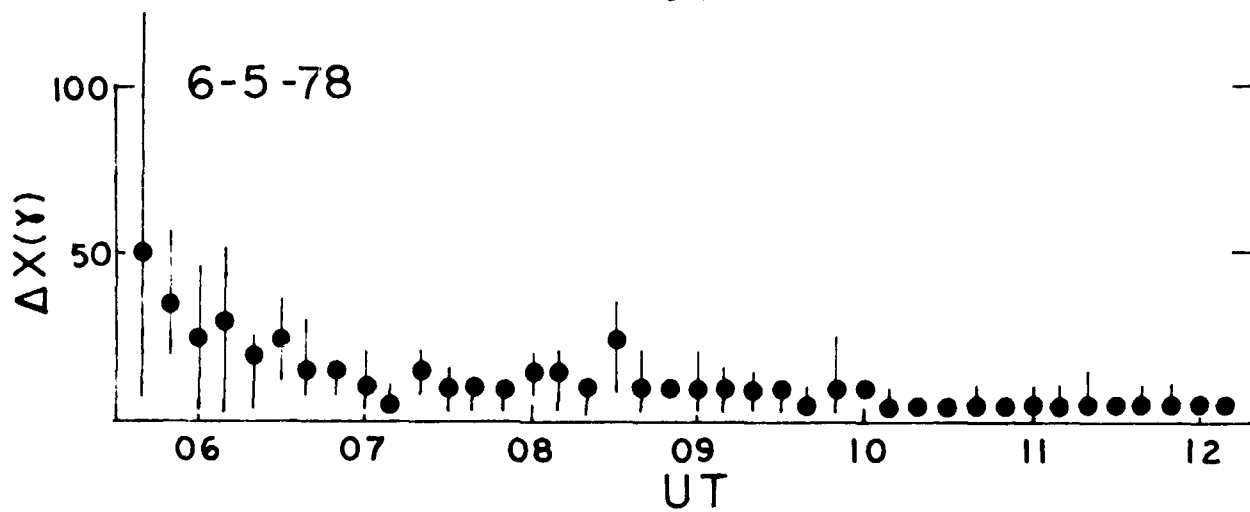
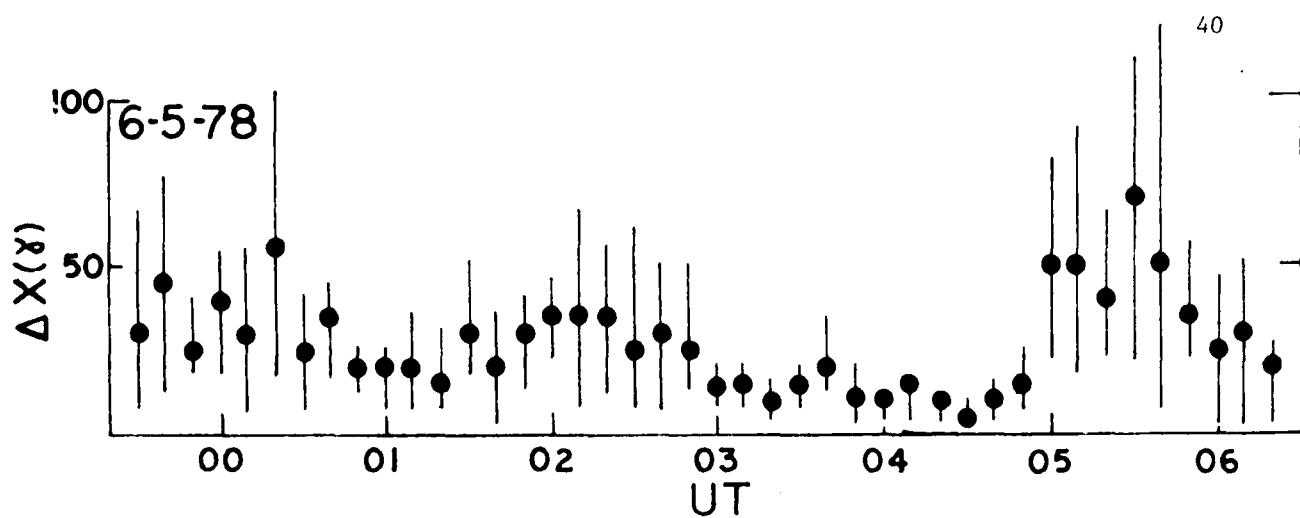


Figure 2.15c

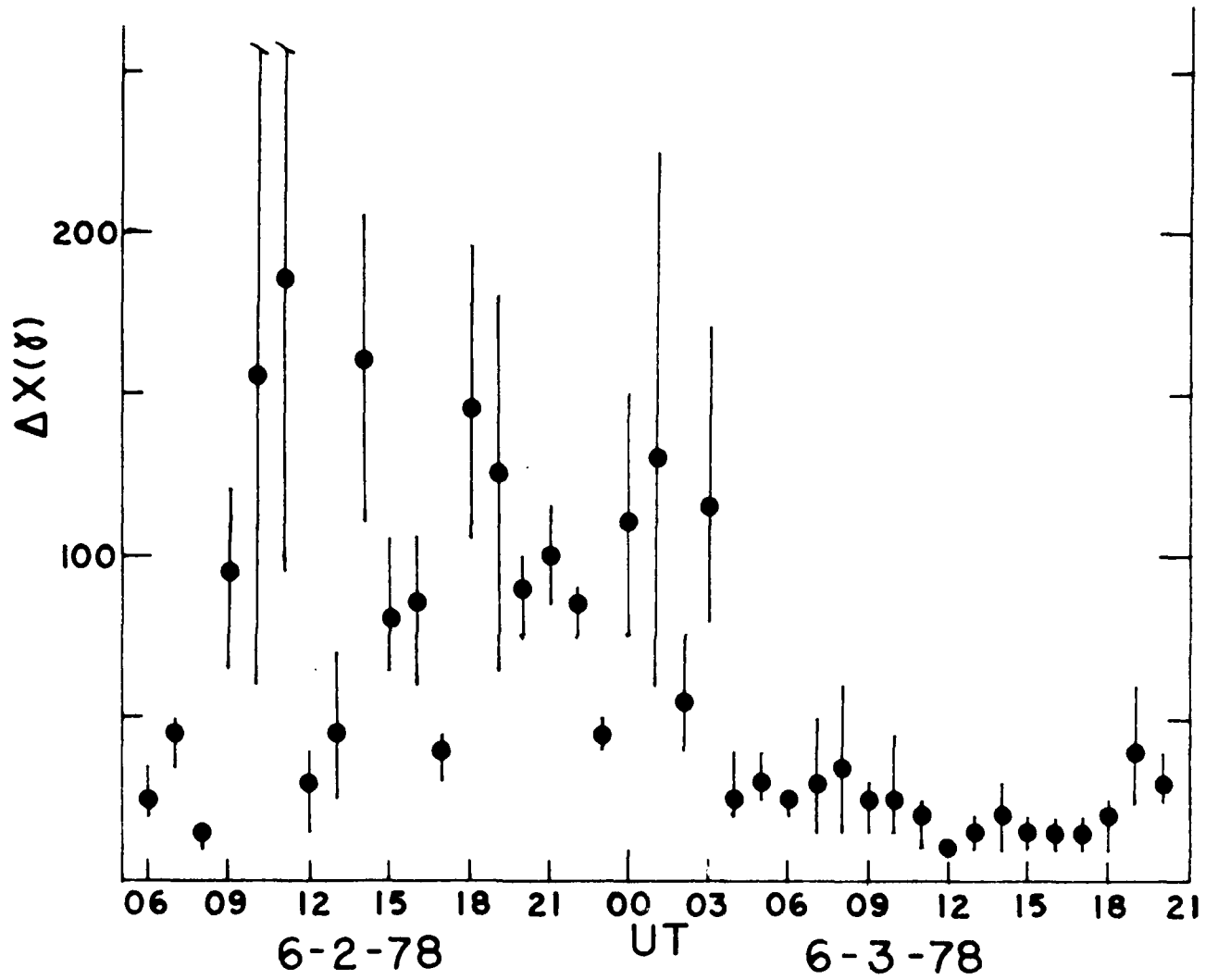


Figure 2.16 Same format as Figure 2.15. 1 hour time intervals (June 2 (0600 UT) - June 3 (2100 UT), 1978).

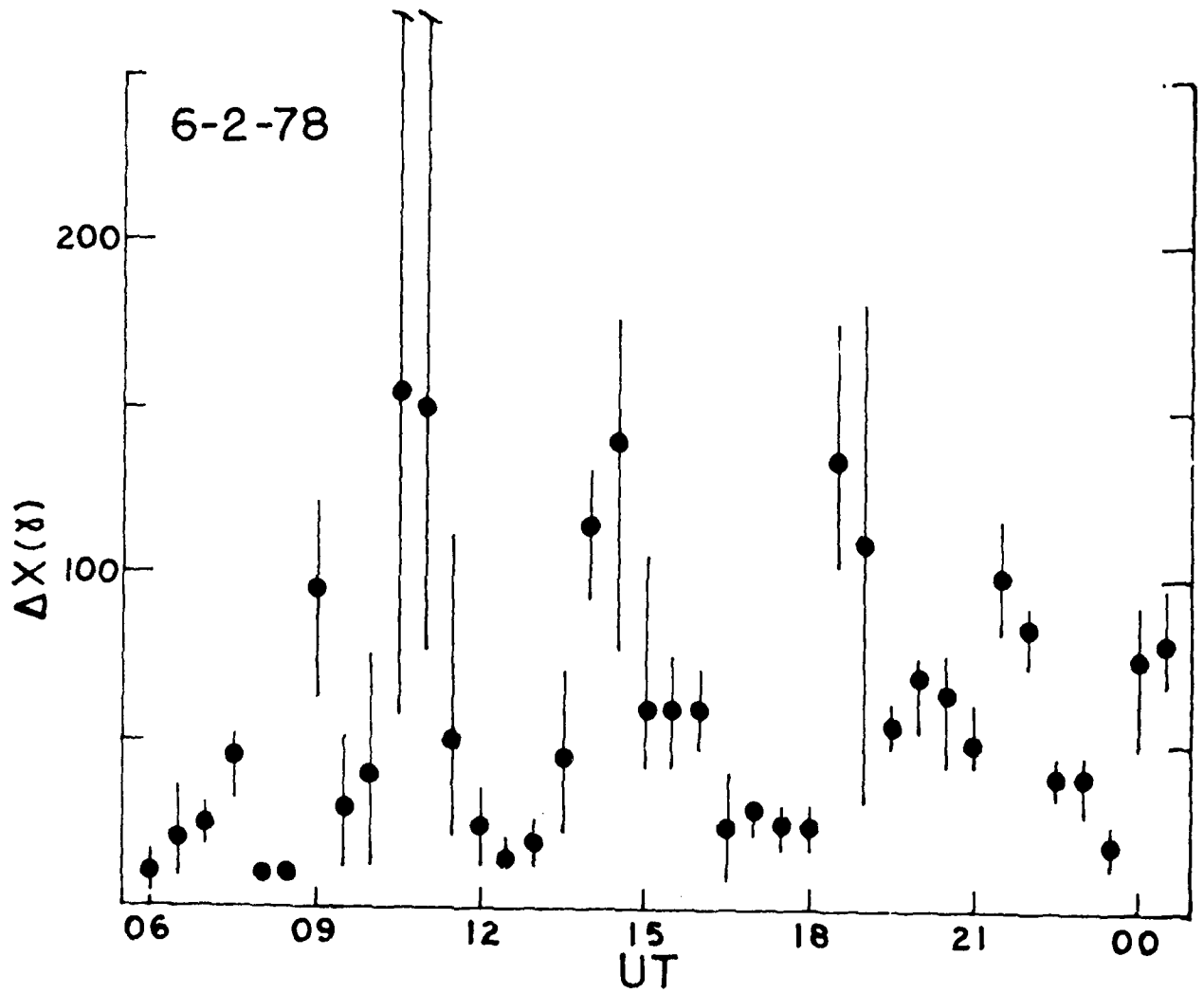


Figure 2.13a Same format as Figure 2.15. 1/2 hour time intervals (June 2 (0600 UT) - June 3 (2100 UT), 1978).

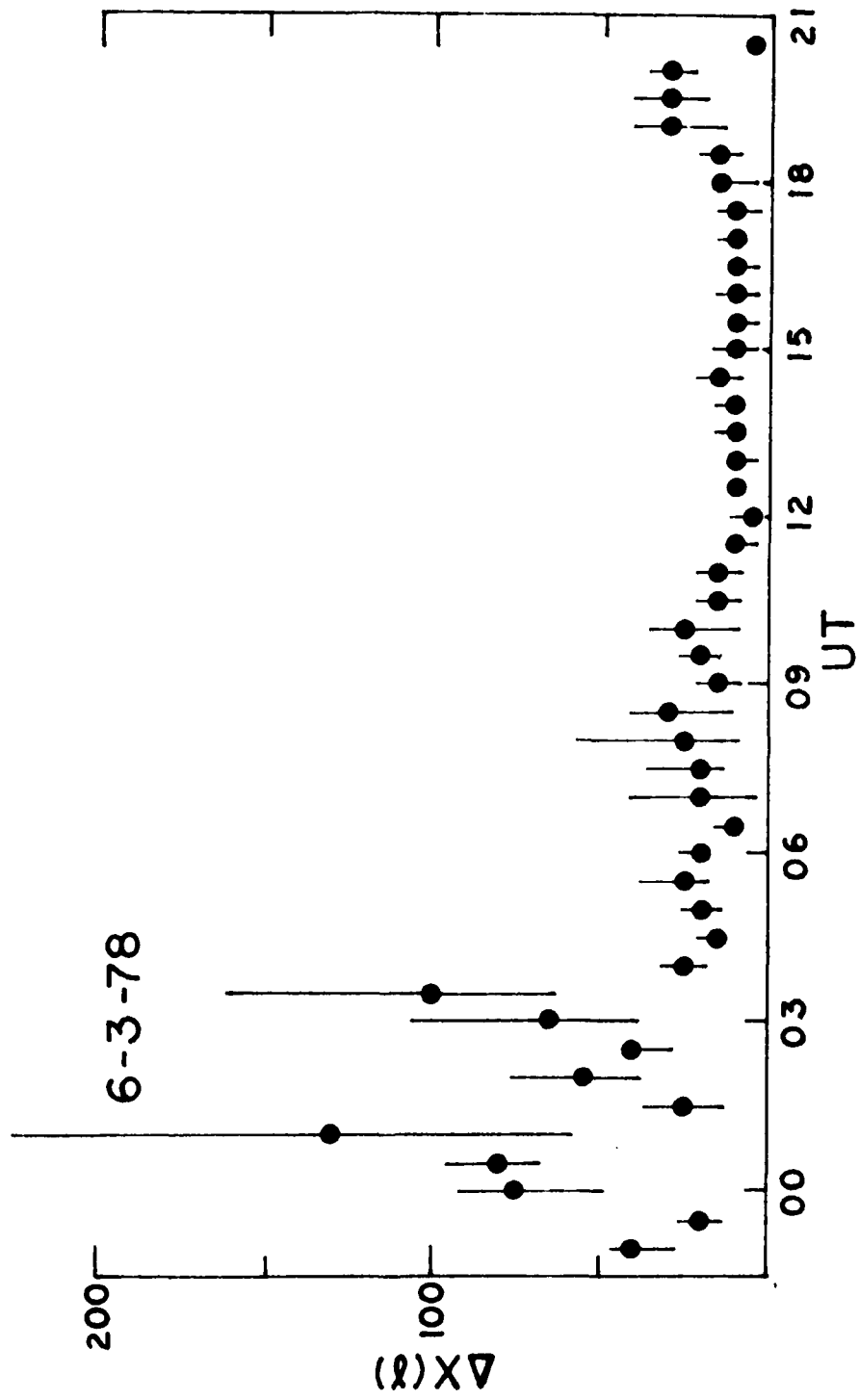


Figure 2.17b Same format as Figure 2.17a.

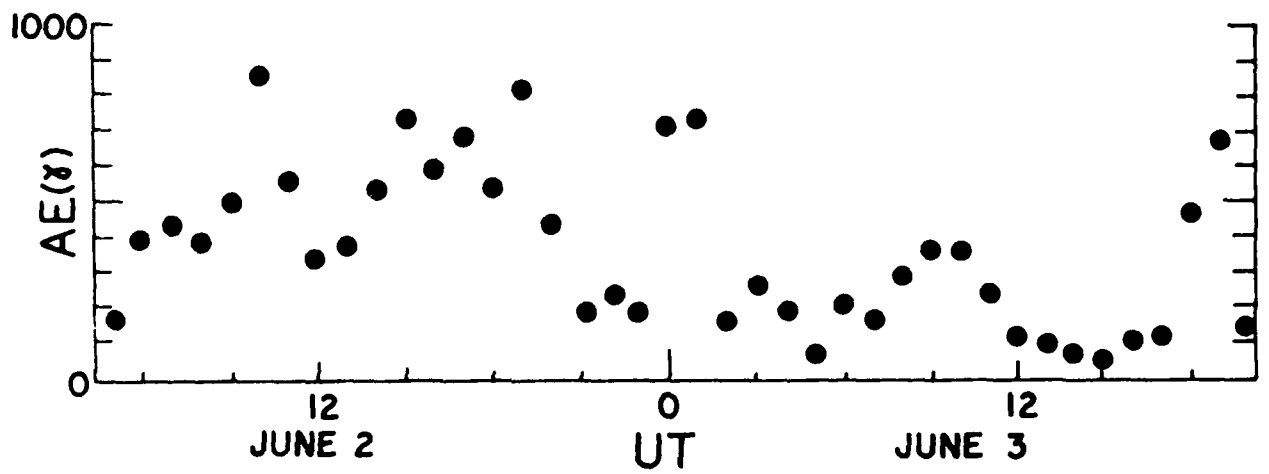


Figure 2.13 Maximum AE achieved in each hour, June 2 (0500 UT) - June 3 (2100 UT), 1978. Four auroral zone stations employed, Tixie, Dixon, Great Whale River, and Fort Churchill.

than one day before.

Two notable cases of improved time resolution are apparent in Figure 2.15 a-e. A 100 γ variation occurring between 09 and 10 UT on June 2 (Figure 2.16) actually commenced sometime between 0910 and 0920 UT in Figure 2.15a. Later in the same day, a large hourly variation between 1800 and 1900 UT did not take place until 1840 UT.

On a 10 minute time scale, it becomes profitable to refer directly to auroral zone magnetograms (Figures 2.19 a-e). Although two stations alone cannot observe everything taking place, TI and GWR are suitably located nearly 12 hours apart in local time and should give at least an indication of major activity. Scanning the AFGL variation data in Figures 2.15 a-e, we see that activity rose on June 2 at 0910, 1000, 1350, and 1840 UT; on June 3, at 00 and 0320 UT; on June 4, at 2230 UT; and on June 5, at 0500 UT. Each of these occasions was accompanied by an identifiable high latitude event ranging in activity from relatively mild (June 3, 00-03 UT) to severe (June 2, 09-21 UT; June 4-5, 20-12 UT) as seen in Figures 2.19 a-e.

Inevitable exceptions in the overall agreement between Figures 2.15 and 2.19 cannot be overlooked. On June 3, at about 0330 UT, the AFGL data was quite disturbed, but there was curiously little activity at GWR and at Fort Churchill, even though both stations were in the evening sector. In fact, there was more activity at TI and DI than in the morning sector. On June 4, beginning at 03 UT, the AFGL data became very quiet while precisely at that time the Canadian stations began to detect negative bays of about 250 γ in the midnight sector.

We have presented examples demonstrating the ability of magnetic variations at mid and subauroral latitudes to indicate the state of auroral zone magnetic activity. Even when observed in a restricted longitude sector of the size spanned

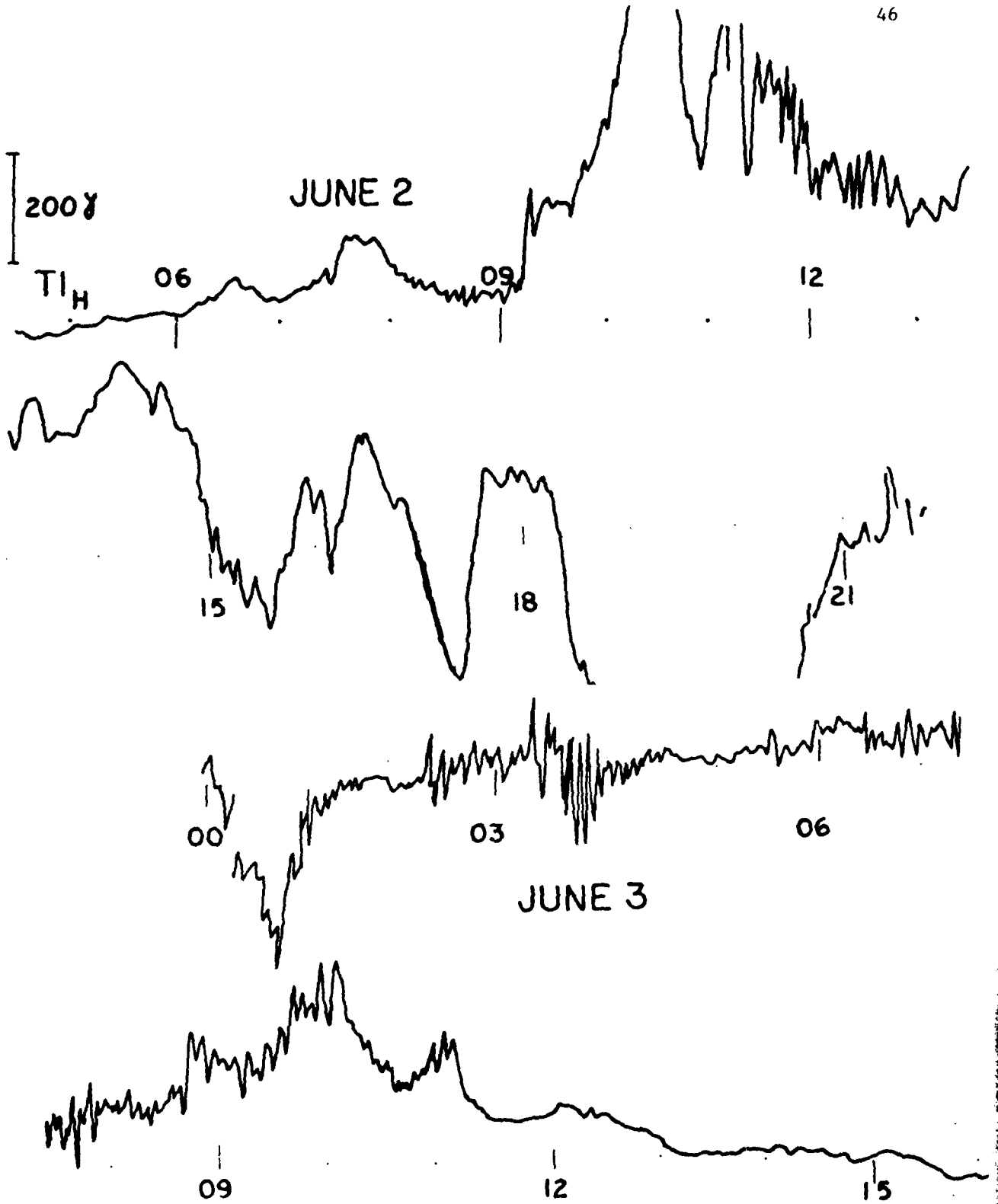


Figure 2.19a H component magnetograms from Tixie Bay on June 2-3, 1978.

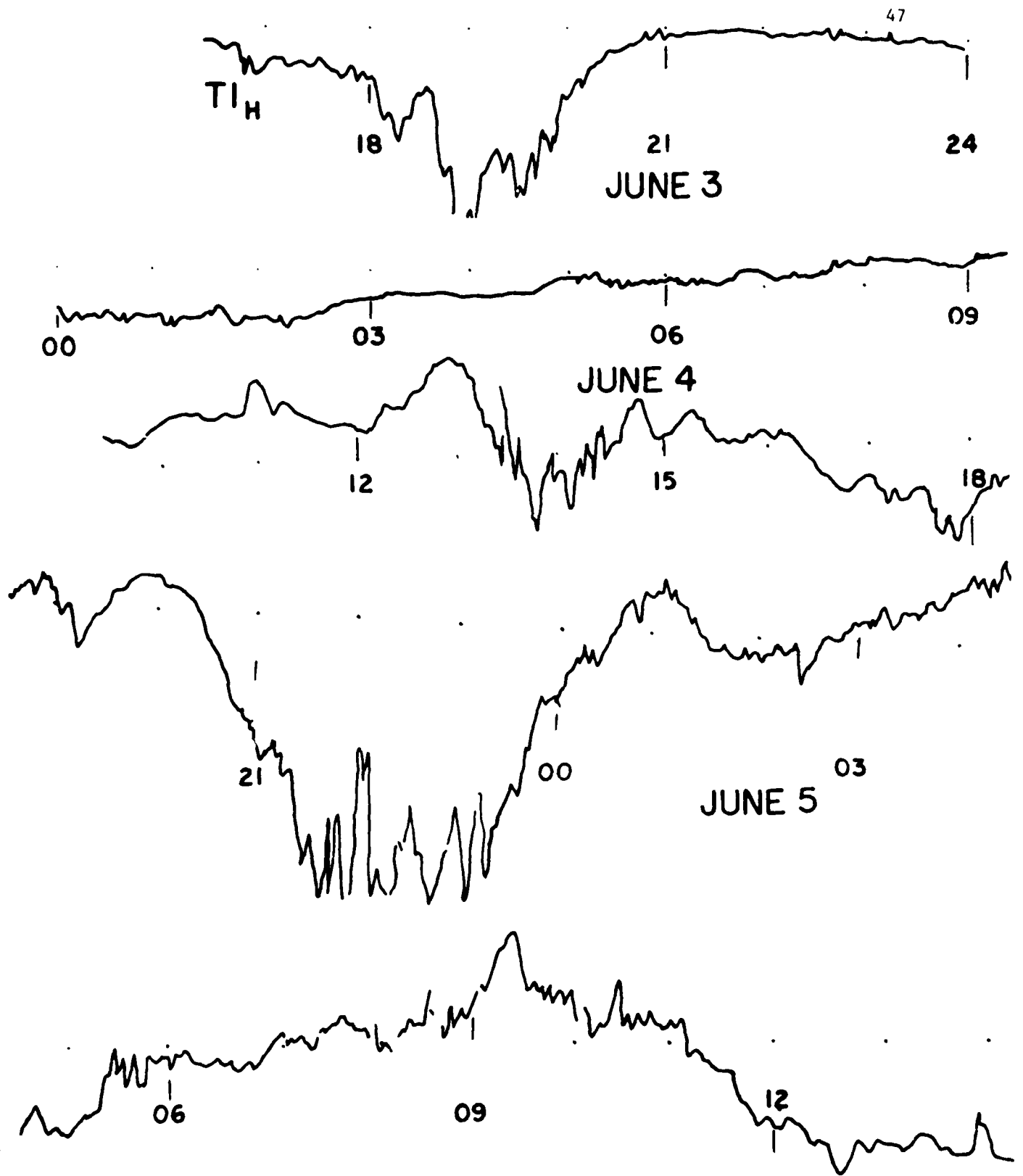


Figure 2.19b H component magnetograms from Tixie Bay on June 3-5, 1978.

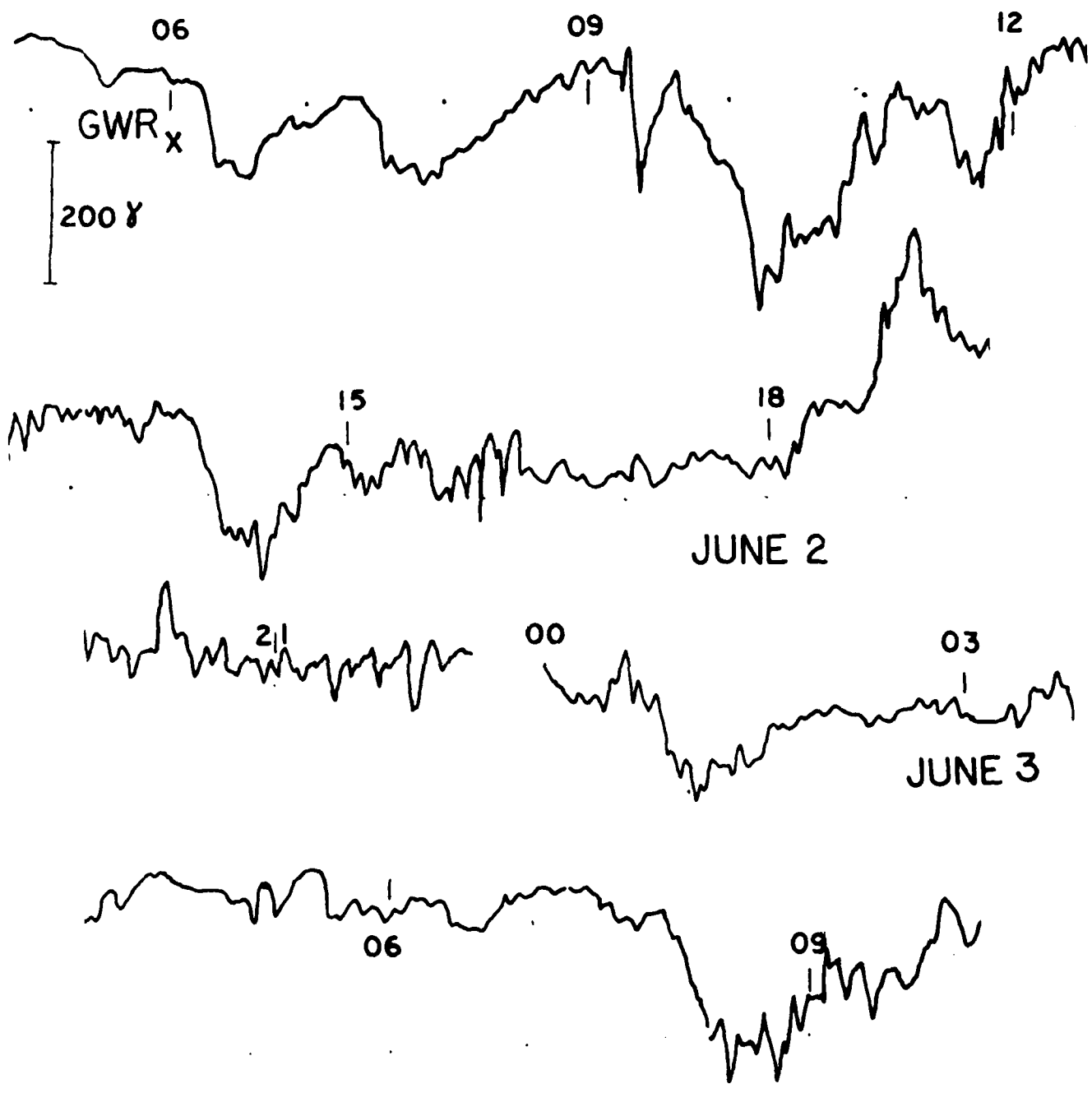


Figure 2.19c. X component magnetograms from Great Whale River on June 2-3, 1978.

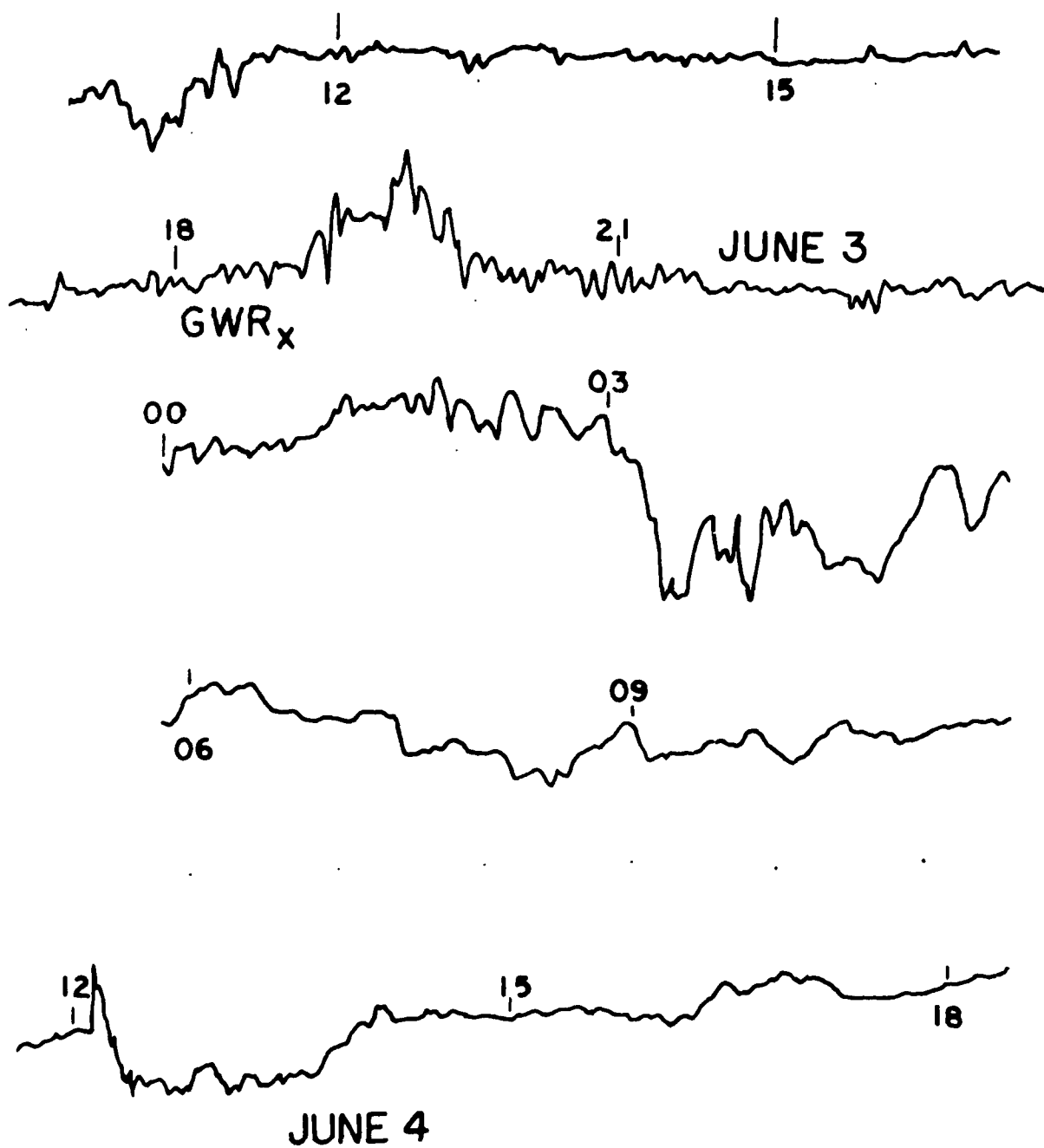


Figure 2.19d X component magnetograms from Great Whale River on June 3-4, 1978.

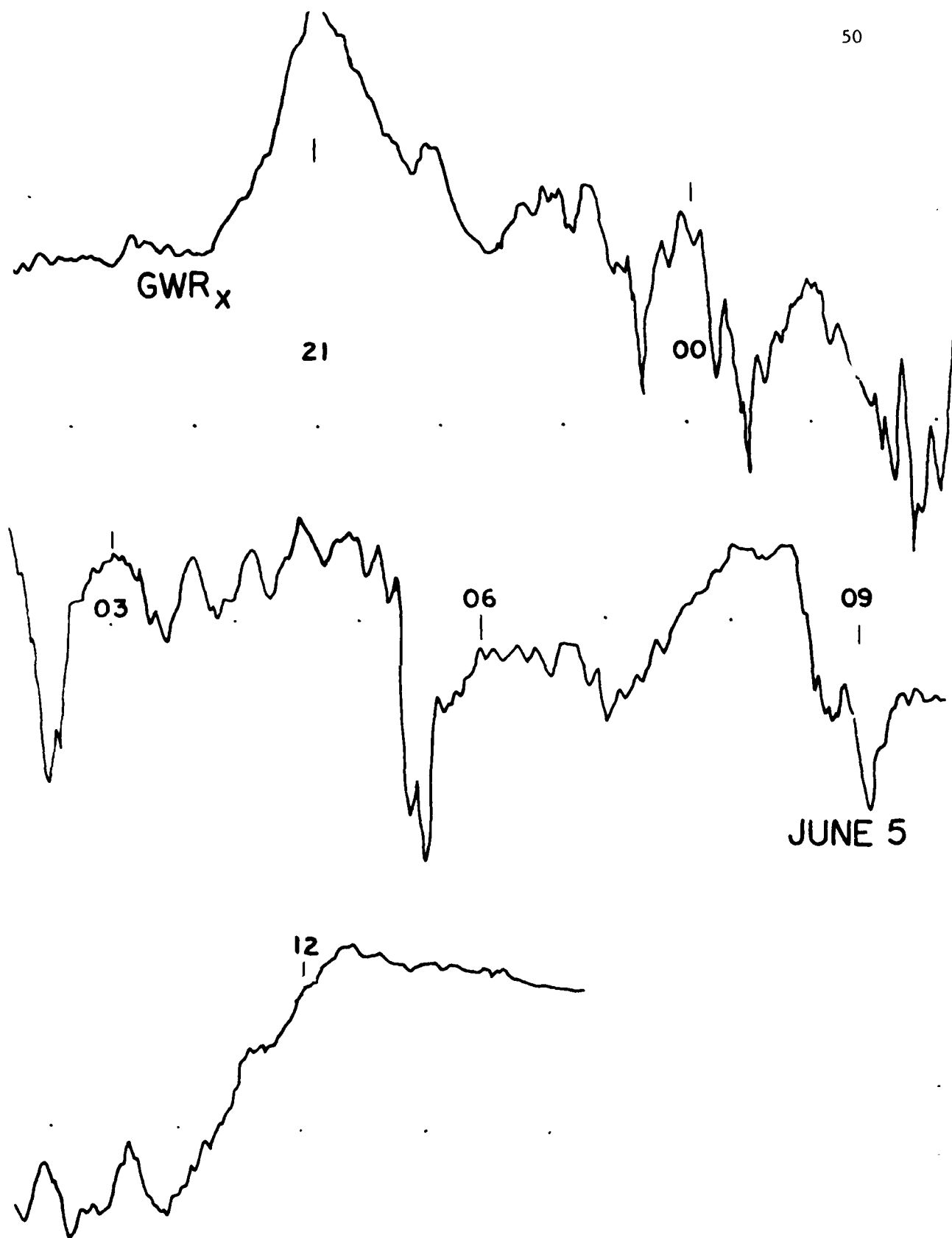


Figure 2.19e X component magnetograms from Great Whale River on June 4-5, 1978.

by the AFGL chain, large substorms with $AE > 400\gamma$ generally produce substantial variations on 1 hour, $\frac{1}{2}$ hour and 10 minute time scales. However, weaker substorms yield less consistent results, ranging from barely detectable to unexpectedly large. Some failures undoubtedly stem from gaps in the AE network or in the particular array of auroral zone stations used to identify substorms. Unless high latitude coverage is extensive, an intense but highly localized disturbance may affect some favorably located stations and give a false impression of activity in the auroral zone, and consequently raise the expectation of mid latitude activity. Insufficient station coverage does not explain satisfactorily the converse problem of large mid latitude magnetic variations but little or no auroral zone activity. In this case, the procedure shows a lack of discrimination between substorm effects and variations coming from other sources. Fortunately, based on the limited number of examples in this study, occurrences of this problem appear to be relatively rare.

F. Summary and Estimate of Reliability

In the preceding sections of this chapter, two related methods for deducing high latitude magnetic activity from mid latitude data were developed and evaluated. The first procedure employs a qualitative 3-level scale of magnetic response which was applied to magnetograms from Fredericksburg and Boulder over a 4 month period. Results from this preliminary study demonstrated that such a scheme, although quite unsophisticated, can detect most substorm activity producing AE enhancements above 400γ if the mid latitude stations are in the night sector, or above 600γ if the stations are in the day sector.

The second method involves net excursions of the magnetic X component recorded at AFGL stations. Figure 2.20 illustrates the procedure with data from the Wisconsin station taken over two 8-hour intervals in December, 1976; boxes delineating hourly excursions are transferred to the ΔX plot directly below. ΔX plots from the other AFGL stations also can be constructed, so that in each time interval

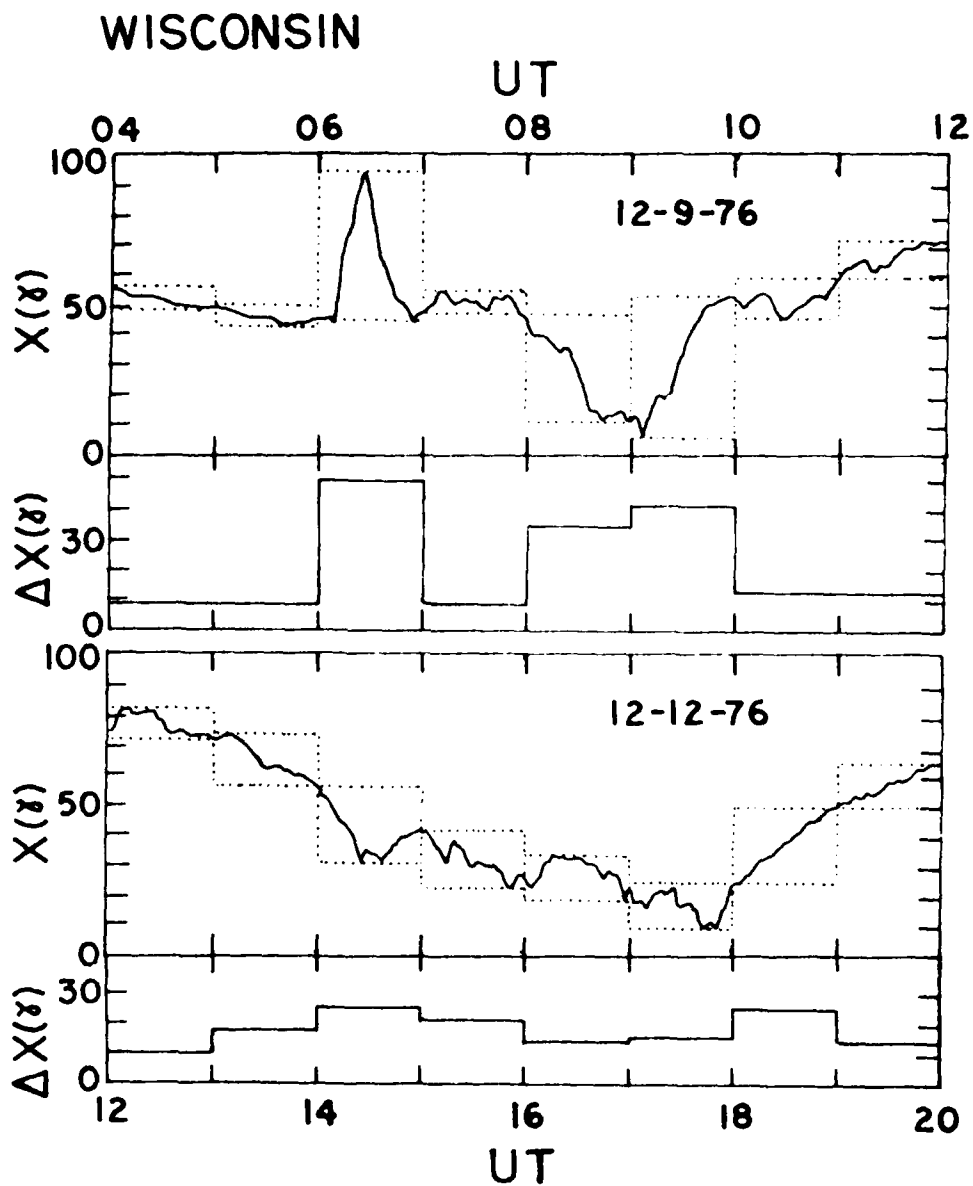


Figure 7.20 Example showing the calculation of ΔX at a chain station. X component magnetograms at Wisconsin (WI) on December 9 and 12, 1976 appear in the top panels. Variations over 1 hour time interval, indicated by dotted boxes in magnetograms, plotted in bottom panels.

up to five basic measurements (ΔX_{MA} , ΔX_{MI} , ΔX_{WI} , ΔX_{SD} , and ΔX_{WA}) can be computed, depending on data availability. From these quantities average ΔX , maximum ΔX , and minimum ΔX (ΔX_{ave} , ΔX_{max} , ΔX_{min}) can be determined easily and plotted, as in Figures 2.15 - 2.17 (Section E). Treating in this manner the limited amount of AFGL data available to us at the time of this study, it was found that 10 minute time intervals yield appreciable values of ΔX_{ave} on the order of 10γ or more when AE exceeds 400γ . This performance holds at all local times.

Although not used explicitly in our analysis, the extreme values of ΔX (ΔX_{max} and ΔX_{min}) indicate the uniformity of disturbance across the chain sector, and also provide some protection against bad data from a single station. For example, a situation where $\Delta X_{MA} = 10\gamma$, $\Delta X_{MI} = 20\gamma$, $\Delta X_{WI} = 30\gamma$, $\Delta X_{SD} = 40\gamma$, and $\Delta X_{WA} = 50\gamma$ yields $\Delta X_{ave} = 30\gamma$, $\Delta X_{min} = 10\gamma$, and $\Delta X_{max} = 50\gamma$. If a bad value from WA makes $\Delta X_{WA} = 500\gamma$, instead of 50γ , then $\Delta X_{ave} = 120\gamma$, $\Delta X_{min} = 10\gamma$, and $\Delta X_{max} = 500\gamma$. The high value of ΔX_{ave} , 120γ , may not be unusual, but the large difference between $\Delta X_{ave} - \Delta X_{min}$ and $\Delta X_{max} - \Delta X_{ave}$, 110γ vs. 480γ , would warn that a station value might be in error.

Although there are not enough examples to determine the statistical reliability of the quantitative procedure outlined above, data from the AFGL chain should equal, if not exceed, the performance indicated by data from Fredericksburg and Boulder (Figures 2.10 and 2.14 a-d). At 55° CGL, the AFGL chain is closer to substorm current systems than FB and BD and spans an additional 1.5 hours in local time. Both factors make it reasonable to expect AFGL chain data to be even more sensitive and reliable than the FB and BD results. More extensive investigations with chain data are needed to assess seasonal effects and wider ranges of magnetic activity. As experience is gained, the procedure can be modified, such as by including the Y component, varying the time interval, or utilizing the sign of the excursion.

Table 2.2 summarizes the procedure and lists some of its advantages and disadvantages. Sensitivity and reliability estimates are based on qualitative and

and quantitative results gathered from FB and BD. Examples from the AFGL chain in December, 1976 and June, 1978 are consistent with these estimates.

- Procedure:
1. Choose time interval (e.g., 1 hour, $\frac{1}{2}$ hour, 10 minutes)
 2. Determine X component excursion during time interval (e.g., $\Delta X_{MA} = X_{max} - X_{min}$), where X_{max} and X_{min} are the maximum and minimum values attained (may occur at beginning or end points of interval, c.f., Figure 2.20).
 3. Calculate ΔX_{ave} (average of ΔX from stations reporting during the interval).
 4. Plot X_{ave} against time. Range of ΔX given by ΔX_{max} and ΔX_{min} from stations reporting during each interval (c.f., Figures 2.15 a-e, 10 minute intervals).

Interpretation: AFGL chain (55° CGL), Sections D and E
 $\Delta X_{ave} > 10\gamma$ (10 minute interval) generally implies
 $AE > 400\gamma$ (c.f., Figures 2.15 a-e, Figure 2.16).

FB and BD (50° CGL), Sections B and C

<u>Local time</u>	<u>Peak AE</u>	<u>Strong responses</u>
night	$> 200\gamma$ $> 600\gamma$	$\approx 50\%$ $\approx 100\%$
day	$> 400\gamma$ $> 600\gamma$	$\approx 50\%$ 70-80%

Advantages

1. Simplicity
2. Can be applied when one or more stations are missing
3. Sensitive to AE disturbances related to substorms
4. Simple local time dependence

Disadvantages

1. Gives only an approximation of AE strength
2. Detection delayed by the time interval employed.

Table 2.2 Summary of procedures and interpretations discussed in Chapter 2.

References

- Akasofu, S.-I., and C.-I. Meng, A study of polar magnetic substorms, J. Geophys. Res., 74, 293, 1969.
- Allen, J.H., and H.W. Kroehl, Spatial and temporal distributions of magnetic effects of auroral electrojets as derived from AE indices, J. Geophys. Res., 80, 3667, 1975.
- Caan, M.N., R.L. McPherron and C.T. Russell, The statistical magnetic signature of magnetospheric substorms, Planet. Space Sci. 26, 269, 1978.
- Clauer, C.R., and R.L. McPherron, Mapping the local time-universal time development of magnetospheric substorms using mid-latitude magnetic observations, J. Geophys. Res., 79, 2811, 1974.
- Crooker, Nancy Uss, and R.L. McPherron, On the distinction between the auroral electrojet and partial ring current systems, J. Geophys. Res., 77, 6886, 1972.
- Cummings, W.D., Asymmetric ring currents and the low altitude disturbance daily variation, J. Geophys. Res., 71, 4495, 1966.
- Davis, T.N., and M. Sugiura, Auroral electrojet activity index AE and its universal time variations, J. Geophys. Res., 71, 785, 1966.
- Eather, R.H., S.B. Mende, and E.J. Weber, Dayside aurora and relevance to substorm current systems and dayside merging, J. Geophys. Res., 84, 3339, 1979.
- Fukunishi, N., and Y. Kamide, Partial ring current models for worldwide geomagnetic disturbances, Rev. Geophys. Space Phys., 11, 795, 1973.
- Gizler, V.A., B.M. Kuznetsov, V.A. Sergeev, and O.A. Troshichev, The sources of the polar cap and low latitude bay-like disturbances during substorms, Planet. Space Sci., 24, 1133, 1976.
- Hughes, T.J., and Gordon Rostoker, Current flow in the magnetosphere and ionosphere during periods of moderate activity, J. Geophys. Res., 82, 2271, 1977.
- Iijima and Potemra, Large scale characteristics of field-aligned currents associated with substorms, J. Geophys. Res., 83, 599, 1978.
- Kamide, Y., S.-I. Akasofu, and E.P. Rieger, Coexistence of two substorms in the midnight sector, J. Geophys. Res., 82, 1620, 1977.
- Kamide, Y., S. Matsushita, Simulation studies of ionospheric electric fields and currents in relation to field aligned currents, 2. Substorms, J. Geophys. Res., 84, 4099, 1979.
- Kokubun, Susumu, and Takesi Iijima, Time sequence of polar magnetic substorms, Planet. Space Sci., 23, 1483, 1975.
- Kokubun, S., R.L. McPherron, and C.T. Russell, Triggering of substorms by solar wind discontinuities, J. Geophys. Res., 82, 74, 1977.

- Linclon, J. Virginia, Geomagnetic Indices, in Physics of Geomagnetic Phenomena, Vol I, p. 67, S. Matsushita and Wallace H. Campbell, ed., Academic Press, New York, 1967.
- Mayaud, P.N., Atlas of K indices (1. Text and 2. Figures), IAGA Bulletin No. 21, IUGG Publication Office, Paris, 1967.
- McPherron, R.L., Satellite studies of magnetospheric substorms on August 15, 1968, 1. State of the magnetosphere, J. Geophys. Res., 78, 3044, 1973.
- McPherron, R.L., C.T. Russell, and M.P. Aubry, Satellite studies of magnetospheric substorms on August 15, 1978, 9. phenomenological model for substorms, J. Geophys. Res., 78, 3131, 1973.
- Nisbet, J. S., M.J. Miller, and L.A. Carpenter, Currents and electric fields in the ionosphere due to field aligned currents, J. Geophys. Res., 83, 2647, 1978.
- Nopper, R.W., and R.L. Carovillano, Polar equatorial coupling during magnetically active periods, Geophys. Res. Lett., 5, 699, 1978.
- Park, C.G., and C.-I. Meng, Distortions of the nightside ionosphere during magnetospheric substorms, J. Geophys. Res., 78, 3828, 1973.
- Pytte, T., R.L. McPherron, and S. Kokubun, The ground signatures of the expansion phase during multiple onset substorms, Planet. Space Sci., 24, 1115, 1976.
- Pytte, T., R.L. McPherron, E.W. Hones, and H.I. West, Multiple satellite studies of magnetospheric substorms: distinction between polar magnetic substorms and convection driven negative bays, J. Geophys. Res., 83, 663, 1978.
- Rostoker, Gordon, Mid latitude transition bays and their relation to the spatial movement of overhead currents, J. Geophys. Res., 71, 79, 1966.
- Rostoker, G., Geomagnetic Indices, Rev. Geophys. Space Phys., 10, 935, 1972.
- Rostoker, Gordon, Current flow in the magnetosphere during magnetospheric substorms, J. Geophys. Res., 79, 1994, 1974.
- Saito, T., K. Yumoto, and Y. Koyama, Magnetic pulsation P12 as a sensitive indicator of magnetospheric substorm, Planet. Space Sci., 24, 1025, 1976.
- Wang, C.S., T. Lee, and J.S. Kim, Substorm associated long period hydromagnetic waves, J. Geophys. Res., 82, 2867, 1977.
- Yashuhara, F., Y. Kamide, and S.-I. Akasofu, A modeling of the magnetospheric substorm, Planet. Space Sci., 23, 575, 1975.
- Yashuhara, F., Y. Kamide, and S.-I. Akasofu, Field aligned and ionospheric currents, Planet. Space Sci., 23, 1355, 1975.

3. MICROPULSATIONS AS INDICATORS OF GEOMAGNETIC ACTIVITY

A. Introduction

The question of correlation between geomagnetic activity and micropulsations (ultra-low-frequency oscillations in the geomagnetic field) is an intriguing problem in magnetospheric physics. It is generally accepted that geomagnetic activity is driven by the solar wind (cf., Burch, 1974; Crooker, 1975; and reviews therein, for background). In addition, micropulsation occurrence correlates reasonably well with solar wind parameters (cf., Raspopov and Lanzerotti, 1976; Lanzerotti and Fukunishi, 1974 for theoretical background; and Troitskaya, 1967; Saito, 1969; Jacobs, 1970; and Orr, 1973; for observational information). Thus, since both geomagnetic activity and micropulsations are strongly related to the solar wind and correlate well with many of its parameters, it follows that the two phenomena should correlate with each other. As will be shown later, reasonably good correlation between micropulsation activity and geomagnetic activity has been found in a number of studies.

In this summary, we will first review the background literature on (i) correlations between solar wind parameters and continuous dayside micropulsations; (ii) relationships between the solar wind and geomagnetic activity; and (iii) the relation between micropulsations and geomagnetic activity. Then we will discuss three recent sets of observations which lend strong support to the relationships suggested earlier in the literature. Finally, we will suggest ways in which the data from the AFGL magnetometer network may be used to formulate a micropulsation index which would reflect the state of magnetospheric activity.

Correlative studies have shown strong relationships between continuous micropulsations and solar wind parameters. These include solar wind velocity (Troitskaya, 1967), magnitude of the IMF (Gul'yel'mi and Bol'shakova, 1973), and the angle between the IMF and the sun-earth line (Plyasova-Bakunina, 1972).

The work by Plyasova-Bakunina is in agreement with external wave generation at the bow shock, as predicted by Greenstadt's mechanism; the correlation is shown in Figure 3.1. Note that Plyasova-Bakunina shows a high occurrence frequency of Pc 2-4 when the projection of the angle between the IMF and the sun-earth line is small. This correlation was supported by the observations of Greenstadt and Olson (1976) using the amplitudes of Pc 3-4 measured at Calgary ($L = 3.6$) and the angle between the IMF and the sun-earth line.

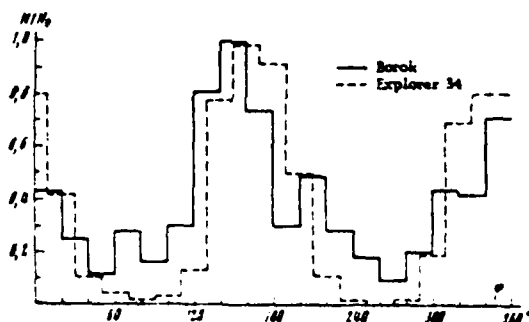


Figure 3.1. From Plyasova-Bakunina (1972): Occurrence frequency of pulsations for intervals of angle γ measured in the solar wind at Imp 3,4. γ is the projection onto the ecliptic plane of the angle between the IMF and sun-earth line.

B. General Background

i) The Solar Wind and Micropulsations. It was originally suggested by Dungey (1954) that micropulsations are the result of hydromagnetic oscillations of the earth's geomagnetic field in the magnetosphere. Following that work, micropulsation theory developed around the ideas of field line resonance and resonance of the magnetospheric cavity. Observations from latitudinal chains of magnetic observatories stimulated the extension of those resonance theories to coupled waves to take account of non-uniformities in the plasma and field distributions, and to account for latitude localization of micropulsation activity (Radoski, 1974; Southwood, 1974; Lanzerotti et al., 1974; Chen and Hasegawa, 1974a,b). Subsequent observations supported the theory that Pc 3-5 micropulsations are the result of excitation of resonant field lines inside the magnetosphere by oscillations at the magnetopause (Arthur et al., 1977; Hughes et al., 1977).

If micropulsations are generated by oscillations on the magnetopause, what is the original driving force? Two mechanisms have been proposed for this driving force. The first is the Kelvin-Helmholtz instability generated at the magnetopause by the flow of magnetosheath plasma along the flanks of the magnetosphere (Southwood, 1968). Under the Kelvin-Helmholtz mechanism, waves would be generated given a high solar wind speed and large angle between the magnetosheath flow direction and the magnetic field directions on either side of the magnetopause. The second magnetopause wave generation mechanism is the direct transmission of waves through the magnetosheath from the bow shock (Greenstadt, 1972). Under this mechanism, waves would be generated preferentially for small angles between the sun-earth line and the direction of the solar wind magnetic field.

ii) The Solar Wind and Geomagnetic Activity. It is generally accepted that geomagnetic activity is driven by the solar wind. Whereas the mechanisms by which energy is transferred are not well understood, a number of correlation studies (cf., Burch, 1974; Crooker, 1975) strongly indicate that the transfer mechanism involves merging between the IMF and the geomagnetic field. The southward component of the IMF and solar wind speed give excellent correlations with geomagnetic activity (Crooker et al., 1977; Burlaga and Lepping, 1977; and others).

iii) Micropulsations and Geomagnetic Activity. Both dayside continuous micropulsations and geomagnetic activity correlate well with many solar wind parameters. However, the two correlate differently and with different sets of parameters, so that a direct theoretical relationship between geomagnetic activity and micropulsations is difficult to formulate.

Micropulsations made at Borok ($L = 2.9$) have shown a good correlation between micropulsation period and K_p (Troitskaya, 1967). Figure 3.2 shows those results.

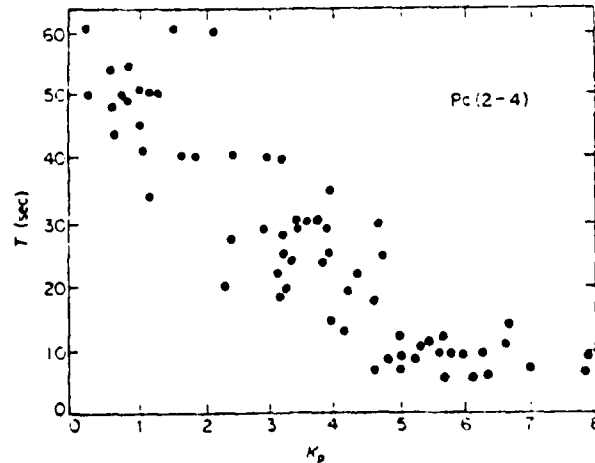


Figure 3.2 From Troitskaya (1967): Dependence of Pc 2-4 periods on K_p at Borok.

C. Recent Results

Three recent pieces of work have given significant credibility to the mechanisms previously proposed for pulsation generation, and have given

support to the possibility of producing a comprehensive micropulsation index which would indicate the level of geomagnetic activity. Two of the studies were based upon satellite observations and the third was based upon ground micropulsation observations. Most importantly, all three studies used digital data, which allowed flexible data manipulation and sophisticated computer analysis.

Recent simultaneous observations of geomagnetic pulsations using three synchronous satellites (Hughes et al., 1978) were in strong agreement with generation of the waves by the Kelvin-Helmholtz mechanism. The data were collected in February, 1975 when, for a few days, the three geosynchronous satellites ATS 6, SMS 1, and SMS 2 were operating in close proximity. The data were cross-spectral-analyzed to obtain phase differences between the spacecraft. All periods of pulsation activity observed on the dayside of the magnetosphere during one week were analyzed. Figure 3.3 shows the results of power spectral analysis upon a typical micropulsation event observed during the local morning. It should be noted that the same spectral peak was observed at all three spacecraft (the separation between adjacent satellites was about 10^0) and that the signals were highly coherent.

During the local morning and early afternoon hours, it was found that when there was a significant peak in the power spectrum at two satellites, there was a fair degree of coherence between the two signals to enable calculation of an m number (representing azimuthal wavelength). In local afternoon after 1400, however, this coherence often did not apply.

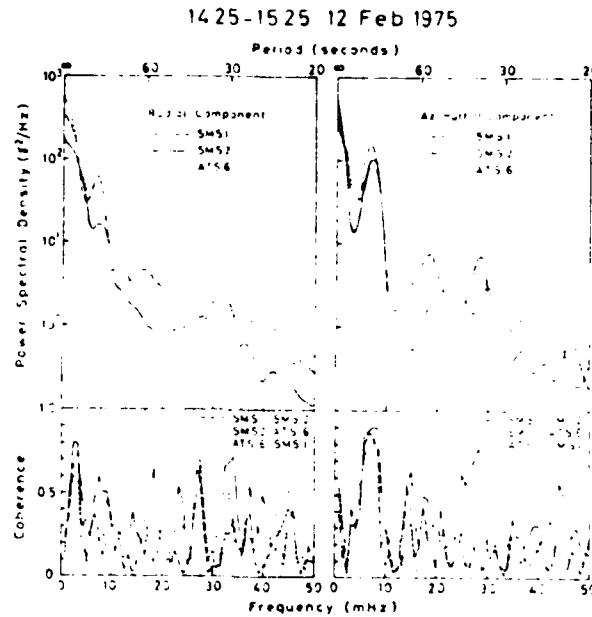


Figure 3.3. Spectra and cross-spectral coherence of the radial and azimuthal magnetic fields obtained by the three space craft during a typical local morning pulsation. From Hughes et al., (1978).

Figure 3.4 shows the variation of m number obtained as a function of time. The results provide support for the Kelvin-Helmholtz wave generation mechanism. In the vast majority of the morning events, the more easterly satellite leads in phase, while around noon this trend is reversed, and in the early afternoon the more westerly satellite leads. This indicates wave propagation away from noon, in the same direction as the flow of the solar wind plasma around the magnetopause.

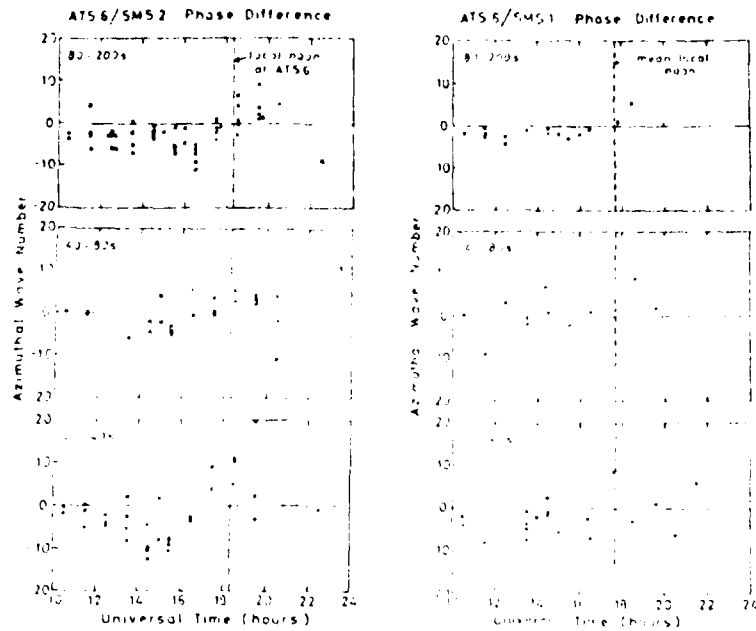


Figure 3.4. The variation of the azimuthal wave number (m) as a function of time. Mean local noon is computed at the midpoint between ATS6 and SMS 1. From Hughes et al., (1978).

The lack of coherence between the signals observed at two different satellites in the late afternoon indicates a strong localization in longitude. A possible source of those pulsations could be hot protons injected from the nightside. Thus, such pulsations would be expected to be associated with individual substorm events, and the power spectral density of those waves would be an indicator of geomagnetic activity level.

A recent study by Greenstadt et al. (1979) indicates that both the Kelvin-Helmholtz mechanism and direct injection of waves through the magnetopause are important sources of micropulsation energy. In that study, hourly distributions of micropulsation activity orientation angle were correlated both with the solar wind alignment of the IMF and with solar wind speed. As shown in Figure 3.5, the results showed positive point correlation with

both speed and orientation. In addition, the joint correlations showed that enhanced magnetic pulsation amplitudes were associated with solar wind speeds above 200-300 km/sec and angles between the IMF and sun-earth line of less than 50° - 60° . The threshold effects further support both the bow shock origin and the Kelvin-Helmholtz generation of daytime micropulsation signals.

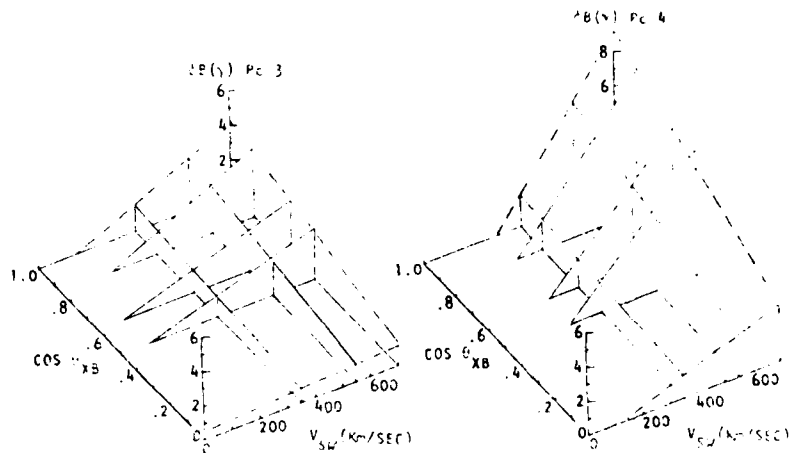


Figure 3.5. Diagrammatical summary of joint δB versus $\cos \theta_{XB}$ and V_{sw} correlations. From Greenstadt et al. (1979).

In another pulsation study using data from the geosynchronous satellite ATS-6, Arthur et al. (1978) calculated the power spectral density of geomagnetic field variations for the month of August, 1974. Two segments of approximately 9 hours each, centered at local noon and at local midnight, were used for the analysis. Figure 3.6 shows the time variation of the power spectral density as well as the ΣKp for the month of data. These results have striking implications on the correlation between micropulsation power content and geomagnetic activity. It is significant that the power spectral density is directly related to ΣKp on both the dayside and the nightside. Smaller

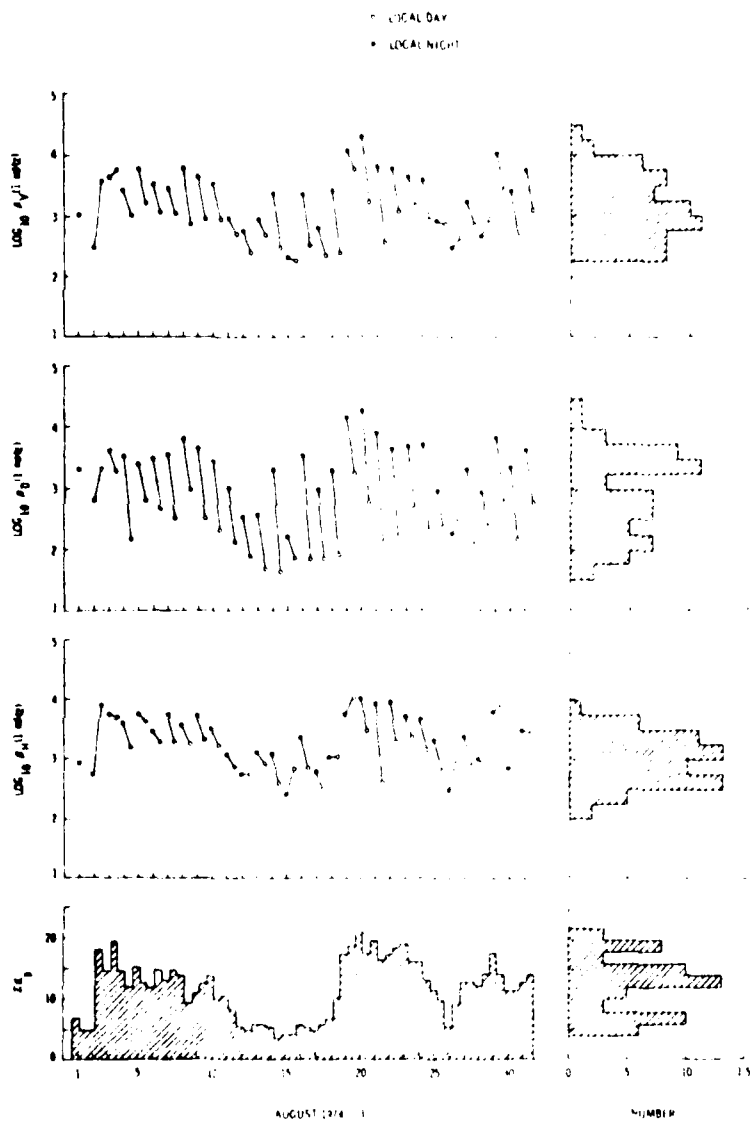


Figure 3.6. Time dependence of distributions of the autospectra of each magnetic field component measured at ATS-6. From Arthur et al. (1978).

(larger) E_{kp} corresponds to smaller (larger) values of power spectral density.

Arthur et al. also compared the average characteristics of power spectra at synchronous orbit with observations from other regions of interest in magnetospheric physics: the interplanetary medium, the magnetosheath, the outer magnetosphere near the magnetopause, and the surface of the earth. Figure 3.7 shows the average spectrum for each of the five regions. The

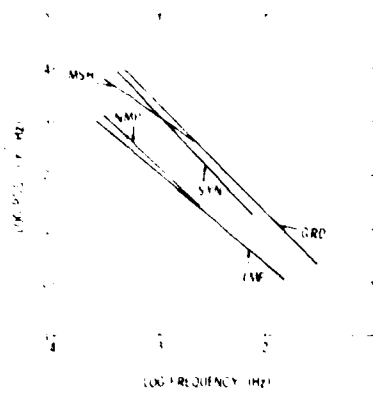


Figure 3.7. Average power spectra for the five regions, interplanetary, magnetosheath, magnetopause, synchronous orbit, and ground. From Arthur et al. (1978).

results in Figure 3.7 indicate that, except for the magnetosheath, which is known to be very disturbed, the power levels in each region increase from the interplanetary medium inward to the surface of the earth. Thus, given a good source of comprehensive digital data, ground observations should be at least as sensitive an indicator of geomagnetic activity as those reported by Arthur et al.

D. Summary and Recommendations

The results indicated herein suggested that:

- i) both the Kelvin-Helmholtz mechanism and direct injection of waves from the bow shock are important sources of micropulsation energy (Hughes et al., 1978; Greenstadt and Olson, 1979).

ii) micropulsation period is a possible indicator of geomagnetic activity level (Troitskaya, 1967),

iii) and the power spectral density of micropulsations may be used as an indicator of geomagnetic activity level (Arthur et al., 1978).

The AFGL magnetometer network is an ideal tool for formulating a micropulsation index for the level of geomagnetic activity. The AFGL data is also ideal for comparison with observations from other chains of magnetometers. Since the AFGL data is digital, it would be straightforward to perform power spectral analysis. And since all facilities used for the network are dedicated to the network, the data are available uninterrupted for long periods of time.

Two possible approaches may be used to formulate and calibrate a micropulsation index from the AFGL magnetometer network data.

The first, and simplest, approach would be to pass the data through a suite of filters, each passband carefully chosen to cover a particular part of the micropulsation spectrum. The output of each filter would then be time averaged and correlated with geomagnetic activity, e.g., K_p . After appropriate study, the filter band passes could be precisely defined so as to cover the spectrum in a way that the most significant channels could be isolated. At that point, the superfluous channels could be eliminated (although they probably should be retained for future study).

A second, more sophisticated, approach would be as follows. Compute the power spectral density matrix for an appropriate time interval (one hour, as a start). Retain the power spectral density for each component of the magnetic field. Careful comparison of shifts of spectral peaks with changing geomagnetic activity would verify or refute the possibility of using micropulsation period as the key indicator of activity level.

Following the technique of Arthur et al. (1978), the level of the spectrum (characterized by key spectral estimates) could be correlated with geomagnetic activity. Based on the success of this approach at synchronous orbit, it is likely that a micropulsation index using this technique on AFGL magnetometer network data could be a reliable indicator of geomagnetic activity.

In this report, we have emphasized dayside continuous micropulsations as possible indicators of geomagnetic activity. However, it is apparent that irregular micropulsations, especially Pi2, may also be good indicators of the level of activity. Pi2 are transient pulsations associated with substorms, with maximum effect at middle and low latitudes. Pi2 are known to correlate with Kp (Troitskaya, 1967). A possible future study of the potential of Pi2 occurrence as a geomagnetic activity index using the AFGL network data should be considered at some point.

References

- Arthur, C. W., R. L. McPherron, and W. J. Hughes, A statistical study of Pc 3 magnetic pulsations at synchronous orbit, ATS 6, J. Geophys. Res., 82(7), 1149-1157, 1977.
- Arthur C. W., R. L. McPherron, L. J. Lauzcrotti, and D. C. Webb, Geomagnetic field fluctuations at synchronous orbit, J. Geophys. Res., 83, 3859-3865, 1978.
- Burch, J. L. Observations of interactions between interplanetary and geomagnetic fields, Rev. Geophys. and Space Phys., 12, 363-378, 1974.
- Burlaga, L. F., and R. P. Lepping, The causes of recurrent geomagnetic storms, Planet. Space Sci., 25, 1151-1160, 1977.
- Chen, L., and A. Hasegawa, A theory of long-period magnetic pulsations: 1. Steady state excitation of field line resonance, J. Geophys. Res., 79,(7), 1024-1032, 1974a.
- Chen, L., and A. Hasegawa, A theory of long-period magnetic pulsations: 2. Impulse excitation of surface eigenmode, J. Geophys. Res., 79 (7), 1033-1037, 1974b.
- Crooker, N. U., Solar wind-magnetosphere coupling, Rev. Geophys. Space Phys., 13, 955-958, 1021-1025, 1975.
- Crooker, N. U., J. Feynman, and J. T. Gosling, On the high correlation between long-term averages of solar wind speed and geomagnetic activity, J. Geophys. Res., 82, 1933-1937, 1977.
- Dungey, J. W., Electrodynamics of the outer atmosphere, Penna. State Univ. Ionos. Res. Lab. Rept. No. 69, 1954.
- Greenstadt, E. W., Field-determined oscillations in the magnetosheath as possible source of medium-period, daytime micropulsations, in Proceedings of the Symposium on Solar Terrestrial Relations, Ed. D. Venkatesan, Univ. of Calgary, Alberta, Canada, p. 515, 1972.
- Greenstadt, E. W., and J. V. Olson, Pc 3,4 activity and interplanetary field orientation, J. Geophys. Res., 81(34), 5911-5920, 1976.
- Greenstadt, E. W., H. J. Singer, C. T. Russell, and J. V. Olson, IMF orientation, solar wind velocity, and Pc 3-4 signals: a joint distribution, J. Geophys. Res., 84, 527-532, 1979.
- Gul'yel'mi, A. V., and O. V. Bol'shakova, Diagnostics of the interplanetary magnetic field from ground-based data on Pc 2-4 micropulsations, Geomagn. Aeron., 13, 459-461, 1973.

- Hughes, W. J., R. L. McPherron, and C. T. Russell, Multiple satellite observations of pulsation resonance structure in the magnetosphere, J. Geophys. Res., 82(4), 492-498, 1977.
- Hughes, W. J., R. L. McPherson, and J. N. Barfield, Geomagnetic pulsations observed simultaneously on three geostationary satellites, J. Geophys. Res., 83, 1109-1116, 1978.
- Jacobs, J. A., Geomagnetic Micropulsations, Springer-Verlag, New York, Berlin, Heidelberg, p. 171, 1970.
- Lanzerotti, L. J., and H. Fukunishi, Modes of magnetohydrodynamic waves in the magnetosphere, Rev. Geophys. Space Phys., 12(4), 724-729, 1974.
- Lanzerotti, L. J., H. Fukunishi, and L. Chen, ULF pulsation evidence of the plasmopause: 3. Interpretation of polarization and spectral amplitude studies of Pc 3 and Pc 4 pulsations near $L = 4$, J. Geophys. Res., 79(31), 4648-4653, 1974.
- Orr, D., Magnetic pulsations within the magnetosphere: A review, J. Atmosph. Terr. Phys., 35(1), 1-50, 1973.
- Plyasova-Bakunina, T. A., Effect of the interplanetary magnetic field on the characteristics of Pc 2-4 pulsations, Geomagn. Aeron., 12, 675-677, 1972.
- Radoski, H. R., A theory of latitude dependent geomagnetic micropulsations: The asymptotic fields, J. Geophys. Res., 79(4), 595-603, 1974.
- Raspopov, O. M., and L. J. Lanzerotti, Investigation of Pc 3 frequency geomagnetic pulsations in conjugate areas around $L = 4$: A review of some USSR and US results, Rev. Geophys. Space Phys., 14(4), 577-589, 1976.
- Saito, T., Geomagnetic pulsations, Space Sci. Rev., 10(3), 319-412, 1969.
- Southwood, D. J., The hydromagnetic stability of the magnetospheric boundary, Planet. Space Sci., 16, 587-605, 1968.
- Southwood, D. J., Some features of field line resonances in the magnetosphere, Planet. Space Sci., 22, 483-491, 1974.
- Troitskaya, V. A., Micropulsations and the state of the magnetosphere, in Solar-Terrestrial Physics, eds. J. W. King and W. S. Newman, Academic Press, London, New York, pp. 213-274, 1967.

4. IONOSPHERIC ELECTRIC FIELDS AND CURRENTS DRIVEN BY BIRKELAND CURRENTS

A. Introduction

A significant observational finding of the past decade is the discovery of magnetospheric electric currents that flow along magnetic field lines and enter the ionosphere in the auroral regions. These so-called Birkeland, or field-aligned currents, constitute a major coupling between the magnetosphere and the ionosphere. Other recent observations suggest that certain ionospheric phenomena, that may occur at all latitudes from the polar cap to the equator, are causally connected to the electric field, current, and conductivity variations that occur in the auroral regions. For the purpose of eventually relating observed mid latitude field signatures to magnetospheric-ionospheric current configurations, we have developed a model for the global distribution of ionospheric currents generated by a specified input-output Birkeland current configuration. The model developed is discussed in this chapter and some principal results are included in the three publications reprinted at the end of this chapter.

The model developed of global distributions of electric fields and currents driven by field aligned currents is useful in several ways. To cite three reasons: (1) Within the model, the ionospheric distribution of electric currents that result from various models of geomagnetic events, such as substorms, are determined, and from these currents, ultimately, the magnetic disturbance patterns can then be calculated for such events. These modeled events are then used in conjunction with actual records (magnetograms, say, at middle latitude) to infer the behavior of the high latitude ionosphere. (Carrying out this procedure is discussed in more detail later in this chapter.) (2) The electric fields in the ionosphere are determined globally for model events. Since a great many plasma phenomena, e.g., at the dip equator, depend

upon the local electric field, one could use such a model to determine the relationship between, say, equatorial ionospheric plasma observations and Birkeland currents. (3) This gives quantitative insight into the relative contributions of various electrodynamic effects that are operative (such as Birkeland currents, neutral winds, conductivity structure, etc.) in determining the resultant distributions of ionospheric electric fields and currents. Thus, in summary, the kind of modeling developed serves to enhance our understanding of the connection between magnetospheric dynamics and various electrodynamic effects in the global ionosphere. This improved understanding, in turn, will enable us to develop ways to exploit the connection for practical purposes.

B. Definition of the Model

The definition of our model is as follows. The ionospheric height-integrated tensor conductivity and the distribution of field-aligned currents into and out of the ionosphere are specified (i.e., taken as known variables) for each model event considered. The basic condition imposed at each point in the ionosphere is that charge is conserved. This is done through the continuity equation, which, using Ohm's law, has the form

$$I(\text{field-aligned}) = \nabla_2 \cdot \underline{\underline{\Sigma}}(\theta, \gamma) \cdot \nabla_2 \phi(\theta, \gamma)$$

The left-hand side of this equation is provided by the given Birkeland current distribution at the ionosphere. $\phi(\theta, \gamma)$ is the electric potential in the (height-integrated) ionosphere at the colatitudinal and azimuthal angles θ and γ . The ionospheric electric field and current distribution are determined by the relations:

$$\begin{aligned} \underline{E}(\theta, \gamma) &= -\nabla_2 \phi(\theta, \gamma), \\ \underline{J}(\theta, \gamma) &= \underline{\underline{\Sigma}}(\theta, \gamma) \cdot \underline{E}(\theta, \gamma). \end{aligned}$$

The subscript on the gradient indicates that only transverse derivatives (tangential to the spherical ionosphere) are operative.

The conductivity tensor $\underline{\underline{\Sigma}}(\theta, \gamma)$ is assumed known and includes the principal

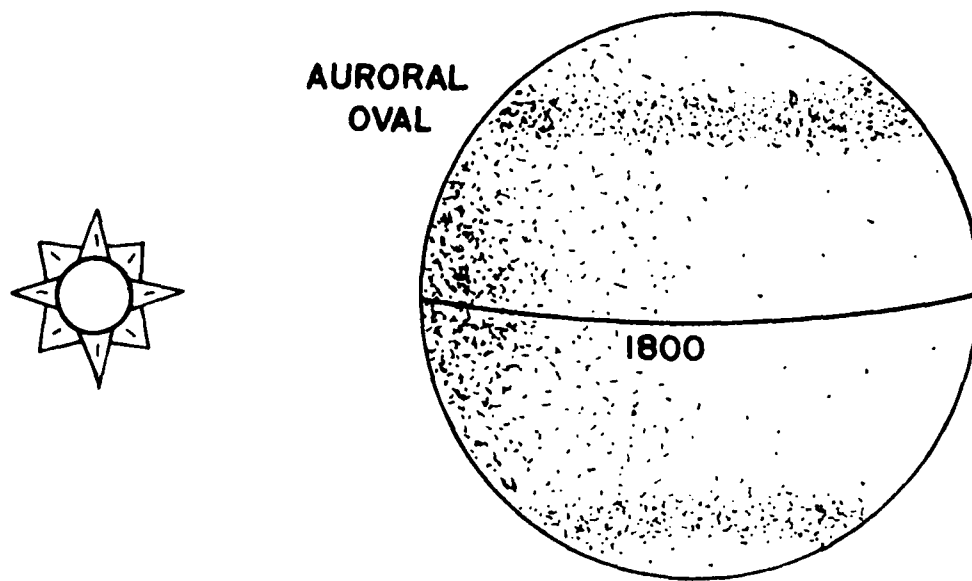
spatial variations: a large increase of dayside over nightside conductivity due to solar photoionization (i.e., the solar-zenith angle variation); and a large increase in the auroral regions due to energetic particle precipitation. These variations are depicted schematically in Figure 4.1. In addition, the layer conductivity formulation employed leads to enhancements of the diagonal conductivities and a zero of the off-diagonal conductivities at the equator (as shown in Figure 1 of the third reprinted paper in this chapter (Nopper and Carovillano, 1979b)). The assumed distribution of driving currents is adapted from the Triad satellite observations (c.f., Figure 2 of the second reprinted paper in this chapter (Nopper and Carovillano, 1979a)). With these modeling parameters, we are able to represent a range of magnetospheric conditions from very quiet to quite disturbed.

The numerical scheme employed to solve the continuity equation is an iterative method using successive relaxations. Iterations are made to a finite difference representation of the continuity equation on a hemispherical grid. This well-known technique (Forsyth and Wasow, 1960; Binns and Lawrenson, 1973) yields reliable numerical results, as tested independently using Gauss's Law in two dimensions on the final output, and gives accurate electric fields and currents to within a few percent almost everywhere.

C. Applications of the Model

In this section, we briefly describe the situations modeled and the determined equipotential patterns and electric field distributions. We also summarize here the results contained in the three reprinted papers included in section D of this chapter. We shall refer to those three papers as Paper I (Nopper and Carovillano, 1978), Paper II (Nopper and Carovillano, 1979a), and Paper III (Nopper and Carovillano, 1979b).

PHYSICAL IONOSPHERIC CONDUCTIVITIES



$$\begin{pmatrix} J_x \\ J_y \\ J_z \end{pmatrix} = \begin{pmatrix} \sigma_p & -\sigma_H & 0 \\ \sigma_H & \sigma_p & 0 \\ 0 & 0 & \sigma_0 \end{pmatrix} \begin{pmatrix} E_x \\ E_y \\ E_z \end{pmatrix}$$

Figure 4.1 Schematic representation of the distribution of ionospheric conductivity used in the model. Conductivity is proportional to density of stippling. Features shown include the solar-zenith (i.e., day-night) variation, and enhanced conductivity in the auroral ovals.

The basic quiet-time (or weakly disturbed) pattern of field-aligned currents discerned by the Triad satellite includes a "Region 1" (poleward) pair, with current into the dawnside and out of the duskside ionosphere, at the high latitude edge of the auroral oval; and a "Region 2" (equatorward) pair, with opposite polarity to the Region 1 set, at the equatorward edge of the oval; Region 1 currents, at 10^6 A, are typically twice the strength of the Region 2 currents during quiet periods. (See Figure 2a of Paper I (Nopper and Carovillano, 1978) for our idealization of this structure; this figure also shows the equipotentials for this set of source currents). Systematic findings are that the dusklike equipotentials are pushed up toward the pole, while the dawnside equipotentials are drawn down toward the equator; in addition, the polar cap equipotentials are pushed over toward the dawnside of the polar cap. These distortions are understood (Wolf, 1970; Nopper and Carovillano, 1979b) to result from the contrast in conductivity between the day and night sides of the earth, and are present in all models with such a conductivity structure. A consequence of this asymmetry appears in the electric field distribution. Thus, Paper I (Nopper and Carovillano, 1978) shows the quiet-time east-west electric field at the equator as a function of local time; one sees that the field is eastward over three-quarters of the day and westward for only about six hours from 2300-0500 LT, and that the field is stronger during its westward orientation than its eastward (a consequence of the requirement that $\oint \underline{E} \cdot d\underline{l} = 0$). Quiet-time electric field components at latitudes 54° and 30° , as functions of local time, are displayed in Figures 4 and 5 of Paper II (Nopper and Carovillano, 1979a) where the local-time asymmetries are also evident.

During disturbed periods, observations indicate that the topology of the field-aligned currents remains the same as for quiet times, but that the strengths of the currents increase to roughly 3×10^6 A in both the Region 1

and Region 2 pairs. Thus, not only do the currents increase in strength during active conditions, but also the Region 2 current becomes approximately as strong as in Region 1 (in quiet time, Region 1 dominates). The general effect on the equipotential pattern can be seen in various figures in Papers I, II, and III. Thus, changes in the electric fields are evident in Figures 2a and 3 of Paper I, and Figures 8 and 9 of Paper II. The change in equipotential pattern is seen in Figures 2a and 2c of Paper III. A striking result is that, during disturbed periods, the east-west component of the electric field reverses its quiet-time direction at the equator (and other latitudes) at most local times.

Using models of the field-aligned currents during quiet and disturbed periods as just discussed, we show in Paper I that the source currents as observed during active times generate equatorial electric fields of sufficient strength and in the proper direction to account for the fluctuations and reversals of the electric field seen in equatorial records. Originally inferred from magnetic observations, these disturbances in the equatorial electric field have now been seen directly as actual ionospheric effects by radar and other sensing techniques, and often occur simultaneously with high-latitude disturbances. Thus, Paper I establishes the ionospheric conductivity as a contributing mechanism to the coupling of electric fields from high latitudes, where driving forces of magnetospheric origin are applied, to low ionospheric latitudes.

The consequences of global spreading of electric fields of magnetospheric origin are examined further in Paper II. Here, in addition to the polar-equatorial coupling discussed above, we conclude that the electric fields due to Birkeland currents are comparable or exceed in magnitude those generated in neutral wind models at all latitudes, and generally have large subdiurnal (12, 8, ... hour) components. Thus, even during quiet periods, neutral wind models are insufficient

to model ionospheric electric fields and currents, and the effects of magnetospheric sources must be included. It was also observed in Paper II that during disturbed times, the electric field in the polar cap deviates from its canonical dawn-to-dusk direction and re-orientes toward the sun.

This last effect is the topic of Paper III where the polar cap electric field is examined under various disturbance conditions. The principal result is that the structure of equipotentials, globally and in the polar cap, depends sensitively on the relative strengths of the field-aligned current pairs. For Region 1 currents much stronger than Region 2 (a very "quiet" condition), the average electric field direction in the polar cap is about 60° east of noon. As the Region 2 currents increase in strength, corresponding to magnetic conditions becoming increasingly active, the orientation of the polar cap electric field rotates clockwise (as seen from above the pole) towards noon and would actually point into the pre-noon sector should the intensity of Region 2 currents slightly exceed Region 1 currents. In Paper III, Figures 2a-c show the smooth progression of equipotential patterns for Region 1/Region 2 intensity ratios of 2:1 (quiet conditions) through 1:1 (disturbed conditions) to 1:2 (intensely and probably unrealistically disturbed conditions). The electric field direction, measured counterclockwise from noon, is given in Figure 4.2 as a function of the intensity ratio. Because the intensity of Region 2 currents is directly dependent upon geomagnetic activity conditions, an important implication of our work is that the electric field orientation in the polar cap should also correlate with geomagnetic activity.

D. Reprinted Publications (Papers I, II, and III)

The reprints mentioned in the foregoing text and briefly discussed in Section C as Papers I, II, and III are presented in this section.

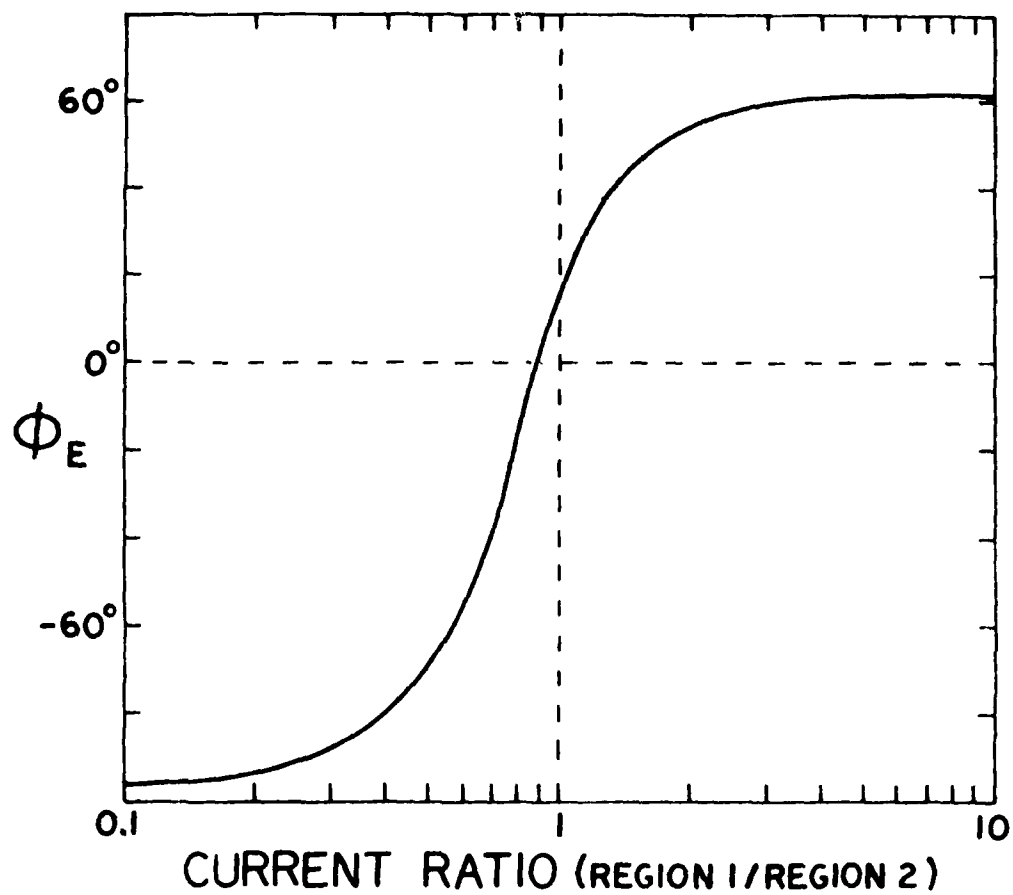


Figure 4.7 The orientation of the model electric field at the north pole, measured counterclockwise from noon, as a function of the ratio of total Region 1 current to total Region 2 current.

POLAR-EQUATORIAL COUPLING DURING MAGNETICALLY ACTIVE PERIODS

R. W. Nopper, Jr. and R. L. Carovillano

Department of Physics, Boston College, Chestnut Hill, Massachusetts 02167

Abstract. Observational evidence indicates that high-latitude magnetic activity can be causally related to fluctuations and reversals of the equatorial electric field. Using Birkeland currents as the driving forces, we have made numerical calculations of the ionospheric electric fields and currents that distribute globally. Our calculations utilize a fairly realistic empirical ionospheric conductivity model and the field-aligned current distribution inferred from TRIAD measurements. The results presented here demonstrate that the field-aligned currents observed during disturbed periods can account for the equatorial fluctuations and reversals in electric field and associated magnetic disturbances noted during such times. In this way, magnetospheric dynamics has a direct and significant influence on the equatorial ionosphere through the ionospheric conductivity.

Introduction

A body of observational evidence has been accumulating for decades that high-latitude and equatorial ionospheric electric fields and currents are coupled during active times. The first evidence involved ground magnetometer measurements from equatorial and high-latitude observatories which showed variations closely correlated in time [Akasofu and Chapman, 1963, 1967; Onwumehili et al., 1973]. These fluctuations were often attributed to a coherent, extensive ionospheric current system generated during polar substorms with "return currents" that affected the dayside equatorial electrojet. However, there was no immediate way to rule out the explanation that such ground magnetic effects were of extra-ionospheric origin, e.g., from ring currents. Thus a causative polar-equatorial ionospheric coupling could not be established from magnetic records alone. With the rise of ionospheric sounding techniques such as incoherent scatter and VHF Doppler radar, in conjunction with ground magnetic records, observational evidence now indicates that high-latitude and equatorial magnetic activity often correlate well with each other and with details of equatorial electric field variations. For example, Matsushita and Balsley [1972] found that 100% changes in geomagnetic H at equatorial Huancayo correlated well with radar-measured decreases in westward electron drift velocity during a period when the ring current was too weak to account for H. Using VHF Doppler radar, Carter et al. [1976] found cases where equatorial fluctuations in E_z velocity with time scales of 20-60 minutes correlated with geomagnetic H and in turn with the high-latitude fluctuations seen on the Dixon Island magnetogram. Heger et al. [1976] found that fast

reversals in the equatorial electrojet current occurred both day and night during times of high K_p, when polar magnetic activity is statistically more frequent. Thus, at least for certain disturbances, radar measurements support the inference from magnetic records that the high-latitude and equatorial ionospheres are coupled electrically.

We will use the term "polar-equatorial coupling" to refer to such coupling of ionospheric electric fields and currents. In our approach, the coupling results from driving forces in the high-latitude ionosphere, and the connection with magnetospheric dynamics is from Birkeland currents. The results reported below essentially establish the role of the ionospheric conductivity in explaining the observed polar-equatorial coupling. The major improvements in our results over past efforts in the area [Iwasaki and Nishida, 1967; Wolf, 1970; Jaggi and Wolf, 1973; Maeda and Maekawa, 1973; Lyatsky et al., 1974; Yasuhara et al., 1975] are in our improved representations of field-aligned current distributions and conductivity, and especially in our careful treatment of the equatorial conductivity. Because of these improvements we are able to determine the magnitudes of low- and equatorial-latitude effects accurately. Modeling parameters can be better specified than in the past mainly because of the synoptic pictures provided by the TRIAD Satellite of the driving field-aligned currents under different conditions, and the improved empirical knowledge of the ionospheric conductivity provided by techniques such as incoherent scatter. In the following sections we describe our models and the calculated results.

The Models

Our approach is to solve the equation of continuity for the height-integrated ionospheric current, given the high-latitude distribution of the driving field-aligned currents and the ionospheric layer conductivities. In these calculations we only obtain the ionospheric electric fields that result from magnetospheric coupling, and therefore do not take into account other dynamical effects such as neutral winds. This is probably not a serious deficiency in modeling the present effects, for which the global coherence in time occurs on scales considerably shorter than the response time of the global wind system, which is perhaps a couple of hours [Fedder and Banks, 1972].

The picture of the field-aligned currents adopted is taken from the TRIAD results [Iijima and Potemra, 1976]. Briefly, TRIAD reports two distinct sets of large-scale field-aligned currents: a poleward set (region 1) which is permanent, and an equatorial set (region 2), which is more transient. The distributions are roughly

Received at the Geophysical Research Office, Boston College, Chestnut Hill, Massachusetts, May 10, 1978.

© 1978 by the American Geophysical Union.

0893-9479/78/050601-07\$01.00/0

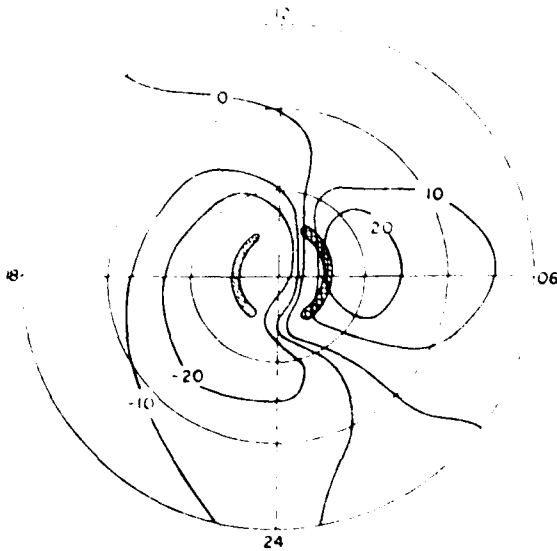


Fig. 1a. Polar plot of equipotential pattern (in kV) due to a region 1 current set of 10^6 A at 72° : into the ionosphere (cross-hatching) on the dawnside, outward (stippling) on the duskside. Noon is at the top, dusk to the left, etc.; the outer circle represents the equator, and the inner circles are at 30° and 60° latitude.

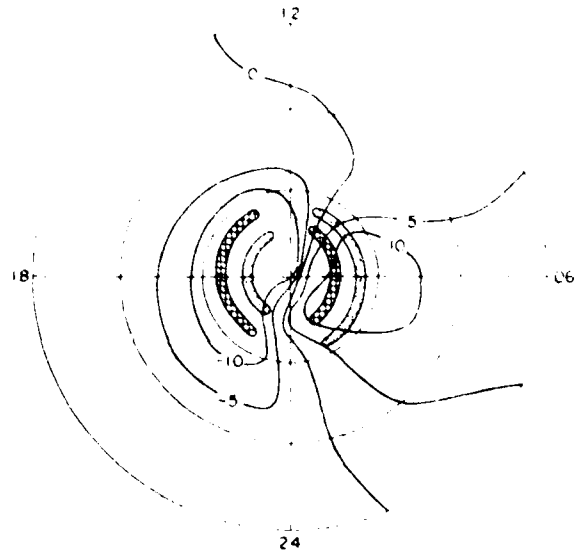


Fig. 2a. Equipotential pattern of region 1 currents of 10^6 A at 72° and region 2 currents of 5×10^5 A at 66° . This scenario approximates the quiet-time TRIAD observations.

symmetrical northern to southern hemisphere. Region 1 currents flow into the ionosphere on the dawnside and out on the duskside; region 2 currents are of opposite polarity. The regions have a large spread in local time and overlap near midnight. During quiet times, region 1 currents are stronger than the region 2 currents (which may even be absent) and amount to $\approx 10^6$ A. During active times the intensities of both sets increase and become equal to about 3×10^6 A [Iijima and Potemra, 1978]. At all times, evidence is that the net current into the ionosphere equals the net current out. For our present idealization of the TRIAD synoptic observations, we placed the current sources along arcs of constant latitude with a longitudinal extent of 132° and distributed the current uniformly along these arcs. This structure is illustrated in Figures 1a and 2a.

The direct, Pedersen, and Hall conductivities were represented by simple functions that reproduce the observed major structures of the ionospheric conductivity, the solar-zenith angle variation and the auroral enhancement. The coefficients were selected as typical or most characteristic values from measurements of Rowe and Mathews [1973], Brekke et al. [1974], Kennel and Rees [1972], and others. With θ the colatitude and ϕ the longitude measured eastward from noon, the height-integrated conductivities for the calculations presented here are (in mhos):

$$\text{Pedersen: } \sigma_p(\theta, \phi) = 0.3 + 5.0 \exp\{-[\cos^{-1}(\sin\theta \cos\phi)]^2 / 1.804\} + 3.0 \exp\{-(\theta - 0.35)^2 / 0.01\}$$

$$\text{Hall: } \sigma_H(\theta, \phi) = 2.0 \sigma_p(\theta, \phi)$$

$$\text{direct: } \sigma_o(\theta, \phi) = 31.62 \sigma_p(\theta, \phi)$$

The first two terms in σ_p provide a low value at night and a smooth solar-zenith angle variation on the dayside which closely approximates the measured form of Van Zandt [1967]; the day-to-

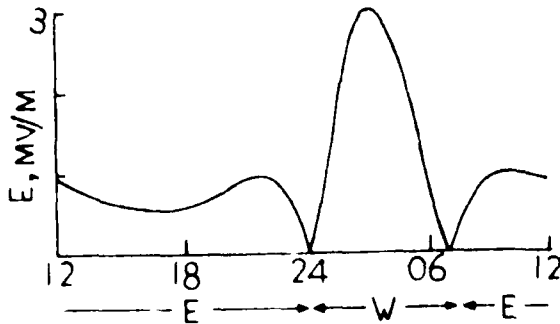


Fig. 1b. Electric field as a function of local time at the equator. The letters E and W at the bottom of the figure give the sense, east or west, of the equatorial field.

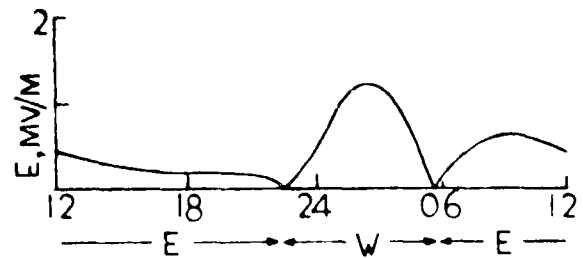


Fig. 2b. Electric fields for the quiet-time model (same format as Figure 1b).

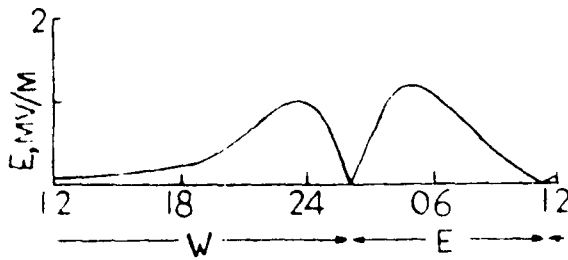


Fig. 3. Electric fields for the case of equal region 1 and region 2 currents (10^6 A). The format is the same as in Figure 1b and 2b. Comparison with Figure 2a shows that the equatorial electric field is oppositely directed over most local times.

night conductivity contrast is about 20 to 1. The last term provides a broad auroral enhancement zone of 15° width peaking at 69° . These functions represent a compromise between the "best" observed or phenomenological models and the requirements of suitable smoothness for the numerical calculational scheme. The above expression for the conductivities were used in the usual layer formulas (cf., Rishbeth and Garriott [1969]) to obtain the two-dimensional or thin-shell conductivity tensor Σ , taking the earth's magnetic field to be dipolar. The continuity equation

$$\nabla \cdot (\text{source}) = \nabla_2 \cdot (\Sigma \cdot \nabla V)$$

is solved numerically using difference formulas on a 30×30 grid. The resulting algebraic equations are solved for the ionospheric potential V , from which the electric field and current density are determined. Our model has north-south symmetry so that calculations are made in the northern hemisphere with the boundary condition of zero current crossing the equator [Wolf, 1970]. North-south symmetry eliminates the consideration of coupling between conjugate hemispheres, e.g., along plasmaspheric field lines. Numerical accuracy of the solutions was carefully monitored, and an additional independent constraint was imposed to improve the quality of the results. This constraint is derived from Gauss's law in two dimensions and basically expresses the local requirement of continuity of ionospheric current that the correct solution must satisfy. The largest numerical errors in the results presented are a few percent.

Results and Discussion

We model quiet and active conditions in the following way. For very quiet times, the steady poleward field-aligned current set is given an intensity of 10^6 A and the equatorward set is absent or weaker in intensity. Active times are modeled making both sets equal with an intensity of several times 10^6 A. In these calculations, we do not vary the auroral current densities.

Figure 1a shows the resulting equatorial equipotential and the electric field produced by region 1 and region 2 currents of 10^6 A. The field is eastward (westward) over most local times, which is opposite

to the situation in the case of region 1 currents only. The field is pulled poleward (pushed equatorward) on the dusk (dawn) side is due to the conductivity contrast between day and night [Wolf, 1970]. The tendency of the subauroral equipotentials to rotate toward later local times was attributed by Wolf [1970] and Vasyliunas [1970] to the enhanced model auroral conductivity. Figure 1b shows the resulting electric field morphology at the equator as a function of local time. Note that the electric field at the equator is westward over just a brief sector of local time (essentially the midnight-dawn quadrant). The equatorial electric field is about 1-2 mV/m. This large magnitude suggests that impulsive activation or enhancement of field-aligned currents during disturbed times could contribute electric fields which are of proper polarity and great enough strength at low latitudes to produce significant fluctuations in (and even reversals of) the quiet-time pattern. For a quiet-time equatorial morphology, we regard the observational picture of Woodman [1970] to be typical: eastward field of ~ 0.5 mV/m over most of the dayside, with a sharp increase to 1 mV/m near dusk, followed by a reversal to ~ 0.5 mV/m in a westward direction over most of the nightside.

Figure 2a gives the equipotential pattern that results from adding region 2 currents of 5×10^5 A at 60° to the current pattern of Figure 1a. This modeling situation corresponds to the quiet-time TRIAD measurements. Here, one associates the region 1 currents with the magnetospheric convection electric field and the region 2 currents with the shielding currents coming from the inner edge of the plasma sheet (e.g., Wolf [1975]). Figure 2a shows the penetration of the equipotentials to low latitudes to be greatly restricted, and Figure 2b shows correspondingly that the electric fields at low latitudes are significantly reduced by the region 2 source, though their directions are more or less the same as in Figure 1b. Our quiet-time results at the equator resemble the quiet-time morphology of Woodman [1970]. To represent active conditions, the strength of the region 2 source is increased to match that of region 1, namely, 10^6 A. Under these conditions the direction of the equatorial electric field is reversed compared to quiet conditions over most local times, as shown in Figure 3. Fujita and Petemra [1976] associated the strength of region 2 currents with the level of auroral electrojet activity. The region 2 currents presumably originate in the inner edge of the plasma sheet/ring current, which is often the source of high-latitude ionospheric activity. As suggested by the TRIAD measurements, during active periods current intensities reach 3×10^6 A and the scales of Figure 3 are to be multiplied by about three. For these conditions, the equatorial reversal of the quiet-time morphology of Woodman [1970] is quite pronounced. If active periods are modeled by impulsive, out-of-phase fluctuations of region 1 and region 2 current sets, then equatorial electric field reversals would appear as in the sequence of Figures 2b, 3, 2b, 3, etc. Such a possibility was suggested by Tostoyev and Lyatsky [1978] for the quiet fluctuations.

In summary, the present calculations indicate the degree to which the ionospheric conductivity couples electric fields driven by high-latitude field-aligned currents to the equatorial ionosphere. The coupling is sufficient to account for the fluctuations and reversals in the equatorial electric field which occur in active periods. Our model gives a consistent picture of magnetically quiet and active periods by incorporating essential features of the observed behavior of field-aligned currents to infer associated equatorial effects. Future applications will deal with selected modeling conditions associated with several classes of magnetic activity.

Acknowledgments. The authors are grateful to N. U. Crooker, G. L. Siscoe, and M. A. Heinemann for discussions on various aspects of this research. This research was supported by the Atmospheric Sciences Section, National Science Foundation, under Grant ATM75-72873 and by the Air Force Geophysics Laboratory under Contract F19628-77-C-0085.

References

- Akasofu, S.-I. and S. Chapman, The enhancement of the equatorial electrojet during polar magnetic storms, *J. Geophys. Res.*, **68**, 2375-2382, 1963.
- Akasofu, S.-I. and S. Chapman, The normality of the SD variation at Huancayo and the asymmetry of the main phase of geomagnetic storms, *Planet. Space Sci.*, **15**, 205-207, 1967.
- Brekke, A., J. R. Doupnik, and P. M. Banks, Incoherent scatter measurements of E region conductivities and currents in the auroral zone, *J. Geophys. Res.*, **79**, 3773-3790, 1974.
- Carter, D. A., B. B. Balsley, and W. L. Ecklund, VHF Doppler radar observations of the African equatorial electrojet, *J. Geophys. Res.*, **81**, 2786-2794, 1976.
- Fedder, J. A. and P. M. Banks, Convection electric fields and polar thermospheric winds, *J. Geophys. Res.*, **77**, 2328-2340, 1972.
- Fejer, B. G., D. T. Farley, B. B. Balsley and R. F. Woodman, Radar studies of anomalous velocity reversals in the equatorial ionosphere, *J. Geophys. Res.*, **81**, 4621-4626, 1976.
- Iijima, T. and T. A. Potemra, The amplitude distribution of field-aligned currents at northern altitudes observed by Triad, *J. Geophys. Res.*, **81**, 2165-2174, 1976.
- Iijima, T. and T. A. Potemra, Large-scale characteristics of field-aligned currents associated with substorms, *J. Geophys. Res.*, **83**, 599-615, 1978.
- Iwasaki, N. and A. Nishida, Ionospheric current systems produced by an external electric field in the polar cap, *Rep. Ionos. Space Res. Jap.*, **21**, 17-28, 1967.
- Jaggi, R. K. and R. A. Wolf, Self-consistent calculation of the motion of a sheet of ions in the magnetosphere, *J. Geophys. Res.*, **78**, 2852-2866, 1973.
- Kennel, C. F. and M. H. Rees, Dayside auroral-oval plasma density and conductivity enhancements due to magnetosheath electron precipitation, *J. Geophys. Res.*, **77**, 2294-2302, 1972.
- Leont'yev, S. V. and V. B. Lyatskiy, Three-dimensional current system of a partial ring current: relation between DP2 and Sq variations, *Geomagn. Aeron.*, **15**, 91-94, 1975.
- Lyatskiy, W. B., Yu. P. Maltsev, and S. V. Leont'yev, Three-dimensional current system in different phases of a substorm, *Planet. Space Sci.*, **22**, 1231-1247, 1974.
- Maeda, H. and Maekawa, A numerical study of polar ionospheric currents, *Planet. Space Sci.*, **21**, 1287-1300, 1973.
- Matsushita, S. and B. B. Balsley, A question of DP2, *Planet. Space Sci.*, **20**, 1259-1267, 1972.
- Onwumehili, A., K. Kawasaki, and S.-I. Akasofu, Relationships between the equatorial electrojet and polar magnetic variations, *Planet. Space Sci.*, **21**, 1-16, 1973.
- Rishbeth, H. and O. K. Garriott, *Introduction to Ionospheric Physics*, p. 138, Academic Press, New York, 1969.
- Rowe, J. F., Jr. and J. D. Mathews, Low-latitude nighttime E region conductivities, *J. Geophys. Res.*, **78**, 7461-7470, 1973.
- Van Zandt, T. E., The neutral atmosphere and the quiet ionosphere, in *Physics of Geomagnetic Phenomena*, ed. by S. Matsushita and W. H. Campbell, Academic Press, New York, 1967.
- Vasyliunas, V. M., Mathematical models of magnetospheric convection and its coupling to the ionosphere, in *Particles and Fields in the Magnetosphere*, ed. by B. M. McCormac, Reidel, Dordrecht-Holland, 1970.
- Wolf, R. A., Effects of ionospheric conductivity on convective flow of plasma in the magnetosphere, *J. Geophys. Res.*, **75**, 4677-4698, 1970.
- Wolf, R. A., Ionosphere-magnetosphere coupling, *Space Sci. Rev.*, **17**, 537-562, 1975.
- Woodman, R. F., Vertical drifts and east-west electric fields at the magnetic equator, *J. Geophys. Res.*, **75**, 6249-6279, 1970.
- Yasuhara, F., Y. Kamide and S.-I. Akasofu, Field-aligned and ionospheric currents, *Planet. Space Sci.*, **23**, 1355-1368, 1975.

(Received June 17, 1978;
accepted July 10, 1978.)

AD-A090 017

BOSTON COLL CHESTNUT HILL MA DEPT OF PHYSICS F/6 8/14
PHENOMENOLOGICAL AND THEORETICAL STUDIES ON MAGNETIC INDICATORS--ETC(U)
MAR 80 R L CAROVILLANO, R E SHEEHAN F19628-77-C-0085

UNCLASSIFIED

AFGL-TR-80-0094

NL

2-1-8
AN
ADVISOR

END
DATE
FORMED
10-80
DTIC

Reprinted from Geophysical Monograph, Vol. 21

IONOSPHERIC ELECTRIC FIELDS DRIVEN BY FIELD-ALIGNED CURRENTS

R. W. Nopper, Jr. and R. L. Carovillano

Department of Physics, Boston College
Chestnut Hill, Massachusetts 02167

Abstract. Field-aligned currents provide an important coupling between magnetospheric and ionospheric processes, driving ionospheric electric fields on a global scale. We have developed a model in which global distributions of electric fields and currents are calculated using mathematical boundary conditions on field-aligned currents that are chosen to correspond to observations made on the Triad satellite. The ionospheric conductivity tensor is represented empirically and includes spatial inhomogeneities resulting from the solar-zenith angle variation and a local auroral zone enhancement. Numerical results are accurate over the entire latitude range, pole to equator.

One application made was to examine the role of the ionospheric conductivity in coupling electric fields from high to low latitude. Ground magnetic observations and direct measurements of equatorial ionospheric phenomena have indicated that magnetospheric coupling effects penetrate at least to $L = 3.2$ during quiet times and to the equator during disturbed times. Calculations using quiet-time sources as observed by Triad yield electric fields at all latitudes which are at least comparable in strength to those produced by dynamo wind models and which have non-diurnal morphologies. In our calculations for disturbed times, imposed fluctuations in the strength of the field-aligned (Region 2) currents are found to produce large variations in the mid- and low-latitude electric field and account for reversal from its quiet time configuration, as is often observed. The electric field in the polar cap is shown to vary significantly in response to substorm conditions when Region 2 currents are appreciable. We conclude that under both quiet and disturbed conditions magnetospheric sources produce ionospheric effects on a global scale.

Introduction

Most past efforts at modeling the coupling between the magnetosphere and ionosphere have excluded proper consideration of the low-latitude ionosphere. The importance of auroral zone effects on the coupling has recently been emphasized with the observations that have established Birkeland currents to be a permanent feature at high latitudes. Important low-latitude effects occur essentially by leakage of current from high latitudes. Thus, calculated ionospheric results of Wolf [1970], Jaggi and Wolf [1973], Maeda and Maekawa [1973], Lyatsky et al. [1974], Yasuhara et al. [1975], and others are generally adequate at high latitudes but are not designed to apply at middle and low latitudes.

558 IONOSPHERIC ELECTRIC FIELDS DRIVEN BY FIELD-ALIGNED CURRENTS

Ionospheric evidence is now available that suggests a direct relationship between high- and low-latitude phenomena. Thus, during disturbed times, rapid magnetic variations closely correlated in time are observed at auroral zone and equatorial stations (e.g., Akasofu and Chapman [1963]; Onwumechili et al. [1973]). Ionospheric electric fields and currents sometimes fluctuate and reverse in concert with this class of magnetic fluctuations as shown by correlative studies of magnetograms and radar measurements of mid- and low-latitude ionospheric plasma drift episodes (e.g., Balsley [1966], Van Zandt et al. [1971], Carter et al. [1976], Fejer et al. [1976]), and other ionospheric phenomena, such as the sudden disappearance of equatorial sporadic-E and vhf radar echoes (Cohen and Bowles [1963], Rastogi [1977], Rastogi et al. [1977], Patel [1978]). Thus the existence of a polar-equatorial ionospheric coupling during disturbed times is documented observationally.

At quiet times, Matsushita [1971] and Leont'yev and Lyatskiy [1975] proposed that the Sq equivalent current system might be driven in part by magnetospheric sources, the conventional generating mechanism being the E-region dynamo. Observationally, F-region plasma drift measurements at Millstone Hill by Carpenter and Kirchhoff [1974, 1975] corroborate a magnetospheric origin for the quiet-time electric field down to $L = 3.2$. More recently, Gonzales et al. [1978] have shown that only in extremely quiet times is the classical dynamo effect dominant over magnetospheric sources in plasma drifts seen at Millstone Hill. It remains an open question how far equatorward the quiet-time configuration of magnetospheric sources exerts a measurable effect.

Our motivation to calculate the distribution of ionospheric electric fields was to evaluate the degree of coupling between the high- and low-latitude ionospheres. As detailed in the next section, our modeling procedure utilizes a realistic model of the ionospheric conductivity and the observed field-aligned current distribution; careful numerical treatment of dip-angle effects in the equatorial regions renders the calculation accurate globally. These inputs (conductivity and Birke-land current) can be modified to conform to improved empirical requirements or special physical circumstances. Model results are presented both for quiet and for disturbed periods. We find that magnetospheric sources contribute on an equal footing with calculated dynamo sources to the quiet-time electric field morphologies at all latitudes; on the other hand, magnetospheric sources alone produce large enough electric field variations at middle and low latitudes to account for observed disturbed-time fluctuations and reversals. Thus effects of magnetospheric coupling to the ionosphere are significant at all latitudes during both quiet and disturbed times.

Definition of the Model

Our approach is to solve the equation of continuity of the height-integrated ionospheric current, given the ionospheric conductivity distribution $\Sigma(\theta, \phi)$ and the driving field-aligned currents $J(\text{source})$. The electric fields we calculate may not be the total ionospheric field; for example, we do not include neutral wind effects. We impose boundary conditions that require north-south symmetry in the conductivities and sources. If (θ, ϕ) denote the co-latitude and azimuth and ∇_{\perp} is the transverse gradient, we obtain the ionospheric potential $\phi(\theta, \phi)$ from the equation of continuity

$$J(\text{source}) = \nabla_2 \cdot \underline{\Sigma}(\theta, \phi) \cdot \nabla_2 \phi(\theta, \phi)$$

by numerically relaxing its finite difference representation on a 30 x 30 grid of nodal points covering the northern hemisphere ionosphere. Southern hemisphere results are determined by the symmetry condition of zero current crossing the equator. The numerical accuracy is verified by checking that the calculated current is locally conserved among adjacent nodal points to a good approximation. The calculated electric fields are accurate solutions to the continuity equation (with assumed source and conductivity models) within a few percent everywhere on the grid.

The ionospheric height-integrated conductivities are expressed by simple functions multiplied by adjustable coefficients. These expressions give a good fit to the principal structures observed, namely, a base level constant conductivity (denoted by subscript "K") a solar-zenith angle variation (subscript "X"), and an auroral enhancement (subscript "A"):

$$\begin{aligned} \text{Pedersen} \quad \Sigma_p(\theta, \phi) &= \Sigma_{PK} + \Sigma_{PX} \exp \{-[\cos^{-1}(\sin\theta \cos\phi)]^2/1.804\} \\ &\quad + \Sigma_{PA} \exp \{-[\theta - 0.35]^2/0.01\} \text{ mhos,} \end{aligned}$$

$$\begin{aligned} \text{Hall} \quad \Sigma_H(\theta, \phi) &= \Sigma_{HK} + \Sigma_{HX} \exp \{-[\cos^{-1}(\sin\theta \cos\phi)]^2/1.804\} \\ &\quad + \Sigma_{HA} \exp \{-[\theta - 0.35]^2/0.01\} \text{ mhos,} \end{aligned}$$

$$\text{direct} \quad \Sigma_O(\theta, \phi) = 31.62 \Sigma_p(\theta, \phi) \text{ mhos.}$$

Here, θ and ϕ (measured eastward from noon) are in radians. The coefficients are chosen to reproduce the most characteristic or typical values from Kennel and Rees [1972], Rowe and Mathews [1973], Brekke et al. [1974], and others. Those employed in the present modeling are as follows:

	Σ_{PK}	Σ_{PX}	Σ_{PA}	Σ_{HK}	Σ_{HX}	Σ_{HA}
Quiet	0.3	5.0	3.0	0.6	10.0	6.0
Disturbed	0.3	5.0	6.0	0.6	10.0	18.0

These conductivities are then adjusted for dip angle effects in the usual way [Rishbeth and Garriott, 1969] to yield the elements of the tensor $\underline{\Sigma}(\theta, \phi)$ used in the continuity equation. Figure 1 illustrates the variation in Σ_{p0} as a function of θ along the noon-midnight meridian. Note the different auroral enhancements, peaking at 69° latitude, for quiet and disturbed times, and the 20 to 1 contrast between day and night values.

For driving currents we utilize the Triad results reported by Iijima and Potemra [1976, 1978], shown in Figure 2. These consist of two large-scale current structures: Region 1, often associated with magnetospheric convection, which flows into the ionosphere on the dawn-side and out on the dusk-side; Region 2, often correlated with auroral electrojet activity, which has the opposite polarity. In our idealiza-

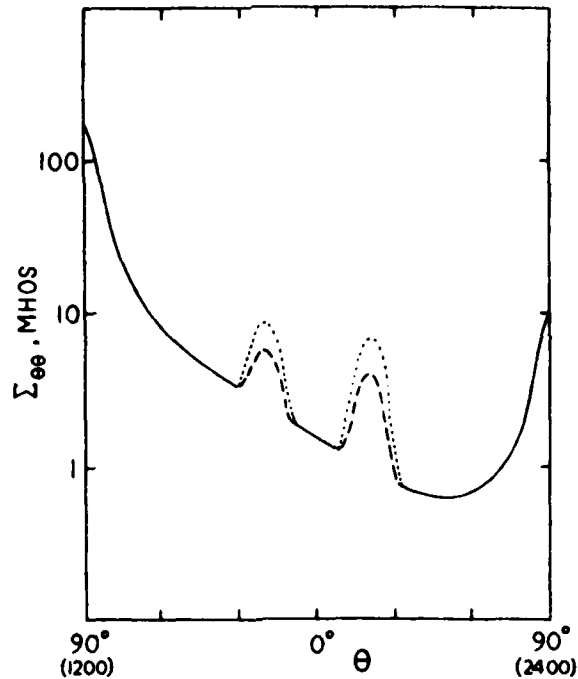


Fig. 1. Variation of conductivity tensor element $\Sigma_{\theta\theta}$ along the noon-midnight meridian from the dayside to the pole to the nightside equator. The dashed (dotted) portions give the model auroral conductivity values during quiet (disturbed) times.

tions, Region 1 currents are located at latitude 72° , and Region 2 at 66° . We abstract the quiet- and disturbed-time current strengths from the Triad results to be:

	<u>Region 1</u>	<u>Region 2</u>
Quiet	10^6 A	5×10^5 A
Disturbed	10^6 A	10^6 A

It is characteristic of quiet times that the Region 1 currents are roughly twice as strong as the Region 2, whereas during more active periods the two sets carry equal currents, from 10^6 A (as tabulated here) to several times 10^6 A.

At present there is no definitive empirical evidence available that specifies the origin or the time-dependent behavior of the field-aligned currents. Likewise, theoretical simulation efforts of the dynamical

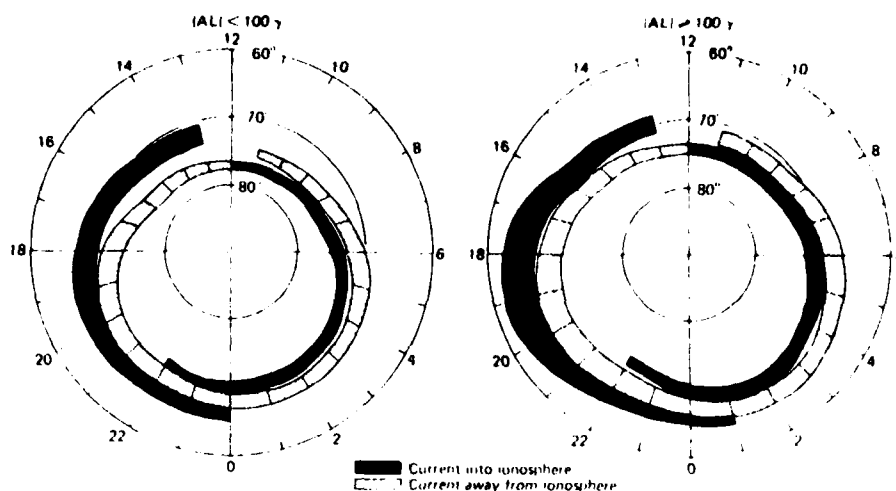


Fig. 2. The field-aligned current distributions determined using the Triad satellite [Iijima and Potemra, 1978].

processes that couple the magnetosphere and ionosphere are in their early stages of development. (See the paper by Harel et al., this volume.) The Triad results adopted in our modeling scheme have only a statistical significance; thus our calculated results would only have statistical significance and would not necessarily be representative of particular events on a case by case basis. Rather, our results should characterize typical distributions of ionospheric electric fields and currents that are generated by typically observed field-aligned currents.

Quiet-Time Results

Our main interest in this first application is to determine the contribution made by the field-aligned currents to the quiet time electric field morphology at middle and low latitudes. In Figure 3 the equipotential curves are given for the quiet-time modeling parameters presented above. It is seen that a two-cell pattern results from the quiet time pattern of Region 1 and Region 2 currents. This agrees with the two-cell convection patterns of Heppner [1977]. The polar-cap field is directed roughly dawn to dusk with magnitude 23 mV/m. There is a striking dusk-dawn asymmetry, in which duskside equipotentials are pushed toward higher latitudes and those on the dawnside are pulled to lower latitudes. This effect was explained by Wolf [1970] as due to the difference in conductivity between day and night. It is interesting to note, since the ionospheric currents are likewise asymmetrical, that even for a symmetrical disposition of field-aligned currents (as taken here) the resulting ground magnetic effect will be asymmetrical dusk to dawn.

Figure 4 shows the meridional (or θ) component of the electric field as a function of local time at the latitudes of Millstone Hill (54°)

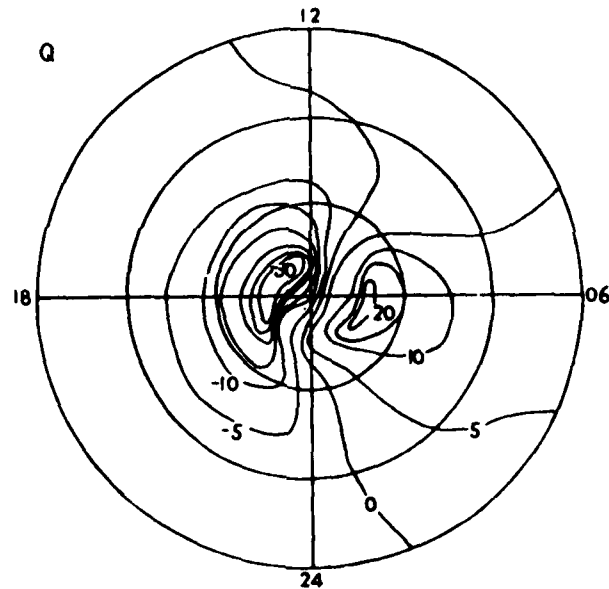


Fig. 3. Polar plot of the equipotential curves, in kV, for quiet times. Here, the Region 1 currents are twice as strong as the Region 2, and the auroral conductivity is moderate. Circles are centered at the pole at colatitude 30° , 60° , and 90° (the equator). The total cross-polar-cap potential drop is about 50 kV in this model.

and Arecibo (30°); E_θ at the equator is identically zero in these models. This field component would correspond to an eastward component of drift of ionospheric plasma. The calculated magnitudes, 5 mV/m at 54° and 1.5 mV/m at 30° , are approximately as large as those generated in neutral wind models [Matsushita and Tarpley, 1970]. Thus, magnetospheric sources and neutral winds must both be included and play comparable roles in modeling quiet time effects at low latitudes. Figure 4 displays a predominantly diurnal morphology at 54° , where maximum and minimum electric field values occur about twelve hours apart. In our model, the premidnight field is northwards and this would generate a westward F-region plasma drift at Millstone Hill; this drift is observed by Gonzales et al. [1978] on all but the quietest days. The classical dynamo effect, which gives southward fields in this sector, would be dominant over magnetospheric driving effects, according to our results, only during very quiet times.

In Figure 5 the azimuthal (or ϕ , positive eastwards) quiet-time electric fields are given at 54° , 30° , and the equator, corresponding to northward plasma drifts. Again the calculated magnitudes are com-

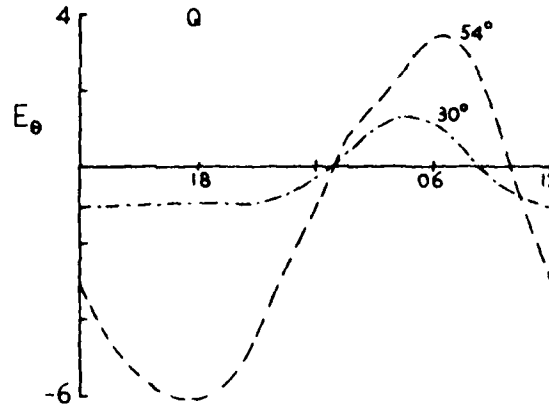


Fig. 4. Meridional component of the electric field, in mV/m, at 54° and 30° latitude, as a function of local time, for the quiet-time model (Q). Positive E_θ corresponds to a southward directed electric field.

parable to those from neutral wind models. A new result is that this component has strong non-diurnal Fourier components, with principal maxima and minima occurring about six hours apart. This results as a beating effect between the diurnal field-aligned source structure and the diurnal but out-of-phase conductivity distribution. To see the magnitude of the non-diurnal components, we idealize the morphologies of Figure 5 and show the Fourier amplitude spectrum of this signal in Figure 6. We find that the 12 hour component dominates over the diurnal, and that the 8 hour component is also quite strong. Thus the subdiurnal harmonics in observed quiet-time plasma drift morphologies (e.g., Blanc et al. [1977]) may have significant contributions from magnetospheric sources (as well as from the atmospheric dynamo).

Disturbed-Time Results

Our goal in modeling active times is to investigate the fluctuations and reversals observed in the otherwise quiet-time electric field at low latitudes. In order to do this it is necessary to impose a time-dependence in our modeling parameters. According to observations, Region 2 currents tend to be variable and roughly equal in intensity to the relatively fixed Region 1 currents during disturbed times [Iijima and Potemra, 1976, 1978]. In addition, the auroral conductivities increase, due to enhanced particle precipitation, during times when the auroral electrojets are active. Thus we adopt the basic disturbed-time model parameters as tabulated above in section 11. Fluctuations are considered to be alternating sequences of the quiet and disturbed model-results.

The disturbed time equipotential pattern is given in Figure 7. The

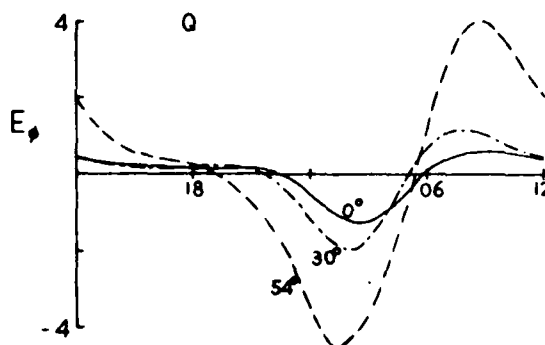


Fig. 5. Azimuthal component of the electric field (mV/m) at 54° , 30° , and 0° , as a function of local time, for quiet times (Q). Positive E_ϕ corresponds to an eastward directed field.

enhanced Region 2 source has moved the formerly prominent duskside vortex to the noon sector and reduced it in size. The equipotential curves tend to be distorted poleward (equatorward) on the dusk (dawn) side, as in the quiet-time model. An interesting feature of this case is the sunward-directed electric field over the polar cap. The magnitude and intensity of the polar cap electric field is a sensitive function of characteristics of the Region 2 current system. The sunward direction of the electric field shown in Figure 7 results because in this case the Region 1 and Region 2 currents have equal intensities. The direction would rotate towards dusk if the Region 2 intensity were decreased, and towards dawn if increased. The polar cap electric field is weak (8 mV/m her. because of the opposite polarity and equal strength of the Region 1 and Region 2 currents. Polar cap convection in this case is directed dawn-to-dusk. Such deviations from quiet-time antisunward convection are occasionally seen during disturbed periods (e.g., Heppner [1977]).

In Figure 8 a comparison is made of the azimuthal electric field components at 30° , between quiet- and disturbed-time results, curves Q and D'. Over most of local times, the strengthened Region 2 currents have reversed the electric field at this latitude. (The added auroral conductivity during disturbed times has little effect upon the reversal, as can be seen from curve D, which uses the sources of D' but the conductivity of Q.) The equatorial electric field is similar to that at 30° , but of roughly half the magnitude, as shown in Figure 9. Since the characteristic Triad active field-aligned current strengths often tend to be several times the value (10^6 A) used in obtaining Figures 7 through 9, it follows that the equatorial electric field can be several times that shown in these figures. Thus strengths up to 2 mV/m can sometimes be obtained and these will, for most local times, be directed oppositely to the quiet-time electric fields. Hence, variations in the Region 2 currents may be responsible for the fluctuations and reversals

NOPPER AND CAROVILLANO

565

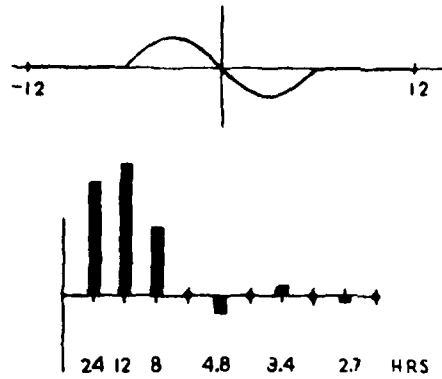


Fig. 6. Idealized morphology of the eastward electric fields in Figure 5, and the Fourier spectrum of this signal.

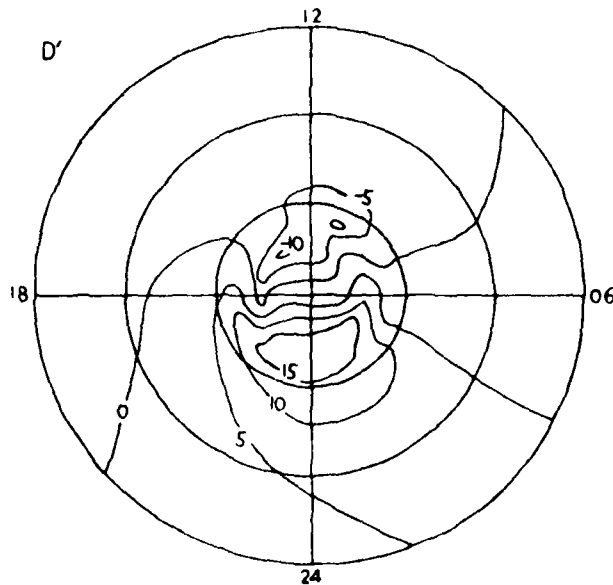


Fig. 7. Equipotential pattern corresponding to the disturbed-time model parameters: equal Region 1 and Region 2 currents and a greatly enhanced auroral conductivity.

566 IONOSPHERIC ELECTRIC FIELDS DRIVEN BY FIELD-ALIGNED CURRENTS

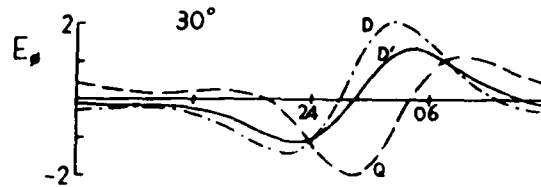


Fig. 8. Azimuthal electric field components at 30° for quiet (Q) and disturbed (D') models. (Model D utilizes sources of D' and conductivities of Q.) Fluctuations in the strength of the Region 2 currents and auroral precipitation would cause this electric field component to vary between Q and D'.

in the equatorial electric field and associated ionospheric phenomena, as referenced earlier. The observed rapid variations in the equatorial field cannot be accounted for by the neutral wind system with its large inertia and slower response time. Further discussion of this case is given in Nopper and Carovillano [1978].

Summary and Conclusions

The principal outcome of our modeling study is the calculation of relatively large electric fields due to magnetospheric sources at all ionospheric latitudes. During quiet times, the observed configuration of field-aligned currents contributes large magnitudes and non-diurnal spectral terms to mid- and low-latitude electric fields and, consequently, to plasma drifts. These effects of magnetospheric origin should not be excluded from models of the quiet ionosphere since they compete with the traditional source of quiet-time variations, dynamo winds. Adopting a plausible model for time variations in the Region 2 currents leads to an explanation of the fluctuations and reversals of the low-latitude electric field observed in disturbed times. Region 2 currents also affect the direction and magnitude of polar cap electric fields in an important way. In summary, the dynamics of the magnetosphere/ionosphere coupled system, as manifest in field-aligned currents,

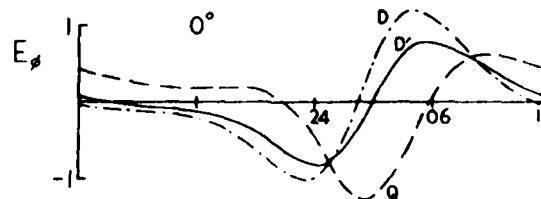


Fig. 9. Same as Figure 8 for the equator.

exerts a global influence on the ionosphere for all but the quietest levels of geomagnetic activity.

Acknowledgements. The authors are grateful to N. U. Crooker, G. L. Siscoe, and M. A. Heinemann for discussions on various aspects of this research. This research was supported by the Atmospheric Sciences Section, National Science Foundation, under Grant ATM75-22873, and by the Air Force Geophysics Laboratory under Contract F19628-77-C-0085.

References

- Akasofu, S. -I. and S. Chapman, The enhancement of the equatorial electrojet during polar magnetic storms, J. Geophys. Res., **68**, 2375-2382, 1963.
- Balsley, B. B., Evidence of the nighttime current reversal in the equatorial electrojet, Ann. Geophys., **22**, 460-462, 1966.
- Blanc, M., P. Amayenc, P. Bauer, and C. Taieb, Electric field induced drifts from the French incoherent scatter facility, J. Geophys. Res., **82**, 87-97, 1977.
- Brekke, A., J. R. Doupnik, and P. M. Banks, Incoherent scatter measurements of E region conductivities and currents in the auroral zone, J. Geophys. Res., **79**, 3773-3790, 1974.
- Carpenter, L. A., and V. W. J. H. Kirchhoff, Daytime three-dimensional drifts at Millstone Hill Observatory, Radio Sci., **9**, 217-222, 1974.
- Carpenter, L. A., and V. W. J. H. Kirchhoff, Comparison of high-latitude and mid-latitude ionospheric electric fields, J. Geophys. Res., **80**, 1810-1814, 1975.
- Carter, D. A., B. B. Balsley, and W. L. Ecklund, VHF Doppler radar observations of the African equatorial electrojet, J. Geophys. Res., **81**, 2786-2794, 1976.
- Cohen, R., and K. L. Bowles, Ionospheric VHF scattering near the magnetic equator during the International Geophysical Year, J. Res. NBS, sect. D., **67D**, 459-480, 1963.
- Fejer, B. G., D. T. Farley, B. B. Balsley, and R. F. Woodman, Radar studies of anomalous velocity reversals in the equatorial ionosphere, J. Geophys. Res., **81**, 4621-4626, 1976.
- Gonzales, C. A., M. C. Kelley, L. A. Carpenter, and R. H. Holzworth, Evidence for a magnetospheric effect on mid-latitude electric fields, J. Geophys. Res., **83**, 4397-4399, 1978.
- Harel, M., R. A. Wolf, and P. H. Reiff, Computer modeling of events in the inner magnetosphere, Quantitative Modeling of Magnetospheric Processes, Geophys. Monogr. Ser., vol. 21, ed. by W. P. Olson, AGU, Washington, D.C., 1979.
- Heppner, J. P., Empirical models of high-latitude electric fields, J. Geophys. Res., **82**, 1115-1125, 1977.
- Iijima, T., and T. A. Potemra, The amplitude distribution of field-aligned currents at northern high latitudes observed by Triad, J. Geophys. Res., **81**, 2165-2174, 1976.
- Iijima, T., and T. A. Potemra, Large-scale characteristics of field-aligned currents associated with substorms, J. Geophys. Res., **83**, 599-615, 1978.
- Jaggi, R. K., and R. A. Wolf, Self-consistent calculation of the motion

568 IONOSPHERIC ELECTRIC FIELDS DRIVEN BY FIELD-ALIGNED CURRENTS

- of a sheet of ions in the magnetosphere, J. Geophys. Res., 78, 2852-2866, 1973.
- Kennel, C. F., and M. H. Rees, Dayside auroral-oval plasma density and conductivity enhancements due to magnetosheath electron precipitation, J. Geophys. Res., 77, 2294-2302, 1972.
- Leont'yev, S. V., and V. B. Lyatskiy, Three-dimensional current system of a partial ring current; relation between DP2 and Sq variations, Geomagn. Aeron., 15, 91-94, 1975.
- Lyatskiy, W. B., Yu. P. Maltsev, and S. V. Leontyev, Three-dimensional current system in different phases of a substorm, Planet. Space Sci., 22, 1231-1247, 1974.
- Maeda, H., and K. Maekawa, A numerical study of polar ionospheric currents, Planet. Space Sci., 21, 1287-1300, 1973.
- Matsushita, S., Interactions between the ionosphere and magnetosphere for Sq and L variations, Radio Sci., 6, 279-294, 1971.
- Matsushita, S., and J. D. Tarpley, Effects of dynamo-region electric fields on the magnetosphere, J. Geophys. Res., 75, 5433-5443, 1970.
- Nopper, R. W., Jr., and R. L. Carovillano, Polar-equatorial coupling during magnetically active periods, Geophys. Res. Lett., 5, 699-702, 1978.
- Onwumehili, A., K. Kawasaki, and S. -I. Akasofu, Relationships between the equatorial electrojet and polar magnetic variations, Planet. Space Sci., 21, 1-16, 1973.
- Patel, V. L., Interplanetary magnetic field variations and the electromagnetic state of the equatorial ionosphere, J. Geophys. Res., 83, 2137-2144, 1978.
- Rastogi, R. G., Coupling between equatorial and auroral ionospheres during polar substorms, Proc. Indian Acad. Sci., 86A, 409-416, 1977.
- Rastogi, R. G., B. G. Fejer, and R. F. Woodman, Sudden disappearance of VHF radar echoes from equatorial E-region irregularities, Indian J. Radio and Sp. Phys., 6, 39-43, 1977.
- Lishbeth, H., and O. K. Garriott, Introduction to Ionospheric Physics, Academic Press, New York, 1969.
- Rowe, J. F., Jr., and J. D. Mathews, Low-latitude nighttime E-region conductivities, J. Geophys. Res., 78, 7461-7470, 1973.
- Van Zandt, T. E., V. L. Peterson, and A. R. Laird, Electromagnetic drift of the mid-latitude F₂ layer during a storm, J. Geophys. Res., 76, 278-281, 1971.
- Wali, R. A., Effects of ionospheric conductivity on convective flow of plasma in the magnetosphere, J. Geophys. Res., 75, 4677-4698, 1970.
- Yasuhara, F., Y. Kamide, and S. -I. Akasofu, Field-aligned and ionospheric currents, Planet. Space Sci., 23, 1355-1368, 1975.

On the Orientation of the Polar Cap Electric Field

R. W. NOPPER, JR., AND R. L. CAROVILLANO

Department of Physics, Boston College, Chestnut Hill, Massachusetts 02167

Using realistic models of the ionospheric conductivity and the field-aligned currents, we have determined how the distribution of the electric field in the polar cap ionosphere is controlled by the day-night contrast in conductivity and by the relative strengths of the region 1 and region 2 field-aligned currents. The sunward directed conductivity gradient acts to set up a space charge in the polar cap which crowds the equipotentials toward the dawn sector for current sources of both region 1 and region 2 polarity, this effectively shifts the polar cap convection pattern toward dawn. Our results show further that for a given conductivity distribution the orientation of the electric field in the central polar cap depends sensitively on the relative strengths of the Birkeland current pairs: for very weak region 2 currents (quiet times) the polar electric field is directed $\approx 60^\circ$ east of noon, for equal region 1 and 2 currents (disturbed times) the direction is $\approx 10^\circ$ east of noon, and for stronger region 2 than 1 currents (which may happen on occasion) the electric field points into the prenoon sector. These findings imply that the orientation of the polar cap electric field should serve as a measure or index of the ratio of region 1 to region 2 net current intensity and should possess correlations with geomagnetic activity similar to those of this ratio. This analysis does not include effects of possible source currents in the region of the polar cusp.

1. INTRODUCTION

Although the electric field in the polar cap is often described as being directed dawn to dusk, it is well known that only rarely is this precisely the case. In fact, both the electric field magnitude and the electric field direction across the polar cap are known to change in response to variations in a number of effects, including the season of the year and the values of various components of the IMF (interplanetary magnetic field) [e.g., Langel, 1974; Heppner, 1977; Fairfield, 1977]. Such observations indicate that the patterns of plasma convection (or electrostatic equipotential lines) frequently differ from uniform antisunward flow.

In recent years the Triad, Isis 2, and S3-2 spacecraft have measured vector magnetic field fluctuations that indicate the presence of field-aligned currents, and a synoptic pattern for these currents has been defined [Iijima and Potemra, 1978]. In addition, atmospheric models are constantly being improved [Jacchia, 1977], and the technique of incoherent scatter radar has been useful in obtaining measurements of ionospheric conductivities, thus allowing fairly realistic conductivity models to be developed. Treating the observed field-aligned currents as driving terms and given the ionospheric conductivity distribution, one can calculate the distributions of ionospheric electric field and current which would result in that model situation. Recent efforts of this sort have been made by Yasuhara *et al.* [1975], Maekawa and Maeda [1978], Nisbet *et al.* [1978], Nopper and Carovillano [1978, 1979], and Kamide and Matsushita [1979]. The last three references utilized conductivity models that represent the principal structure observed (variation with solar zenith angle and auroral enhancement) and are intended to apply globally.

The purpose of this brief note is to discuss properties of the electric field in the polar cap. We note that even for a symmetrical disposition of field-aligned currents, an idealized model situation, the electric field at the pole is usually not directed dawn to dusk. In addition, our calculations show that the direction of the polar cap electric field is a sensitive function of the relative strengths of the field-aligned current sheets (region 1 and 2 current pairs). Since the relative strengths of

these input currents are known to vary with geomagnetic activity, one would expect the polar cap electric field direction to show a similar dependence.

2. THE MODELING SCHEME

We have developed a numerical procedure to solve the equation for the continuity of ionospheric current,

$$J(\text{source}) = \nabla_{\perp} \cdot \Sigma(\theta, \phi) \cdot \nabla_{\perp} \Phi(\theta, \phi)$$

using finite difference methods and an iterative technique. Here, Φ is the ionospheric electrostatic potential, from which the ionospheric electric field and current distributions are obtained. The assumed representations for the height-integrated tensor conductivity Σ and for the driving field-aligned currents $J(\text{source})$ are discussed briefly below. We ignore dynamo winds, which are expected to play a secondary role in the high-latitude region of interest here. The accuracy of numerical results is checked by applying a test based upon Gauss's law in two dimensions to various areas of the numerical grid. This check certifies that ionospheric current is locally conserved everywhere on the grid to within a few percent.

Our empirical conductivity model is given by simple functions of position multiplied by adjustable coefficients. The functions are designed to give reasonable approximations to the solar zenith angle and auroral variations of conductivity, and the coefficients are selected to give agreement to published observed values [e.g., Brekke *et al.*, 1974; Rowe and Mathews, 1973]. With θ the colatitude and ϕ the azimuth measured eastward from noon the conductivity model employed in the present study is, in mhos,

Pedersen

$$\Sigma_p(\theta, \phi) = 0.3 + 5.0 \exp \{ -[\cos^{-1}(\sin \theta \cos \phi)]^2 / 1.804 \} \\ + 3.0 \exp \{ -(\theta - 0.35)^2 / 0.01 \}$$

Hall

$$\Sigma_H(\theta, \phi) = 2.0 \Sigma_p(\theta, \phi)$$

Direct

$$\Sigma_D(\theta, \phi) = 31.62 \Sigma_p(\theta, \phi)$$

Copyright © 1979 by the American Geophysical Union.

Paper number 9A0820
0148-0227/79/009A-0820\$01.00

6489

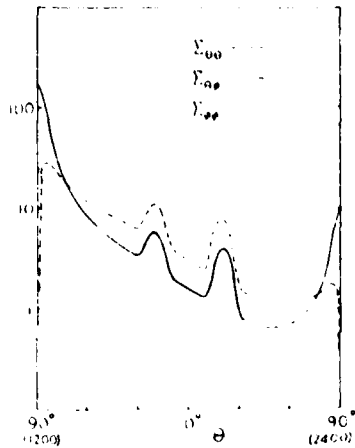


Fig. 1. The variations in tensor conductivity elements $\Sigma_{\theta\theta}$, $\Sigma_{\phi\phi}$, and $\Sigma_{\theta\phi}$ along the noon-midnight meridian (i.e., from the noon equator to the pole to the midnight equator).

These expressions are used in the usual formulas [e.g., *Rishbeth and Garriott, 1969*] for the elements of the layer conductivity tensor $\Sigma(\theta, \phi)$ appearing in the continuity equation. Figure 1 shows the variation of these elements along the meridian from the equator at noon to the pole to the equator at midnight. Azimuthally symmetrical auroral zone enhancements peaked at 69° latitude are superposed on the background conductivity, which has a 20:1 day-to-night contrast. This conductivity model is symmetrical between northern and southern hemispheres. We calculate northern hemisphere results using the boundary condition of zero meridional current at the equator.

The driving currents used are based upon the statistical Triad results reported by *Iijima and Potemra [1978]*. These results indicate the existence of two distinct sets of large-scale

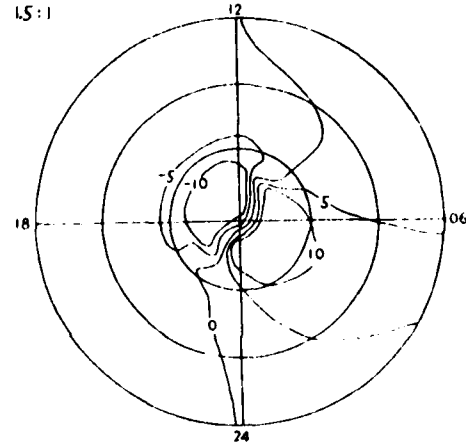


Fig. 2b

field-aligned current: region 1 currents flow into the ionosphere at the high-latitude edge of the auroral oval on the dawnside and out of the ionosphere on the duskside; region 2 currents have the opposite polarity and are located somewhat equatorward of the region 1 set. Both regions have a large spread in azimuth and overlap near midnight. Characteristically, in weakly disturbed periods the region 1 set carries about 10^6 A, and the region 2 half to three quarters of that value. (In quiet periods the region 2 set is weaker and may even be absent.) During active periods, however, the strengths of both sets increase to perhaps 3×10^6 A, and the region 2 set may even exceed the region 1 set in net amperage. For our present purposes we have idealized the above as follows. The region 1 currents are applied in two bands, extending azimuthally from 18° to 150° (duskside) and from 210° to 342° (dawnside) at 72° latitude; the region 2 currents are in bands with the same azimuthal extents but at 66° latitude. Since one purpose of this note is to illustrate the effect of changing the ratio of region 1 and region 2 current strength, the region 1 source is held fixed at 10^6 A, and the region 2 source is varied to give region 1/region 2 ratios of 2:1, 1.5:1, 1:1, 1:1.5, and 1:2. The last two ratios are included here for pedagogical purposes and probably do not occur in practice, since the current intensity in region 2 is rarely reported to exceed that in region

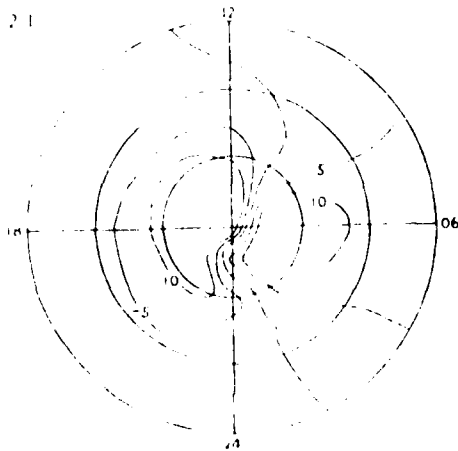


Fig. 2a

Fig. 2. Polar plots of the equipotential patterns for the conductivity model and field-aligned currents given in section 2. In each figure the same five equipotential curves (labeled in kilovolts) are shown. The outer circle is the equator, the inner ones are 30° and 60° latitude. The ratios of region 1 and region 2 current strength are (a) 2, (b) 1.5, (c) 1, (d) 0.67, and (e) 0.5. In all cases the region 1 current was 10^6 A. The resulting polar cap electric field orientations are about (a) $+50^\circ$, (b) 40° , (c) 12° , (d) -48° , and (e) -72° , measured counterclockwise from noon.

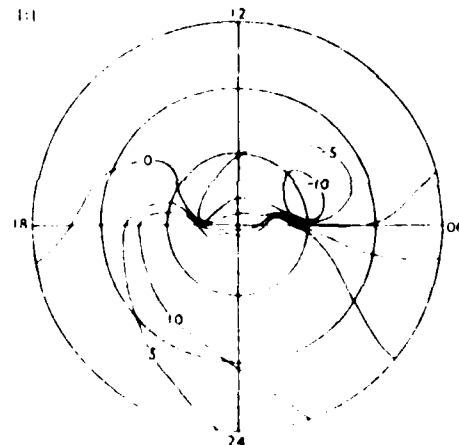


Fig. 2c

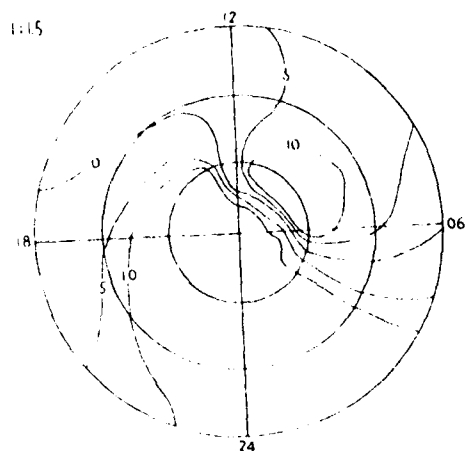


Fig. 2d

1. The effects of input currents in the region of the polar cusp are not included in this analysis.

3. DISCUSSION AND RESULTS

Before considering our calculated results it is useful to review polar cap equipotential patterns under simpler circumstances. In the presence of only symmetrically located region 1 sources, if the Pedersen conductivity were uniform and the Hall conductivity absent then the equipotentials would possess dawn-to-dusk symmetry, and the electric field would essentially point from dawn to dusk. The effect of a nonzero Hall conductivity is demonstrated in the axisymmetrical model of Vasyliunas [1970]; this model has a driving source that is sinusoidal in azimuth, neglects day-night variations in conductivity, and includes an enhanced auroral conductivity band. For this case, polar cap equipotentials remain uniform and sun aligned, although auroral and subauroral equipotentials are rotated because of the band of enhanced auroral conductivity. Thus such axisymmetrical modeling variations have no effect on the orientation of the electric field or the distribution of equipotentials in the polar cap.

The condition of axisymmetry was broken by Wolf [1970], who included a realistic variation with solar zenith angle in the conductivity tensor; however, his model was not applied to the polar cap. Atkinson and Hutchison [1978] have recently presented analytical results for Pedersen and Hall con-

ductivities that decrease exponentially across the polar cap. They find that the steeper the day-night conductivity decrease from noon to midnight is, the more the equipotential lines are squeezed into the dawn sector of the polar cap. The corresponding effect was essentially seen and explained earlier by Wolf [1970] in his analysis of mid-latitude equipotentials. In the polar cap the combined effect of the polarity of the Birke-land currents (in at dawn, out at dusk, or vice versa) and the direction of the conductivity gradient produces an electric field more intense at dawn than at dusk. Equipotential lines are therefore more dense near dawn than at dusk. This effect arises physically because of the charge density (proportional to $-\nabla \Sigma_p \cdot \mathbf{l}$, where \mathbf{l} is the total current) generated by the day-night conductivity gradient. This charge density is negative for region 1 polarity and positive for region 2 polarity, because of the reversed direction of the Hall current, and increases in magnitude toward the dayside. Thus for either polarity the density of the equipotential lines is greater in the dawn sector than in the dusk sector. Of course, the polar cap electric fields generated by region 1 and region 2 polarities are oppositely directed and, for example, give rise to oppositely directed convection patterns.

For a fixed source the distortion of the equipotentials and the direction of the electric field are controlled by the conductivity gradient. This feature can be seen in the results of Atkinson and Hutchison [1978] for symmetrical sources, where the polar cap electric field direction always differs from dawn to dusk and is further altered by the steepness of the conductivity gradient. The effect of the conductivity gradient can also be seen in our earlier work [Nopper and Carovillano, 1978, 1979] and in the calculations of Nisbet et al. [1978] and Kamide and Matsushita [1979]. In our present calculations we show, in addition, how the direction of the polar cap electric field is affected by the relative intensity of the region 1 and region 2 current sources.

In Figures 2a-2e we show the global patterns of the same five equipotential lines for the ratios 2, 1.5, 1, 2/3, and 1/2 of region 1 to region 2 current, as defined in section 2. (Region 1 currents are fixed at 10⁶ A for these calculations.)

Figure 2a would correspond roughly to a quiet time field-aligned current configuration. The mid-latitude equipotential pattern follows the 'midlatitude rules' given by Wolf [1970]: the duskside (dawnside) equipotentials are distorted toward (away from) the pole by the action of the day-night conductivity asymmetry. The polar cap equipotentials are more dense in the dawn sector, as discussed above. The direction of electric field at the pole is about +50° (i.e., east of noon).

The region 2 source intensity increases in strength in the sequence of Figures 2b-e. These figures show the negative vortex to be decreasing in size and rotating about 180° across the dayside toward dawn, while the positive equipotentials rotate in the same sense (clockwise) through midnight toward dusk, eventually to form a large vortex there. (This vortex does not appear in Figure 2e because of our choice of displayed equipotentials.) In all cases the expected behavior of the equipotential shapes, given above, is seen. In the sequence of cases in Figure 2 the direction of the polar cap electric field is seen to rotate clockwise as the region 2 source intensity is increased. The direction goes from about +50° for the ratio 2:1 of region 1 to region 2 current intensities to about -70° for the ratio 1:2. To see the extremes for the cases represented, the polar cap electric field direction is +60° when region 2 currents are absent and -96° when region 1 currents are ab-

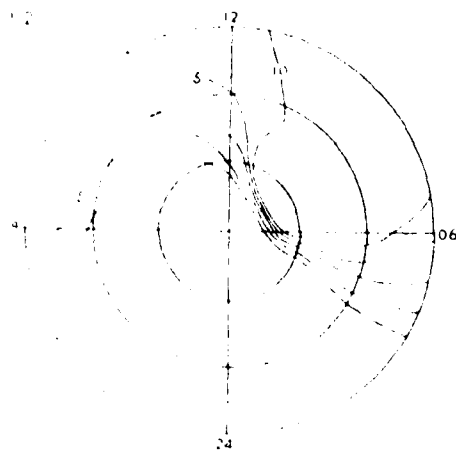


Fig. 2e

sent. The lack of symmetry between these extreme values is because the region 1 and 2 currents are applied at different latitudes. As was discussed earlier, these extreme values depend upon parameters in the conductivity model. (We will publish a further study on this issue.)

In summary, we have discussed how the direction of the polar cap electric field is affected by the day-night conductivity gradient and by the relative strengths of region 1 and region 2 currents. The effect of the conductivity gradient is to increase the density of equipotentials (and hence shift the polar cap convection pattern) in the dawn sector, as shown in the work of several authors [Atkinson and Hutchison, 1978; Nopper and Carovillano, 1978, 1979; Kamide and Matsushita, 1979; Nisbet *et al.*, 1978]. Our principal purpose is to display the dependence of the direction of the polar cap electric field on the ratio of region 1 to region 2 current intensities. This ratio is observed to vary from slightly greater than 2 to less than unity. In our calculations the direction of the polar cap electric field is found to depend sensitively on this ratio. Conversely, this leads us to suggest that measurement of the orientation of the polar cap electric field could serve as an index of the relative strength of region 1/region 2 currents and should possess correlations with geomagnetic activity similar to those of the ratio. Our results do not include effects of currents in the polar cusp region.

Acknowledgments. This research was supported by the Atmospheric Sciences Section, National Science Foundation, under grant ATM75-22873 and by the Air Force Geophysics Laboratory under contract F19628-77-C-0085.

The Editor thanks G. Atkinson and another referee for their assistance in evaluating this paper.

REFERENCES

- Atkinson, G., and D. Hutchison, Effects of the day-night ionospheric conductivity gradient on polar cap convective flow, *J. Geophys. Res.*, **83**, 725-729, 1978.
- Brekke, A., J. R. Doupnik, and P. M. Banks, Incoherent scatter measurements of E region conductivities and currents in the auroral zone, *J. Geophys. Res.*, **79**, 3773-3790, 1974.
- Fairfield, D. H., Electric and magnetic fields in the high-latitude magnetosphere, *Rev. Geophys. Space Phys.*, **15**, 285-298, 1977.
- Heppner, J. P., Empirical models of high-latitude electric fields, *J. Geophys. Res.*, **82**, 1115-1125, 1977.
- Iijima, T., and T. A. Potemra, Large-scale characteristics of field-aligned currents associated with substorms, *J. Geophys. Res.*, **83**, 599-615, 1978.
- Jacchia, L. G., Thermospheric temperature, density, and composition: New models, *Spec. Rep. 375*, Smithsonian Astrophys. Observ., Cambridge, Mass., 1977.
- Kamide, Y., and S. Matsushita, Simulation studies of ionospheric electric fields and currents in relation to field-aligned currents. 1. Quiet periods, *J. Geophys. Res.*, **84**, 4083-4098, 1979.
- Langel, R. A., Near-earth magnetic disturbance in total field at high latitudes. 2. Interpretation of data from Ogo 2, 4, and 6, *J. Geophys. Res.*, **79**, 2373-2392, 1974.
- Mackawa, K., and H. Maeda, Electric fields in the ionosphere produced by polar field-aligned currents, *Nature*, **273**, 849-850, 1978.
- Nisbet, J. S., M. J. Miller, and L. A. Carpenter, Currents and electric fields in the ionosphere due to field-aligned auroral currents, *J. Geophys. Res.*, **83**, 2647-2657, 1978.
- Nopper, R. W., Jr., and R. L. Carovillano, Polar-equatorial coupling during magnetically active periods, *Geophys. Res. Lett.*, **5**, 699-702, 1978.
- Nopper, R. W., Jr., and R. L. Carovillano, Ionospheric electric fields driven by field-aligned currents, in *Quantitative Modeling of Magnetospheric Processes*, *Geophys. Monogr. Ser.*, vol. 21, pp. 557-568, edited by W. P. Olson, AGU, Washington, D. C., 1979.
- Rishbeth, H., and O. K. Garriott, *Introduction to Ionospheric Physics*, Academic, New York, 1969.
- Rowe, J. F., Jr., and J. D. Mathews, Low-latitude nighttime E region conductivities, *J. Geophys. Res.*, **78**, 7461-7470, 1973.
- Vasyliunas, V. M., Mathematical models of magnetospheric convection and its coupling to the ionosphere, in *Particles and Fields in the Magnetosphere*, edited by B. M. McCormac, D. Reidel, Hingham, Mass., 1970.
- Wolf, R. A., Effects of ionospheric conductivity on convective flow of plasma in the magnetosphere, *J. Geophys. Res.*, **75**, 4677-4698, 1970.
- Yasuhara, F., Y. Kamide, and S.-I. Akasofu, Field-aligned and ionospheric currents, *Planet. Space Sci.*, **23**, 1355-1368, 1975.

(Received April 3, 1979;
revised May 21, 1979;
accepted May 21, 1979.)

E. Refinements of the Model

As indicated by the foregoing discussions, global ionospheric modeling is a worthy means to gain understanding of many physical effects and offers a wide range of possibilities for comparing theory and observation. To advance the utility of our model, a number of refinements are needed both in representing our input parameters in a more realistic fashion and in addressing a new class of physical effects. Here we shall briefly discuss possible improvements to the global modeling scheme.

The conductivity model used is adequate for general studies but can be refined to accord with the latest improved ionospheric models (e.g., Mehta, 1979), and particularly with auroral region incoherent scatter results (e.g., Vondrak and Vickrey, 1979; de la Beaujardiere et al., 1977) which provide a far more realistic picture of high-latitude conductivities for both quiet and active times. In order to maintain numerical accuracy, the high-latitude portion of the mesh will need to be refined, as observation shows the highly conducting auroral regions to possess abrupt gradients. Similar numerical techniques used for our model can be applied to the modeling of individual auroral arcs. Given the field-aligned currents over an arc and the ionospheric conductivity in that region, the distributions of electric field and current (electrojets) can be calculated. The parameters involved in such modeling can be determined in case studies from the ground and/or from rockets, so that a tight control on the calculations may be available. In addition to upgrading the auroral region conductivity, it would be useful to include a seasonal dependence in the model, in which the latitude of the subsolar point (where the conductivity is largest) changes with time of year. This seasonal effect would give rise to very large effects in the electric fields and currents at the equator and polar caps. For

example, the summer polar cap is much more conducting than the winter polar cap, and during equinox there is a strong gradient across the polar cap (Paper III). Thus, quantities which depend significantly upon polar cap conductivities, such as electric fields, convection patterns (equipotentials), and currents, can be expected to depend sensitively upon time of year.

In addition to the two major pairs of field-aligned currents modeled at present, there is another set observed in the cusp region (Iijima and Potemra, 1976) which seem to depend upon the y-component (B_y) of the interplanetary magnetic field (IMF) (Iijima et al., 1978; McDiarmid et al., 1977, 1978a, b, 1979; Wilhjelm et al., 1978). This is of importance because evidence has been accumulating that the interplanetary magnetic field affects the global ionosphere and hence could profitably be introduced into our modeling. For example, Maezawa (1976) and Burke et al. (1979) have postulated a correlation between the high latitude convection pattern and IMF B_z ; Heppner (1972, 1977), Friis-Christensen and Wilhjelm (1975), Wilhjelm et al. (1978), and McDiarmid et al. (1978b, 1979) have studied the relation of high latitude convection and IMF B_y . In middle latitudes, Matsushita (1975) has shown the dependence of the S_q current system focus on IMF B_y . At low latitudes, studies relating ionospheric electrodynamic effects and IMF B_z have been published by Patel (1978), Rastogi (1977), Rastogi and Chandra (1974), Rastogi and Kroehl (1978), Rastogi and Patel (1975), and Rastogi et al. (1978); correlation between ionospheric effects and B_y have been shown by Bhargava and Rangarajan (1977) and Galperin et al. (1978). A schematic summary of the salient observations for the northern high latitude region is given in Figure 4.3. Unfortunately, the inclusion of cusp currents to introduce an IMF-dependent effect into the modeling would greatly enlarge the computational task. These currents are anti-symmetrical (northern-to-southern hemisphere) whereas the Region 1 and 2 current sources used in our

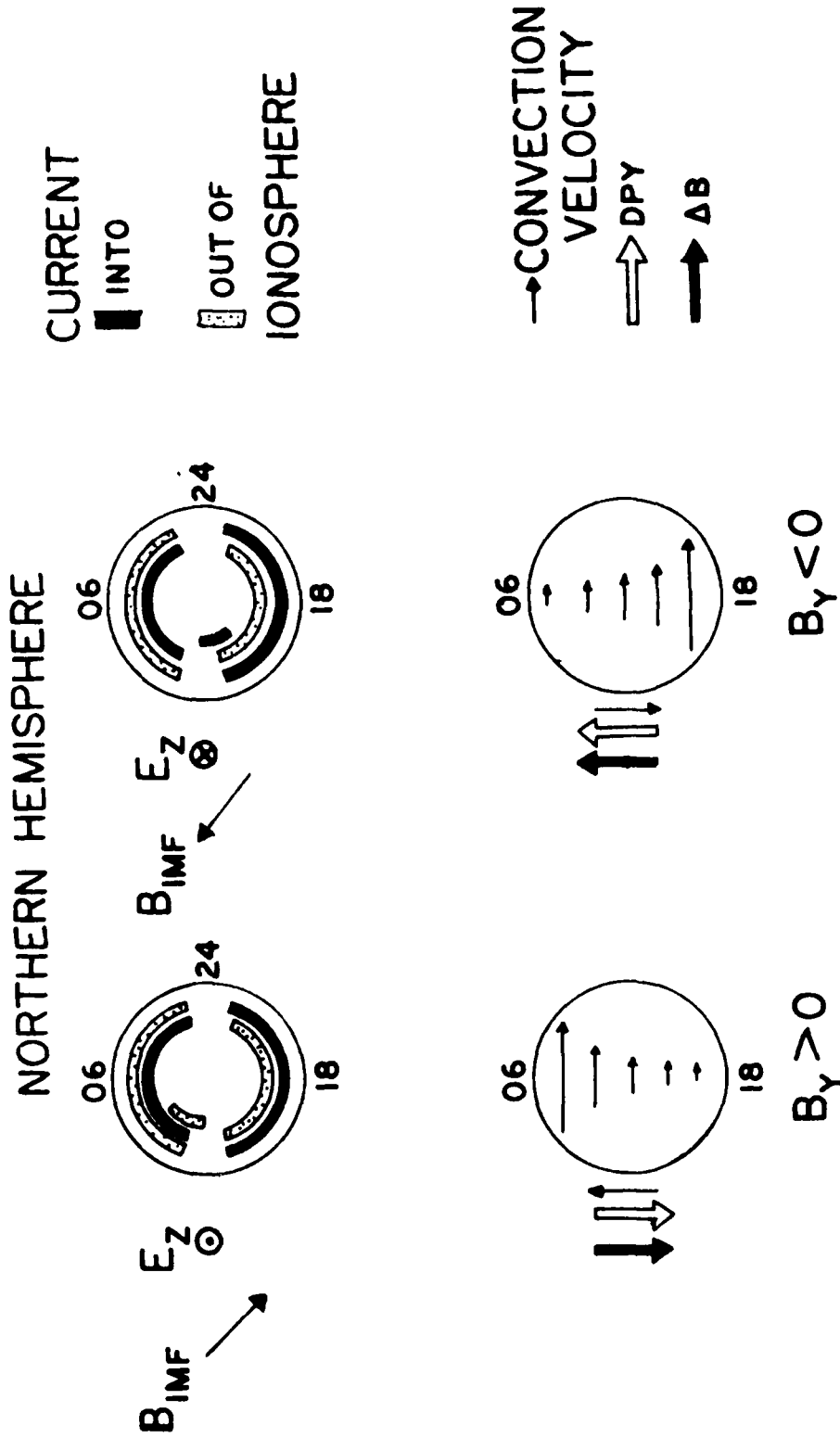


Figure 4.3 Illustration of northern hemisphere structure of observed field-aligned currents and correlative high-latitude phenomena for IMF B_y positive (left) and negative (right). The top panels show interplanetary magnetic and electric field components and observed Region 2, 1, and cusp currents. The bottom panels indicate Heppner's (1972) convection velocities in the polar cap, and the DPY equivalent currents (Fris-Christensen and Wilhelm, 1978) and ΔB of McDiarmid, et.al. (1978) in the cusp region.

present model are symmetrical. With symmetrical sources we are able to impose a boundary condition at the equator that greatly improves numerical accuracy and reduces the size of the calculational effort. With cusp-currents included, both hemispheres will need to be explicitly modeled and solutions obtained over the complete globe.

For a more complete picture of the ionospheric electric fields and currents during quiet and disturbed times, it would be necessary to include neutral winds in the dynamo (E) region of the ionosphere. For wind field \underline{u} , magnetic field \underline{B} , and conductivity $\underline{\Sigma}$, this source term has the form $\nabla \cdot \underline{\Sigma}(\underline{u} \times \underline{B})$. Strictly speaking, the neutral wind speed \underline{u} to be used in our formulation should be height-independent. Unfortunately, models of neutral winds do not provide such modes for us to adopt (Forbes and Lindzen, 1976); one exception is the (1,-2) mode, which fortuitously is the main contributor in quiet times (J. Forbes, pvt. communication). At the present time, there is actually no comprehensive dynamo wind model that has general acceptance. This problem limits the possibility of including neutral winds in our modeling scheme with a high degree of confidence, at least for the immediate future.

F. Magnetic Ground Signatures

The culmination of our model would be to relate predictions to ground magnetic signatures. Difficulties to be overcome to accomplish this task are discussed in this section. The problem is complicated by many factors, but significant advances are certainly possible if the proper time and effort is devoted to the task. Ground magnetic signatures are treated more specifically in chapter 5 within a well defined context.

There is a prodigious amount of information available to the space physics community in the form of magnetograms from thousands of station-years. Magnetic observatories are relatively inexpensive to instrument and operate and, since recent efforts at installing high-quality instruments in chains and/or networks

have been exerted, magnetic records will continue to form the core of our ground data base. Two ways in which magnetograms have been used for many years are: (1) the records from one or a small number of stations are inspected to infer limited information about nearby current systems (e.g., the use of auroral zone magnetograms to investigate electrojets); (2) the records from a global collection of stations are processed into "equivalent current systems" (see Stern (1977) for a discussion of the procedure). Recently, the equivalent current system concept has been greatly upgraded by the use of magnetometer arrays, which by virtue of a relatively dense distribution of instruments on a regular grid allows more information to be extracted from magnetic variation data than otherwise possible. Even with dense global coverage on the ground, however, it is not possible to infer the current system uniquely that is responsible for a given magnetic disturbance distributed over the globe. Special assumptions are needed to obtain a current system that corresponds to a given magnetic disturbance. Thus, to derive "equivalent current systems," the ansatz is made that all currents flow in the ionosphere (which is demonstrably false).

The task of inferring currents from a given magnetic disturbance is an "inverse problem" to the usual task of calculating the magnetic disturbance that results from a given set of currents in space. For specified boundary conditions, the magnetic field resulting from a given current configuration is unique. In contrast, the inverse problem is not unique. For example, Fukushima (1969) considered the problem of a vertical line current along the z-axis entering a uniformly conducting plane located at right angles to the z-axis. This current configuration - vertical line current plus distributed currents in the horizontal plane at $z=0$ - produces no magnetic field below the conducting plane (i.e., at $z<0$). Thus, if the ionosphere is approximated by a plane conductor, even at times of zero magnetic disturbance at the surface of the

earth there may or may not be overhead currents of magnetospheric origin. This simple example demonstrates that inferences to be made from ground magnetic observations of ionospheric and/or magnetospheric currents can only be made within the context of a model. In the "equivalent current" representation, the ground magnetic signature is assumed to be generated by currents confined completely to the ionosphere.

The development of realistic models to represent the magnetic signatures of ground observations is further complicated by induction effects within the earth. These induction effects "contaminate" the magnetic record in reflecting the external current system. For example, Nopper and Hermance (1974) have shown that, for substorm-like events, induction effects alter magnetic component disturbance magnitudes and introduce significant phase shifts. Early methods of quantifying effects of induction were the construction of "induction arrows" and the separation of magnetic fluctuations into internal and external parts using analytic techniques (e.g., Price, 1967). With the refinement of mathematical techniques and the introduction of arrays, more quantitative characterization of source and induced fields are now available (e.g., Schmucker, 1970a, b; Alabi et al., 1975). Gregori and Lanzerotti (1980) have reviewed this subject. Most of these studies have been aimed at determining earth conductivity structure and not ionospheric current configurations. The determination and removal of the effects of induction from ground magnetic observatory records constitutes a major field of research in itself.

Other recent considerations of the inverse problem are those of Kamide et al. (1976) and Oldenburg (1978). Kamide et al. (1976) have developed an automated technique to solve Poisson's equation for the magnetic potential by a finite-difference method to obtain an equivalent current system.

Oldenberg (1978) used a linear inverse theory to construct a most probable current system compatible with the ground disturbance pattern. Both of these efforts are, of course, subject to the difficulties mentioned above, namely, the necessity to constrain the currents to flow in a particular configuration in order to obtain results.

The calculation of a ground magnetic signature from a given current distribution may be performed without the inherent ambiguity of the inverse problem. Thus, magnetic field signatures have been obtained from wire models (Cummings, 1966), from direct integration over distributed currents using the Biot-Savart law (Crooker and Siscoe, 1974; Kisabeth, 1972), from wire-model simulations (Olson, 1974) and from a magnetic charge representation (Kisabeth, 1979); these computations are generally straightforward but tedious. The difficulty with these direct approaches derives from our lack of knowledge of the actual spatial configurations of the contributing currents, which are known to include ionospheric, field-aligned, ring, tail, magnetopause, and earth components. An unfortunate practical difficulty of assumed current models is that several of these components of a complete current system in a given event-model contribute on a roughly equal footing, and some in opposing senses (e.g., Fukushima and Kamide, 1974; R. Wolf, pvt. communication; Alabi et al., 1975). As a result, the calculated ground signature is quite sensitive to details of the model current system, whose correspondence with reality is poorly known. These limitations are apparent, in context, in the simple model described in Chapter 5 of the ground signature for the Birkeland current system.

References

- Alabi, A.D., P.A. Camfield, and D.I. Gough, The North American Central Plains conductivity anomaly, Geophys. J. Roy Astr. Soc., 43, 815, 1975.
- Bhargava, B.N. and G.K. Rangarajan, Low latitude geomagnetic bays and IMF sector polarity, Planet. Space Sci., 25, 161, 1977.
- Binns, K.J. and P.J. Lawrenson, Analysis and computation of electric and magnetic field problems, second edition, Pergamon Press, Oxford, 1973.
- Burke, W.J., M.C. Kelley, R.C. Sagalyn, M. Smiddy, and S.T. Lai, Polar cap electric field structures with a northward interplanetary magnetic field, Geophys. Res. Lett., 6, 21, 1979.
- Crooker, N.U. and G.L. Siscoe, Model geomagnetic disturbance from asymmetric ring current particles, J. Geophys. Res., 79, 589, 1974.
- Cummings, W.D., Asymmetric ring current and the low-latitude disturbance daily variation, J. Geophys. Res., 71, 4495, 1966.
- de la Beaujardiere, R. Vondrak, and M. Baron, Radar observations of electric fields and currents associated with auroral arcs, J. Geophys. Res., 82, 5051, 1977.
- Forbes, J.M. and R.S. Lindzen, Atmospheric solar tides and their electrodynamic effect I. The global Sq current system, J. Atmos. Terr. Phys., 38, 897, 1976.
- Forsythe, G.E. and W.R. Wasow, Finite-Difference Methods for Partial Differential Equations, Wiley, New York, 1960.
- Friis-Christensen, E. and J. Wilhjelm, Polar cap currents for different directions of the interplanetary magnetic field in the y-z plane, J. Geophys. Res., 80, 1248, 1975.
- Fukushima, N., Equivalence in ground geomagnetic effect of Chapman-Vestine's and Birkeland-Alfven's current systems for polar magnetic storms, Rep. Ionos. Space Res. Jap., 23, 219, 1969.
- Fukushima, N. and Y. Kamide, Contribution to low-latitude geomagnetic DS(H) from field aligned currents in the magnetosphere, Rep. Ionos. Space Res. Jap., 27, 1973.
- Galperin, Yu I., V.N. Ponomarev, and A.G. Zosimova, Equatorial ionospheric anomaly and interplanetary magnetic field, J. Geophys. Res., 83, 4265, 1978.
- Gregori, E.P. and L.J. Lanzerotti, Geomagnetic depth sounding by induction arrow representations: A review, to appear in Rev. Geophys. Space Phys., 1980.
- Hepner, J.P., Polar cap electric field distributions related to the interplanetary magnetic field direction, J. Geophys. Res., 77, 4877, 1972.

- Heppner, J.P., Empirical models of high-latitude electric fields, J. Geophys. Res., 82, 1115, 1977.
- Iijima, T. and T.A. Potemra, Field-aligned currents in the dayside cusp observed by Triad, J. Geophys. Res., 81, 5971, 1976.
- Iijima, T., R. Fujii, T.A. Potemra, and N.A. Saflekos, Field-aligned currents in the south polar cusp and their relationship to the interplanetary magnetic field, J. Geophys. Res., 83, 5595, 1978.
- Kamide, Y., M. Kanamitsu, and S.-I. Akasofu, A new method for mapping world-wide potential contours for ground magnetic perturbations: equivalent ionospheric current representation, J. Geophys. Res., 81, 3810, 1976.
- Kisabeth, J.L., The dynamical development of the polar electrojets, Ph.D. dissertation, University of Alberta, Edmonton, Alberta, Canada, 1972.
- Kisabeth, J.L., On calculating magnetic and vector potential fields due to large-scale magnetospheric current systems and induced currents in an infinitely conducting earth, in Quantitative Modeling of Magnetospheric Processes, Geophys. Monogr. 21, p. 473, ed. by W.P. Olson, AGU, Washington, D.C., 1979.
- Maezawa, K., Magnetospheric convection induced by the positive and negative z components of the interplanetary magnetic field: quantitative analysis using polar cap magnetic records, J. Geophys. Res., 81, 2289, 1976.
- Matsushita, S., IMF polarity effects on the Sq current focus location, J. Geophys. Res., 80, 4751, 1975.
- McDiarmid, I.B., E.E. Budzinski, M.D. Wilson, and J.R. Burrows, Reverse polarity field-aligned currents at high latitudes, J. Geophys. Res., 82, 1513, 1977.
- McDiarmid, I.B., J.R. Burrows, and M.D. Wilson, Comparison of magnetic field perturbations at high latitudes with charged particle and IMF measurements, J. Geophys. Res., 83, 681, 1978a.
- McDiarmid, I.B., J.R. Burrows, and M.D. Wilson, Magnetic field perturbations in the dayside cleft and their relationship to the IMF, J. Geophys. Res., 83, 5753, 1978b.
- McDiarmid, I.B., J.R. Burrows, and M.D. Wilson, Large-scale magnetic field perturbations and particle measurements at 1400 km on the dayside, J. Geophys. Res., 84, 1431, 1979.
- Mehta, N.C., Ionospheric dynamics and its coupling to the magnetosphere, Ph.D. dissertation, UCSD, 1978.
- Nopper, R.W., Jr. and J.F. Hermance, Phase relations between polar magnetic substorm fields at the surface of a finitely conducting earth, J. Geophys. Res., 79, 4799, 1974.

- Nopper, R.W., Jr. and R.L. Carovillano, Polar equatorial coupling during magnetically active periods, Geophys. Res. Lett., 5, 699, 1978.
- Nopper, R.W., Jr. and R.L. Carovillano, Ionospheric electric fields driven by field-aligned currents, in Quantitative Modeling of Magnetospheric Processes, Geophys. Monogr. Ser., vol. 21, ed. by W.P. Olson, AGU Washington, D.C., 1979a.
- Nopper, R.W., Jr. and R.L. Carovillano, On the orientation of the polar cap electric field, J. Geophys. Res., 84, 6489, 1979b.
- Oldenburg, D.W., A quantitative technique for modeling ionospheric and magnetospheric current distributions, J. Geophys. Res., 83, 3320, 1978.
- Olson, W.P., A model of distributed magnetospheric currents, J. Geophys. Res., 79, 3731, 1974.
- Patel, V.L., Interplanetary magnetic field variations and the electromagnetic state of the equatorial ionosphere, J. Geophys. Res., 83, 2134, 1978.
- Price, A.T., Electromagnetic induction within the earth, in Physics of Geomagnetic Phenomena, ed. by S. Matsushita and W.H. Campbell, Academic Press, New York, 1967.
- Rastogi, R.G. and H. Chandra, Interplanetary magnetic field and the equatorial ionosphere, J. Atmos. Terr. Phys., 36, 377, 1974.
- Rastogi, R.G. and V.L. Patel, Effect of interplanetary magnetic field on ionosphere over the magnetic equator, Proc. Indian Acad. Sci., 82, 121, 1975.
- Rastogi, R.G., Equatorial spread F and interplanetary magnetic field, J. Geomagn. Geoelec., 29, 557, 1977.
- Rastogi, R.G., R.F. Woodman, and P.C. Hedgecock, Correlated changes in the equatorial electrojet and in the interplanetary magnetic field during a geomagnetic storm, J. Atmos. Terr. Phys., 40, 867, 1978.
- Rastogi, R.G. and H.W. Kroehl, Interplanetary magnetic field and the equatorial ionosphere, Ind. J. Radio Space Phys., 7, 84, 1978.
- Schmucker, U., An introduction to induction anomalies, J. Geomagn. Geoelec., 22, 9, 1970a.
- Schmucker, U., Anomalies of geomagnetic variations in the Southwestern United States, Bull. Scripps Inst. Ocean., USCD, La Jolla, Cal., 1970b.
- Stern, D.P., Large-scale electric fields in the earth's magnetosphere, Rev. Geophys. Space Phys., 15, 156, 1977.
- Vondrak, R.R. and J.F. Vickrey, Latitudinal variations of auroral zone conductivities and energy dissipation rates, EOS Trans. AGU, 60, 355, 1979.

Wilhjelm, J., E. Friis-Christensen, and T.A. Potemra, The relationship between ionospheric and field aligned currents in the dayside cusp, J. Geophys. Res., 83, 5586, 1978.

Wolf, R.A., Effects of ionospheric conductivity on convective flow of plasma in the magnetosphere, J. Geophys. Res., 75, 4677, 1970.

5. SIMPLE ESTIMATE OF THE GROUND MAGNETIC SIGNATURE OF THE BIRKELAND-IONOSPHERIC CURRENT SYSTEM AT LOW LATITUDES

A. Introduction

Inherent difficulties for the determination of the ground magnetic signature for the complete current configuration generated by Birkeland currents were discussed in Chapter 4. In this chapter, a simple model is developed to obtain first estimates of the ground magnetic signature of the Birkeland-Ionospheric current system. The approach taken was to combine the Fukushima-Vasyliunas theorem and the requirement of induced shielding currents within the earth with a schematic representation of the main Birkeland current systems to reduce the problem to an analytic expression of great simplicity. With this model, we show that the main characteristic of the low latitude disturbance field of such a current system is a harmonic variation in the H-component of the field. The local time of maximum disturbance depends on the nature of the ionospheric closure of the Birkeland current system. One suggestion compatible with our model is the possibility that the classical mid latitude disturbance field asymmetry normally associated with a partial ring current is instead the signature of the Birkeland current system.

The systems of permanent polar Birkeland current first identified by Zmuda and Armstrong (1974) are now believed to be the main electrodynamic links connecting the ionosphere to the magnetosphere and the solar wind. The near-earth distribution of these current systems and their variations in time and space are presently the subjects of intensive investigation (see the review by Potemra, 1979). Already a fairly complete picture of the current patterns has been inferred statistically from data on encounters with the current systems made by low-altitude, polar-orbiting spacecraft (e.g., Iijima and Potemra, 1976;

1978). These patterns were utilized in the modelling calculations presented in Chapter 4. This relatively recent emergence of a new and fairly well defined global current pattern comes after a long history of analysis and interpretation of ground-based magnetic records. The question thus arises: What is the ground magnetic signature of the Birkeland current systems? The signature most likely would be distinctive and be present among the known types of magnetic disturbances, where its interpretation would remain incomplete or incorrect until it is identified.

A strong motivation for identifying the ground magnetic signature of the Birkeland current systems, for our purposes, is that by monitoring the signature, the behavior of the current systems themselves can be inferred. Ground based magnetometer observations have the advantage of high time resolution (essentially continuous) and easy availability compared to satellite observations. For these reasons, we have under the contract taken a number of steps toward the goal of achieving ground based magnetometer characterization of the polar Birkeland current systems. Our approach was to develop theoretical models to determine the types of ground magnetic signature produced by given Birkeland current configurations. Our findings are presented in this chapter.

B. Ionospheric Shielding Effects

The magnetic signature at the surface of earth is created by the combined effects of internal and external currents. Internal currents account for the main field (essentially dipolar) and induction effects due to transient disturbances of external origin. External currents are primarily of magnetospheric and ionospheric origin and constitute complicated three dimensional arrays. The full Birkeland current system (with its full three

dimensional character) is one such external current system. Under certain conditions, it is well known that the ionosphere serves to shield the earth from external magnetic effects. The physical basis for the shielding is nicely demonstrated in the simple theorems stated recently by Fukushima (1969) (planar geometry) and Vasyliunas (1970) (spherical geometry). We begin with a statement and simple derivation of these theorems.

Given: An infinite plane is connected to infinity by straight lines perpendicular to its surface. The lines are all in the same half space (e.g., all extending upwards from a horizontal plane). Along these lines, electrical current flows to and from infinity and closes in the plane, which has uniform, isotropic conductivity. There is no restriction on the number of lines or their location.

Fukushima's Theorem: There is no magnetic field produced by this current system in the current-free half space (i.e., below the horizontal plane).

Given: A spherical surface with uniform, isotropic electrical conductivity is connected to infinity by straight, radial lines. The lines carry electrical current to and from the sphere, and the current closes in the surface of the sphere. There is no restriction on the number or the disposition of the lines.

Vasyliunas' Theorem: There is no magnetic field produced by this current system in the interior of the sphere.

It is understood that these theorems are stated in the context of magneto-statics in the sense that signal propagation times can be ignored. We prove the theorems for one connecting, current-carrying line in each case. Then, since the problem is linear, the theorem follows for an arbitrary number and disposition of lines by linear superposition.

In the case of a single line, we may choose the line to be the axis of a cylindrical polar coordinate system. Since the only source for the field in this case is the current through the line, the fields must be axisymmetric with respect to the line. Also, since $\nabla \cdot \underline{B} = 0$, axial symmetry requires that the magnetic field be of the form

$$\underline{B} = B(r,z,t)\hat{\phi}$$

where r, z and ϕ are the radial, axial, and azimuthal variables of the chosen cylindrical coordinate system, and $\hat{\phi}$ is a unit vector in the azimuthal direction. The magnetic field is to be determined from Ampere's law given in MKS notation by:

$$\nabla \times \underline{B} = \mu_0 \underline{J} + \frac{1}{c^2} \frac{\partial \underline{E}}{\partial t} \quad (1)$$

Application of Stoke's Theorem to equation (1) yields

$$B(r,z,t) = \frac{\mu_0}{2\pi r} (I_c + I_D) \quad (2)$$

where I_c and I_D are the total electric and displacement currents through a circle of radius r centered at the location z on the axis.

Through any point, P , in the current-free half space or in the interior of the sphere we can draw an axis-centered circle. Because of axisymmetry, the circle will lie wholly in the current-free region in both cases. Thus, $I_c = 0$ for any such circle for each point P .

To find the I_D appropriate to the circle through P , we need to know the flux of electric field through the circle. The relevant electric field for the problem is generated by the electrical charges that are carried by the current between infinity and the conducting surface in each case. Because of

the symmetries involved, planar in one case and spherical in the other, the electric field lies wholly between the surfaces and the charges at infinity. We must keep in mind that the charges transferred to the surfaces are compensated for by equal and opposite charges at infinity. Thus the field is confined between the surfaces and infinity in the manner of a parallel plate condenser or a spherical condenser. Hence, we have $I_D = 0$ also.

Since we have shown that I_C and I_D are zero, it follows that $B(r,z,t) = 0$ for any point in the current-free half plane and in the interior of a conducting sphere. Hence, \underline{B} is zero everywhere in these source free regions, and stated in the theorems.

In most intended applications, more than one current-carrying line would be involved, and current could then flow in both directions. In this way the net current can be maintained equal to zero. Also the result is unaffected if the number of current-carrying lines is proliferated to generate distributed current systems.

C. Model Results at Low Latitudes

The application of the theorem to the case of Birkeland current systems is fairly direct. The Birkeland field-aligned currents would correspond to the radial currents and the ionosphere to the conducting, spherical surface. Field lines at high latitudes are approximately radial. For example, at a geomagnetic colatitude of 20° , the field is inclined 10° with respect to the radial direction. The main contribution to the surface magnetic field produced by a field-aligned current is made by the near-earth, quasi-radial portion of the field line (Crooker and Siscoe, 1974). Thus, the Birkeland field-aligned current systems approximate the radial currents for which the theorem strictly applies.

With sufficient accuracy for some purposes the Birkeland current systems can be represented as four separate radial line currents directed toward or away from the ionosphere, as illustrated in Figure 5.1. At not a very great depth in the earth, the conductivity is large enough that earth shielding currents are induced and have the effect of cancelling the Birkeland current field at greater depths, but increasing the field at the surface. It is easy to demonstrate that the field at the surface produced by the Birkeland currents and their shielding currents is approximately the same as the field produced by extending the Birkeland currents through the earth, as suggested by the dashed lines on the figure. (One should, in fact, also retain a current-free gap between the level at which the shielding currents flow and the ionosphere. But this is a small correction at low latitudes.)

The largest perturbation in the H-component at low latitudes produced by the Birkeland currents systems occurs along the noon-midnight meridian. The value at point A on the noon equator is

$$H_A = -\frac{\mu_0}{\pi R_e} (I_1 \sin \alpha_1 - I_2 \sin \alpha_2) \quad (3)$$

where H_A is measured positive northward, I_i ($i = 1, 2$) is the total current in the region i current system, and α_i is the colatitude of the region i current system. By symmetry:

$$H_B = -H_A \quad (4)$$

The ionospheric closure currents provide shielding and tend to reduce the perturbation magnetic field at the surface. As we have seen, if the conductivity of the ionosphere were isotropic and uniform, the closure current would cancel the field of the Birkeland current everywhere under the ionosphere.

The conductivity of the ionosphere is neither isotropic nor uniform. The presence of Hall currents and of spatial gradients in the conductivities violate the conditions necessary for perfect cancellation of the Birkeland current field at the surface of the earth. There are two limiting cases which illustrate the range of the surface fields that result. In the direct closure limit, the Birkeland currents close in narrow, latitudinally confined electrojets. In the other limit, the Pederson conductivity is taken to be uniform, so that the field of the Birkeland current plus its Pederson current closure is zero under the ionosphere. However, the associated Hall current produces a non-zero field at the surface.

The direct closure case is represented to a good approximation by equations (3) and (4) for H_A and H_B . The field produced at low latitudes by the direct closure current (subscript D) is considerably smaller than that produced by the Birkeland current (Crooker and Siscoe, 1974). Thus,

$$(H_A)_D = - (H_B)_D = - \frac{\mu_0}{\pi R_e} (I_1 \sin \alpha_1 - I_2 \sin \alpha_2) \quad (5)$$

Also, by symmetry, referring to points C and D in Figure 5.1,

$$(H_C)_D = (H_D)_D = 0 \quad (6)$$

To obtain similar expressions for the case of uniform Pederson conductivity, we assume that the ratio of the Hall to Pederson conductivities is a constant η , i.e., the Hall conductivity is also taken to be uniform. (However, the sign of η must change across the equator to reflect the change in the sign of the vertical component of the earth's magnetic field.) The Hall current, \underline{J}_H , is perpendicular to the Pederson current \underline{J}_p everywhere, in a direction given by $\underline{J}_p \times \hat{r}$ in the northern hemisphere, where \hat{r} is a unit

vector in the radial direction. \underline{J}_H flows in the $-\underline{J}_p \times \hat{r}$ direction in the southern hemisphere. The Hall current streamline pattern is, therefore, everywhere orthogonal to the streamline pattern of the Pederson current. It is easy to demonstrate by means of a sketch of the current streamlines that at middle and low latitudes, the Hall current pattern can be obtained simply by performing a 90° eastward rotation in longitude of the Pederson current pattern. At high latitudes, the two patterns deviate even after rotation, since one closes completely in the ionosphere whereas the other terminates at the ionospheric intersection of the Birkeland currents. The two patterns would coincide exactly after rotation in the limit in which α_1 and α_2 approach zero (c.f., Figure 5.1).

The field at middle and low latitudes is determined mainly by the middle and low latitude part of the current pattern. Hence, the Hall current field is approximately the same as the field of the Pederson current appropriately rotated. But from the Fukushima-Vasyliunas theorem, we know that the surface field of the Pederson current is equal and opposite to that of the Birkeland current. After tracing the connection from the Hall current field to the Pederson and Birkeland current fields, remembering that the Birkeland and Pederson fields have opposite signs, we find that the Hall field is approximately the same as the Birkeland field obtained by rotating the current pattern in Figure 5.1 90° westward. We must also multiply the Birkeland field by the conductivity ratio η to obtain the strength of the Hall field. Thus, we arrive at the results for uniform conductivity (subscript u):

$$\text{noon-midnight:} \quad (H_A)_u = (H_B)_u = 0 \quad (7)$$

$$\text{dusk-dawn:} \quad (H_C)_u = -(H_D)_u \cong \frac{\eta u_0}{\pi R_e} (I_1 \sin \alpha_1 - I_2 \sin \alpha_2) \quad (8)$$

In both limits, the quantity $(I_1 \sin \alpha_1 - I_2 \sin \alpha_2)$ enters and must be supplied empirically. From the review article by Potemra (1979), we extract the statistical values shown in Table 1 for quiet and disturbed conditions.

Table 5.1 Parameters used to evaluate antipodal magnetic disturbances at the equator.

Disturbance Level	I_1^*	I_2^*	α_1	α_2	$(H_A)_D$	$(H_C)_u^+$
Quiet ($ AL < 100 \gamma$)	1.55	1.10	16°	19°	-4.3 γ	8.7
Disturbed ($ AL > 100 \gamma$)	2.70	2.45	18°	21°	2.7 γ	-5.4
				Difference	7.0 γ	-14.1
				Antipodal Difference	14.1 γ	-28.2

* in units of 10^6 amperes

+ $\eta = 2$ assumed

Since the base line for measuring the amplitude of disturbances is established during quiet conditions, the proper measure of the disturbance produced by the Birkeland current systems is the difference between quiet and disturbed conditions. The total amplitude of the global disturbance field is the difference between antipodal points on the equator.

If the disturbance field is represented by a sine wave with zero average, the Table 5.1 gives for its amplitude a value of 7 γ in the direct closure case and 14 γ in the uniform conductivity case. The Hall-to-Pederson conductivity ratio η , was taken to be 2 (Nopper and Carovillano, 1978). The low latitude disturbance field in the direct closure case takes the form of a noon-midnight asymmetry in H, with a positive increment at noon. In the uniform conductivity case, it takes the form of a dawn-dusk asymmetry in H with a negative increment at dusk.

Returning now to the original question of the low latitude ground magnetic signature of the Birkeland currents system, we see that it should take the form

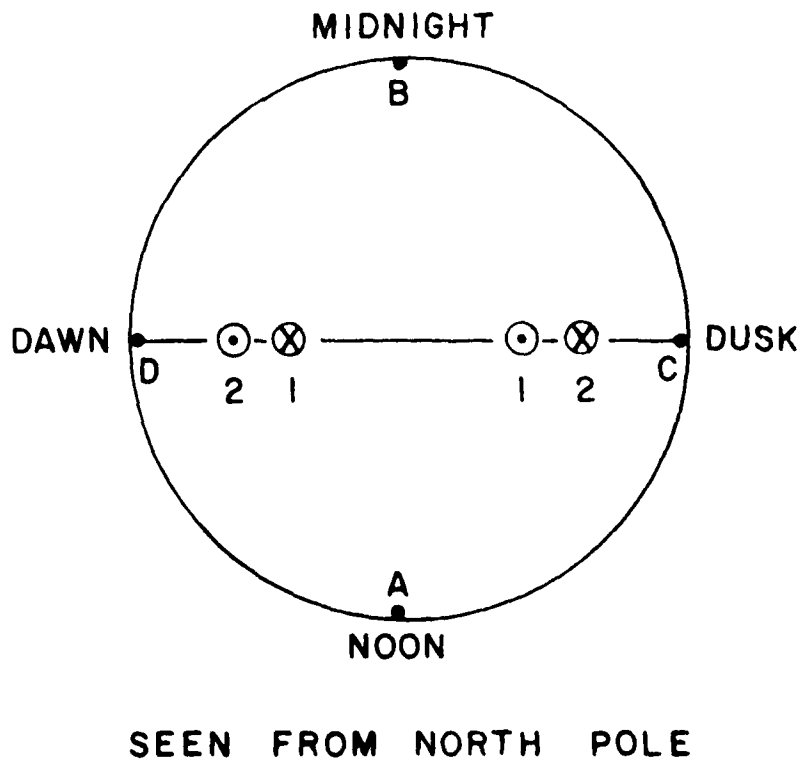
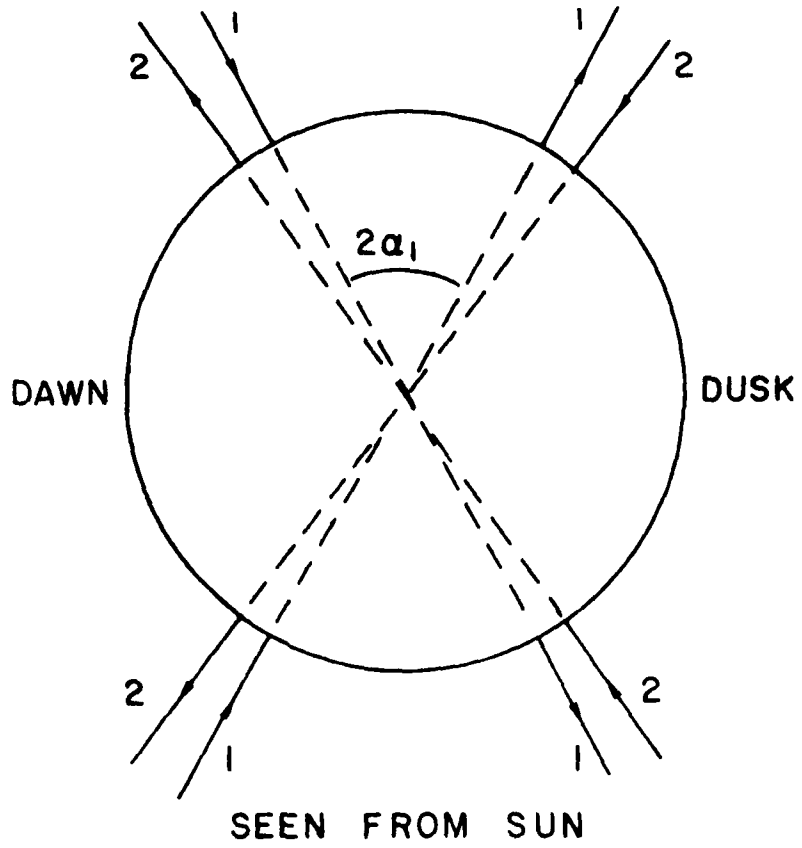


Figure 5.1 Simple representation of Birkeland currents corresponding to Region 1 (quiet time) and Region 2 (active) configurations.

of an antipodal asymmetry in the H-component of the disturbance field, but that the local time meridian of its maximum amplitude depends on the detailed nature of the associated ionospheric current systems. The most notable representative of an antipodal asymmetry at low latitudes is the well-known dawn-dusk magnetic storm disturbance field asymmetry (Sugiura and Chapman, 1960; Crooker and Siscoe, 1971), which since 1966 has been attributed to a partial ring current system (Cummings, 1966; Crooker and McPherron, 1972; Crooker and Siscoe, 1974). This disturbance field is characterized by a negative increment in H in the dusk meridian, and thus conforms to the case of uniform conductivity. The amplitude found in our model is based on averages of numbers representing quiet and disturbed conditions. Individual cases would undoubtedly yield both larger and smaller amplitudes. However, it is true that in previous studies of the low latitude disturbance-field asymmetry, an amplitude of 14γ would be among the very lowest values considered (e.g., Crooker and Siscoe, 1971). The calculation of the asymmetry for values of I_1 and I_2 based on time periods for which $|AL| > 500 \gamma$ or 1000γ , would likely represent more faithfully the conditions under which the low latitude disturbance-field asymmetry is most pronounced.

We note with regard to the amplitude of the low latitude disturbance field produced by the Birkeland current system, that the disturbance fields of the two components of this system, the region 1 and region 2 currents, nearly cancel each other. What remains is a small residual field. For example, the amplitude of the region 2 current system alone in the uniform conductivity, disturbed condition case is $(H_C)_u = -95 \gamma$. It would appear as if the two component systems are coupled in such a way that if they act in direct opposition,

as we have arranged them to do, they nearly cancel each other. In the interest of simplicity, we have perhaps been too strict in imposing exact opposition.

The results of this study were reported at the Geomagnetism Workshop held at AFGL, April 1979. The presentation lead R.A. Wolf and coworkers to use the Rice University magnetospheric convection model to test the general hypothesis that the low latitude disturbance field asymmetry results from the Birkeland current systems (Harel et al., 1979). They indeed found the predicted asymmetry, but they judged that the main factor contributing to it was a downward current into the polar ionosphere in the noon meridian and an upward current in the midnight meridian. The low latitude disturbance field was then produced in the direct closure mode from this noon-midnight current residual. (These currents would not be represented in our models as presented in Chapers 4 and 5.)

A noon-midnight Birkeland current component can be simulated in our two component model by means of a longitudinal offset between the region 1 and region 2 current systems. The region 2 system must be rotated westward with respect to the region 1 system.

In terms of the quantities already defined, if we add an offset angle β , then the direct closure, disturbance field resulting from an uncompensated westward rotation of the region 2 current system is

$$H_C \approx - \frac{\mu_0}{\pi R_e} I_2 \sin \alpha_2 \sin \beta \quad (10)$$

Using disturbance condition parameters and $\beta = 45^\circ$, we find $(H_C)_0 \approx -34 \gamma$. Once again, larger values would result if currents appropriate to more disturbed conditions were used.

D. Recommended Approach

For the reasons indicated in Chapter 4, while magnetic signatures corresponding to our globally determined ionospheric current configurations could easily be calculated, the utility of such results could be limited. Above we presented within the context of a simple model most features necessary to consider in determining the ground magnetic signature. For the purpose of determination of such magnetic signatures, the approach we recommend is to build upon the current Report to: (1) increase the applicability of our models to real events (see section 4E); (2) develop a magnetospheric extension of our current models to provide closure of currents out of the ionosphere (this should be done in recognition of the work of R. Wolf and collaborators); (3) take earth induction effects into account realistically.

References

- Crooker, N. U., and G. L. Siscoe, A study of the geomagnetic disturbance field asymmetry, Radio Sci., 6, 495-501, 1971.
- Crooker, N. U., and R. L. McPherron, On the distinction between the auroral electrojet and partial ring current systems, J. Geophys. Res., 77, 6886-6889, 1972.
- Crooker, N. U., and G. L. Siscoe, Model geomagnetic disturbance from asymmetric ring current particles, J. Geophys. Res., 79, 589-594, 1974.
- Cummings, W. D., Asymmetric ring currents and the low-latitude disturbance daily variation, J. Geophys. Res., 71, 4495-4503, 1966.
- Fukushima, N., Equivalence in ground geomagnetic effect of Chapman-Vestine's and Birkeland-Alfven's current systems for polar magnetic storms, Rep. Ionos. Space Res. Jap., 23, 219, 1969.
- Harel, M., R. A. Wolf, R. W. Spiro, P. H. Reiff and C. K. Chen, Quantitative model of a magnetic substorm: 2. Comparison with observations, to be submitted to J. Geophys. Res., 1979.
- Iijima, T., and T. A. Potemra, The amplitude distribution of field-aligned currents at northern high latitudes observed by Triad, J. Geophys. Res., 81 (13), 2165-2174, 1976.
- Iijima, T., and T. A. Potemra, Large-scale characteristics of field-aligned current associated with substorms, J. Geophys. Res., 83, 599, 1978.
- Nopper, R. W., and R. L. Carovillano, Polar-equatorial coupling during magnetically active periods, Geophys. Res. Lett., 5, 699-702, 1978.
- Potemra, R. A., Current systems in the earth's magnetosphere, Rev. Geophys. Space Phys., 17, 640-656, 1979.

Sugira, M., and S. Chapman, The average morphology of geomagnetic storms with sudden commencement, Abt. Akad. Wiss. Gottingen, Math-Phys. Klasse, Sonderheft Nr. 4, 1960.

Vasyliunas, V. M., Models of ionospheric currents driven by quasi-static magnetospheric convection and their relation to equivalent current systems, presented at Upper Atmosphere Currents and Electric Field Symposium, NOAA and NCAR, Boulder, August 1970.

Zmuda, A. J., and J. C. Armstrong, The diurnal flow pattern of field-aligned currents, J. Geophys. Res., 79, 4611-4619, 1974.

6. AURORAL BOUNDARY LOCATIONS

Magnetospheric conditions affect both the occurrence and location of auroras, but until recently, there was no means of monitoring auroral activity on a global scale. Images from DMSP satellites now provide the opportunity to observe auroras every 1-2/3 hours over each pole. The images sacrifice time resolution compared with all sky camera coverage, but this is more than compensated for by the images' wide spatial coverage, clockwork regularity, and timely reception vital for practical applications. With proper training, DMSP images can be interpreted reliably without very much difficulty. Also, the sensitivity of DMSP images rivals or surpasses the sensitivity of all sky cameras, under good conditions (Eather, 1979). These features make the images useful tools for observing auroral activity and determining boundary positions.

The auroral boundary marks the termination of particle precipitation sufficient to excite aurora above a threshold intensity, which depends on the means of detection. Auroras generally expand both poleward and equatorward with increasing magnetic activity, but the connection is not tight; although particle precipitation may carry some, as yet unknown, fraction of field aligned currents, various definitions of magnetic activity may also reflect electric currents linked only indirectly to auroras, such as the ring current or certain ionospheric currents.

We have studied the relationship between the equatorward auroral boundary and two familiar indices, Kp and AE (Sheehan and Carovillano, 1978). A reprint of the article is included at the end of this chapter. Based on 162 DMSP images taken over the north pole, the Kp dependence of the boundary near

local midnight is consistent with earlier findings by Lui (1975), who used ISIS 2 satellite images, and results from the south pole DMSP images analyzed by Nagata et al. (1975). In Figure 6.1, the average boundary latitude is seen to steadily decrease from 67° CGL ($K_p < 0$) to 63° CGL ($K_p \geq 4$) with increasing magnetic activity. A 2° CGL range of scatter above and below the average locations can be attributed partly to the incompatibility between instantaneous

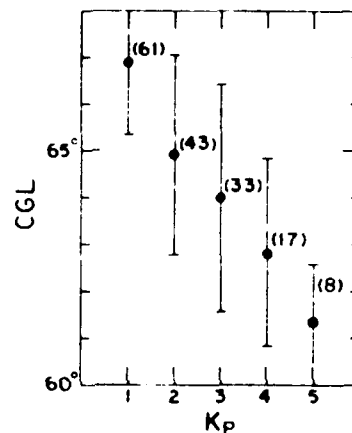


Figure 6.1. Average corrected geomagnetic latitude of the equatorward auroral boundary at 0100 CGLT as a function of K_p . Error bars demark one standard deviation. From Sheehan and Carovillano (1978).

auroral determinations and the 3 hour interval defining K_p , but similar scatter also applies to the boundary latitude with AE, which is a virtually instantaneous index. The average boundary location plotted in Figure 6.1 follow rather well the ionospheric mapping of an injection boundary in the equatorial plane determined empirically by McIlwain (1974), as indicated in Figure 6.2.

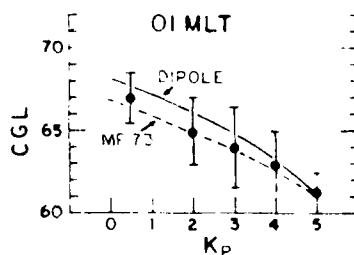


Figure 6.2. Data of Figure 6.1 along with the McIlwain injection boundary mapped to the auroral zone. Two field models shown, dipole (solid line), and empirical Mead-Fairfield (MF73). From Sheehan and Carovillano, 1978.

Thus, the equatorward boundary seen in DMSP images is related to plasma injected near the inner edge of the plasma sheet at the onset of substorms, at least statistically.

Gussenhoven et al. (1978) carried out a similar analysis of auroral boundaries in DMSP images but concentrated on the poleward boundary, which is more difficult to clearly determine than the equatorward one. The authors also considered D_{st} behavior (Figures 6.3 and 6.4, at two local times) with the intention of estimating ring current influence on polar cap size. They found that separating D_{st} affects from AE affects was difficult to accomplish because the general relationship between AE and D_{st} hampered the accumulation of good statistics at extreme values. Nevertheless, the task of mapping auroral locations globally, under various magnetic conditions, remains of great importance in studying the overall state of the magnetosphere.

23-01 GLT

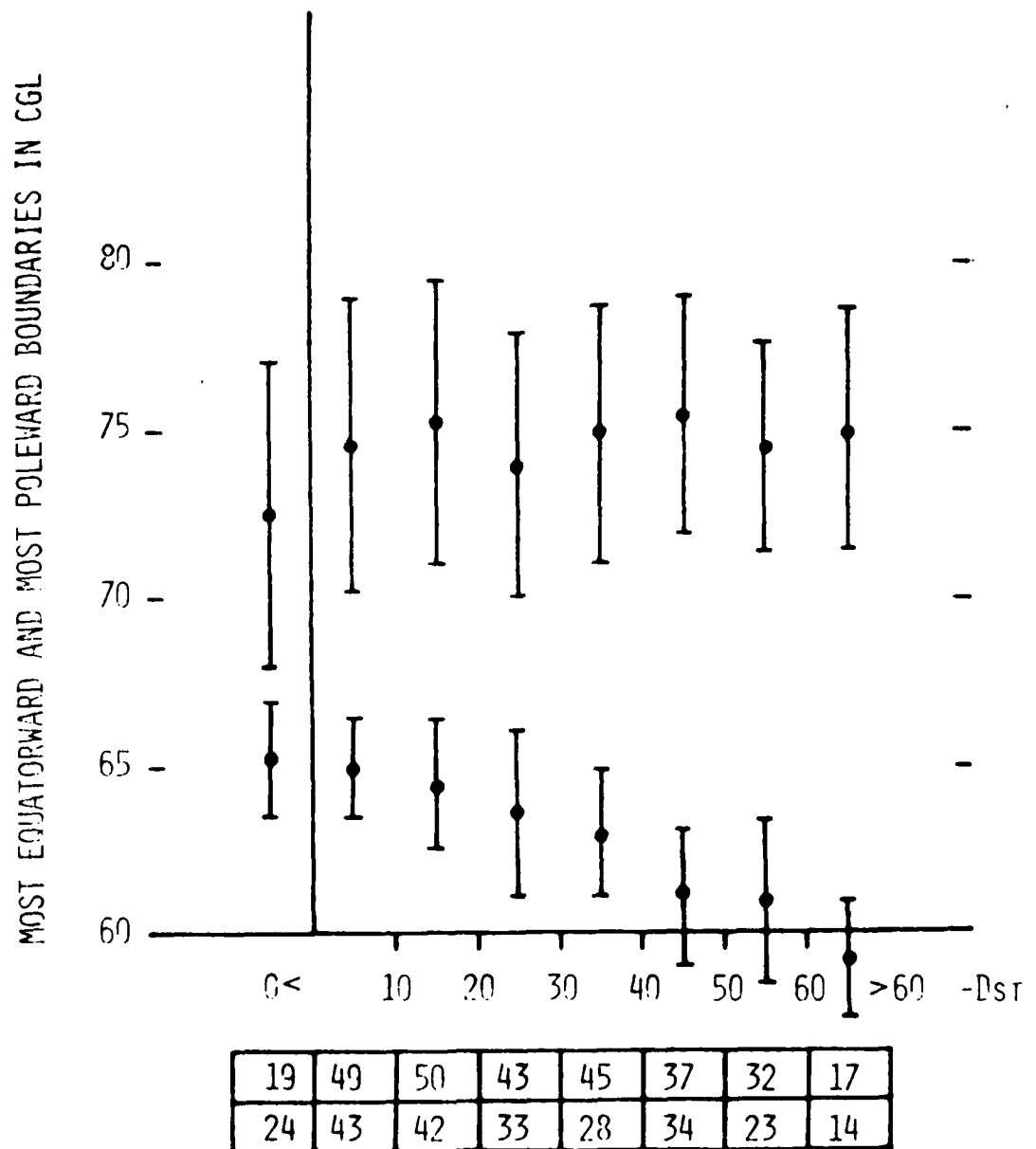


Figure 6.3. Average latitude of the poleward and equatorward auroral boundaries, determined from DMSP images, in the 23-01 local time sector as a function of $-Dst$. Number of poleward and equatorward cases in each Dst interval shown in the upper and lower boxes, respectively. Bars indicate one standard deviation. From Gussenhoven et al. (1978).

04-06 GLT

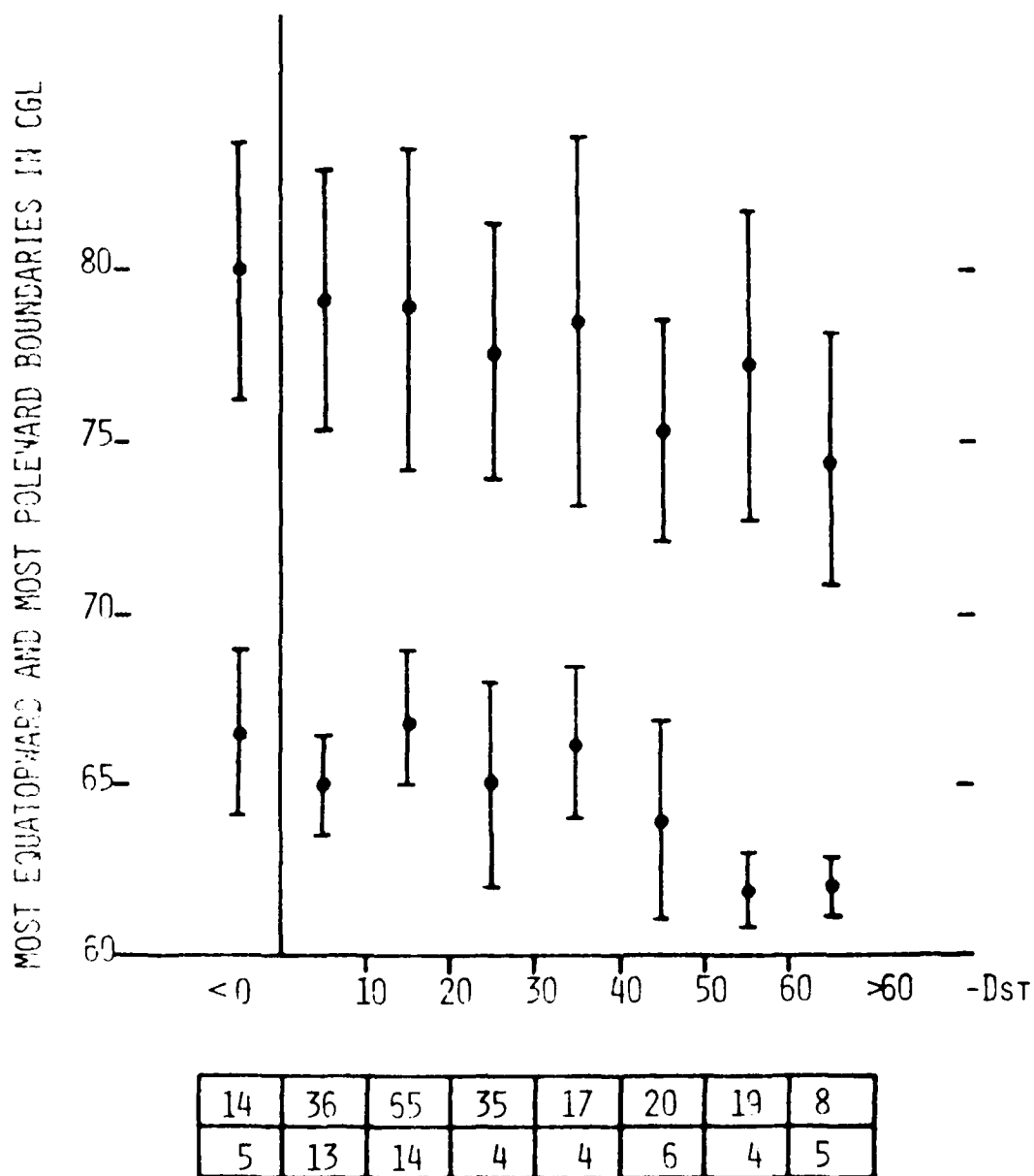


Figure 6.4. Average latitude of the poleward and equatorward auroral boundaries, determined from DMSP images, in the 04-06 local time sector as a function of $-D_{st}$. Number of poleward and equatorward cases in each D_{st} interval shown in the upper and lower boxes, respectively. Bars indicate one standard deviation. From Gussenhoven et al. (1978).

Characteristics of the Equatorward Auroral Boundary Near Midnight Determined From DMSP Images

R. E. SHEEHAN AND R. L. CAROVILLANO

Department of Physics, Boston College, Chestnut Hill, Massachusetts 02167

The latitude of the equatorward auroral boundary near local midnight has been determined for 162 Defense Meteorological Satellite Program (DMSP) images in November–December 1972. When grouped according to K_p and AE , these observations show approximate linear decreases in the average boundary latitude with increasing values of these magnetic indices. There appears also to be a slight diurnal variation in the boundary location. Mapping of the appropriate McIlwain injection boundaries to auroral latitudes shows good agreement with the average DMSP equatorward auroral boundary latitude. Similar analyses at 2000 and 2200 CGLT (corrected geomagnetic local time) using a different set of DMSP images yield similar results, with somewhat poorer agreement under quiet conditions.

INTRODUCTION

Auroral images from satellites have been especially useful in studies of global auroral patterns during substorms [Pike and Whalen, 1974; Snyder et al., 1974; Akasofu, 1974; Carovillano et al., 1974]. Isis satellites provide valuable spectral information. [Liu et al., 1975a, b], while U.S. Air Force satellites in the Defense Meteorological Satellite Program (DMSP) series produce high-resolution images in a broad band extending from long visible to near-infrared wavelengths. Some studies are based on a small number of images selected to complement other data. Work involving large groups of DMSP images [Holzworth and Meng, 1975; Carovillano, 1975; Berkey and Kamide, 1976] requires extensive gridding and analysis, straightforward but tedious by hand and expensive by computer. Even so, statistical studies exploring the gamut of magnetospheric conditions become more inviting and possible as large quantities of images become available.

The primary measurement reported in this paper is the latitude of the equatorward auroral boundary as seen in DMSP images. Orbiting in circular paths with 102-min periods, DMSP satellites travel in either the noon-midnight or the dawn-dusk meridian plane. A radiometer pointing toward earth builds an image by rapidly scanning narrow strips perpendicular to the satellite path projected to the earth's surface (the ground track). The apparent intensity of auroras seen in DMSP images depends on several factors: absolute radiometer sensitivity, original image and copy quality (in our case, 35-mm transparencies from the World Data Center), oblique viewing angles away from the center of the ground track (Van Rijn effect), and uncertain background albedo from ice and clouds (see Carovillano [1975] for a discussion of these effects).

Our data base consists of 162 DMSP images taken by a noon-midnight satellite during the period November 14 to December 15, 1972. A DMSP satellite can produce a maximum of about 430 images in a month, but gaps in the data are rather common, and some images are of doubtful quality for reasons related to the problems mentioned above. In addition, exposure problems and interference by the full moon commonly result in poor-quality images. The data base in this study was chosen because it contained a good sample of high-quality images. Our procedure was to grid each image with a corrected geomagnetic (CG) coordinate system [Whalen, 1970] and to measure the latitude of the equatorward auroral boundary at the 0100 CGLT (CG local time) meridian. This meri-

dian is convenient because of its proximity to the ground track for images from a satellite orbiting in the noon-midnight plane. Because the satellite is stabilized in a fixed plane relative to the earth-sun line, the magnetic coordinates in a series of images shift diurnally as the earth rotates below, and this effect is taken into account by the gridding process.

Generally, diffuse-appearing aurora served to define the measured equatorward boundary. However, DMSP images cannot accurately portray the entire range of possible auroral intensities. Saturation occurs at relatively low brightness levels and often hinders discrimination between diffuse and discrete aurora, based on structure alone. When a distinction is possible, it is based solely on the actual DMSP images and not on complementary information. When comparisons have been possible, our results have been quite consistent with features seen in all-sky camera pictures. Whether diffuse or discrete in appearance, the boundary is usually quite sharp and is measured within $\frac{1}{2}^\circ$ of latitude.

HISTOGRAMS WITH K_p , AE , AND UT AS PARAMETERS

Figures 1a, 1b, and 1c contain histograms showing the distribution of DMSP images by equatorward auroral boundary latitude when grouped parametrically according to the K_p index, the AE index, and image universal time, respectively. In this format, each image has four quantities associated with it: equatorward boundary latitude, universal time, and the appropriate K_p and AE indices. For increasing values of K_p and AE the histograms display shifts in the distributions from about 67° CGL (quiet conditions) to about 62° CGL (active conditions) (CGL is corrected geomagnetic latitude). There are only a small number of cases corresponding to large values of K_p or AE , but the trends are both unmistakable and expected from the definitions of the indices. The distributions for K_p and AE are sharply peaked at 67° CGL during very quiet conditions, but in all cases where there are more than a few images the width of each distribution spans about 5° of latitude. Large scatter is understandable when K_p is used as a parameter because it is a 3-hour-averaged mid-latitude magnetic index and therefore may not represent the wide degree of auroral variability possible within a 3-hour interval. The AE index, however, more nearly provides an instantaneous indication of magnetic activity somewhere in the auroral zone. The scatter in the distributions for the boundary latitude for 50- γ AE ranges means that there is a general, but by no means unique, connection between general high-latitude magnetic conditions and the auroral boundary location.

Copyright © 1978 by the American Geophysical Union.

Paper number SA0567
0148-0227/78/108A-0567\$01.00

4749

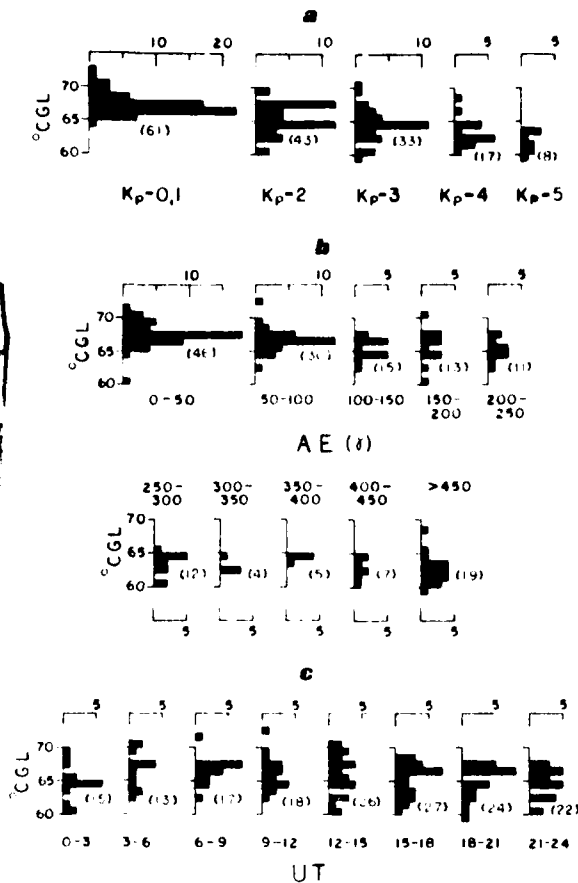
THIS PAGE IS BEST QUALITY PRACTICABLE
 FROM COPY 1 OF ORIGINAL TO DRP


Fig. 1. Histograms of the equatorward auroral boundary grouped according to (a) K_p index, (b) AE index, and (c) UT. Values in parentheses indicate the number of DMSP images for each case.

If auroral activity occurred randomly at any time of the day, the distribution of images by boundary latitude would be broad and flat when grouping was done according to the universal time of the image. Although the small number of cases in each UT interval in Figure 1c makes it difficult to draw firm conclusions, the data in our sample tend to suggest that the auroral equatorward boundary more commonly extends to low latitudes in the latter half of the UT day. Images taken around 0000 UT may be biased, however, because at this time the 0100 CGLT meridian is in a position prone to Van Rijn enhancement. If real, the small diurnal effect exhibited in Figure 1c could be a reflection of a diurnal change in the average polar cap size or possibly of a misalignment of the corrected geomagnetic coordinate system with the average auroral oval. The size of the polar cap cannot be determined accurately from DMSP images except in rare cases because of their limited spatial coverage, but similar trends with no phase lags at several other local times would indicate an overall expansion and contraction of the average nightside auroral oval. If systematic phase differences among the diurnal trends at several local times were observed, this behavior would suggest that a constant average oval pertains which shifts location relative to an eccentric (and perhaps nonlinear) coordinate system as the earth rotates.

VARIATION OF THE AVERAGE EQUATORWARD BOUNDARY LATITUDE WITH K_p AND AE

Figure 2 displays the average and standard deviation of the equatorward auroral boundary latitude distributions at 0100 CGLT versus K_p . Here integer K_p values encompass neighboring fractional cases, and the $K_p = 1$ data point also includes images with $K_p = 0$. The decrease in the average latitude of the equatorward boundary varies approximately linearly with K_p when $1 \leq K_p \leq 5$. When these results are compared with the results of *Lui et al.* [1975b] from Isis 2 data, a general agreement between the two types of imaging is found (Figure 3). Also, the equatorward trend over the K_p range 1-5 is comparable to that shown by *Starkov* [1969] based on all-sky camera data for Q index values ranging from 2 to 6. On the other hand, accord is not as good with an analysis of south pole DMSP images during May-June 1973 by *Nagata et al.* [1975]. As shown in Figure 4, the trends are similar, but our average latitudes are 1° - 2° lower for $K_p = 2, 3$, and 4. These differences could arise from the particular sets of images used in each study or physically from a lack of conjugacy between the northern and the southern hemisphere in the corrected geomagnetic system. The change in the average equatorial latitude versus AE (Figure 5) can be approximated roughly by a linear decrease of about 1° CGLT/100 γ .

Only on exceptional occasions does the aurora extend below 60° CGLT. For example, during the great magnetic storm period in early August 1972 the equatorward boundary approached 55° CGLT only during an extremely disturbed interval when K_p reached 8. A linear extrapolation of Figure 2 to $K_p > 5$ leads to a similar value.

PLASMA INJECTION PHENOMENA

Observations of magnetospheric plasma at synchronous orbit ($\sim 6.6 R_E$) have been reported by *DeForest and McIlwain* [1971]. Those authors exhibit their data in the form of energy-time spectrograms and give fluxes of electrons and protons in a range of energies as a function of time. Characteristic dispersion structures are seen in these spectrograms that indicate that the satellite encounters protons and electrons of different energies at various points along its orbit. As the satellite moves

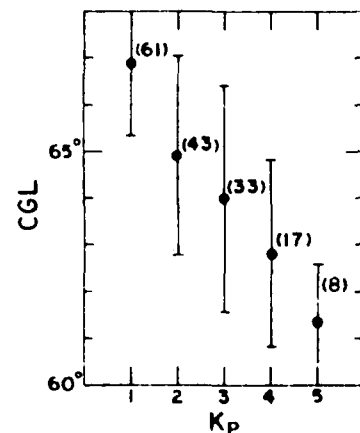


Fig. 2. Average corrected geomagnetic latitude of the equatorward auroral boundary at 0100 CGLT as a function of K_p , using the same data base as was used in Figure 1. Error bars demark one standard deviation.

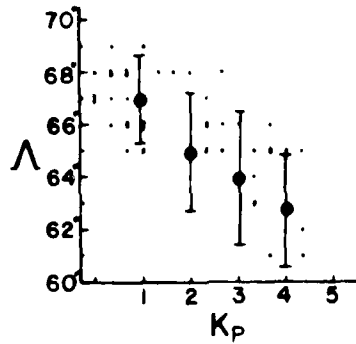


Fig. 3. Data of Figure 2 (large dots) superimposed on the results of *Lee et al.* [1975b] using Isis 2 images. Each small dot represents one Isis 2 image. λ indicates invariant latitude, which is very similar to corrected geomagnetic latitude.

from evening local time toward midnight, high-energy protons are encountered first, followed by successively lower energy protons until there occurs a simultaneous encounter with near-zero-energy protons and electrons (the inner edge of the plasma sheet). Occasionally, protons and electrons of all energies show enhanced fluxes simultaneously, as if a cloud of heated plasma suddenly appeared or was created at the satellite's location. This is called an injection event.

By calculating the particle drift motion caused by magnetic field curvature and gradient and adding the convection of a postulated electric field, DeForest and McIlwain were able to trace particle trajectories backward in time from their locations at the satellite encounter at $6.6 R_E$. If protons and electrons of all energies are traced back in the equatorial plane to a common time of origin, their locus falls on a smooth spiral curving toward the earth from dusk to midnight. The locus (the so-called injection boundary) may be interpreted to be the earthward boundary of a common source region for particles of all energies at the time of injection. *McIlwain* [1974] derived a formula for the statistical injection boundary given by $R_b = (122 - 10 K_p) (\varphi - 7.3)$. R_b is the injection boundary position in units of earth radii at the equatorial plane as a function of

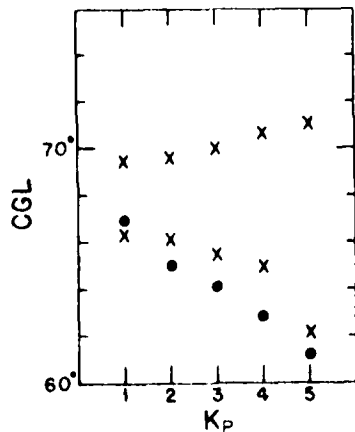


Fig. 4. Data of Figure 2 (dots) compared with the results of a statistical analysis using southern hemisphere DMSP images [*Nagata et al.* 1975]. Upper and lower crosses indicate the average poleward and equatorward limits, respectively, as reported by *Nagata et al.*

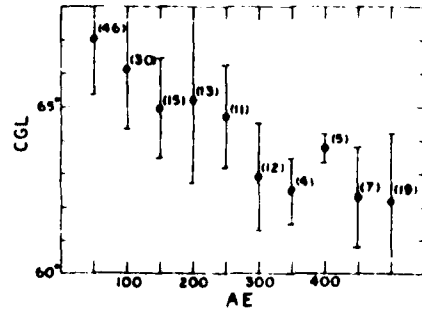


Fig. 5. Same as Figure 2 except for AE, based on data of Figure 1b.

K_p and magnetic local time in hours, φ ($1800 \leq \varphi \leq 2400$ CGLT). *Mauk and McIlwain* [1974] analyzed their ATS 5 data in this way using the value of K_p at the time of encounter with cold plasma and regard R_b to be useful in describing the injection boundary's location when a substorm occurs. Coordinated ground-based photometer and ATS 5 studies by *Father et al.* [1976] give further significance to the injection boundary concept.

DMSP AURORAL BOUNDARY AND THE McILWAIN INJECTION BOUNDARY NEAR LOCAL MIDNIGHT

In Figure 6 a comparison is made between the DMSP boundary location and the McIlwain injection boundary R_b at 0000 CGLT as a function of K_p . The formula for R_b is valid only up to local midnight, and its extension past local midnight is questionable. Although our DMSP data apply to 0100 instead of 0000 CGLT, this should be of little practical significance, since the auroral boundary is generally parallel to circles of constant latitude in the vicinity of local midnight. A simple dipole model (solid line) and an empirical field model (dashed line) are used to map the injection boundary from the equatorial plane to the auroral zone. The realistic magnetic fields used in Figure 6 are the MFQ (quiet, $K_p < 2$) and MFD (disturbed, $K_p \geq 2$) models described by *Fairfield and Mead* [1975]. In a review of magnetic field models, *Walker* [1976] considered the Mead-Fairfield models (MFQ and MFD) to be among the best, principally because they are based on satellite data.

In the equatorial plane the most accurate region of the Mead-Fairfield model is $-5 R_E \geq X \geq -12 R_E$, where X is the distance from the earth's center along the earth-sun line, posi-

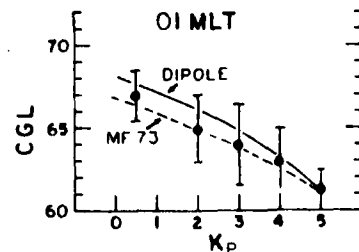


Fig. 6. Data of Figure 2 along with the McIlwain injection boundary mapped to the auroral zone using a dipole magnetic field model (solid line) and the empirical Mead-Fairfield 75 (MF 75) magnetic field model (dashed line). Auroral data are at 0100 CGLT, and McIlwain boundary is at 0000 CGLT.

THIS PAGE IS PART QUALITY PRACTICABLE FROM COPY PROCESSED TO DDG

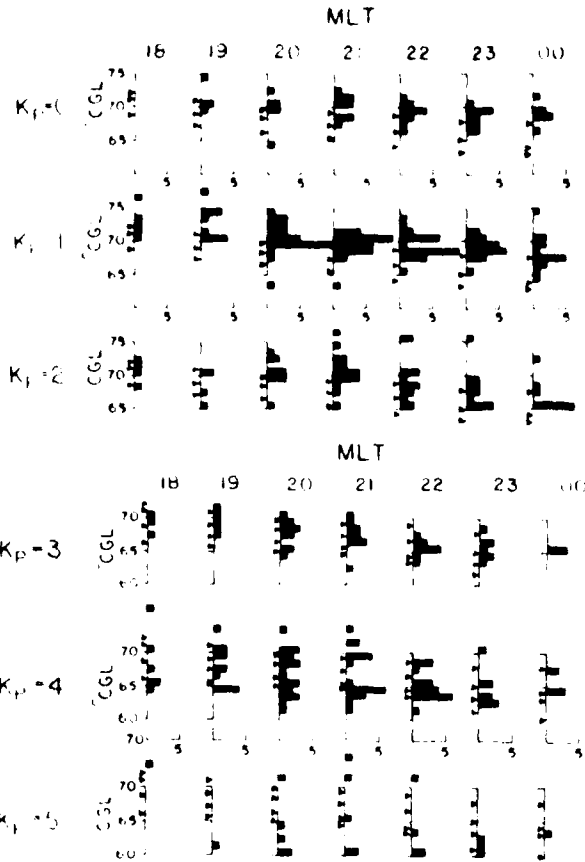


FIG. 7. Histograms showing the number of DMSP images with equatorward auroral boundaries in the indicated 1° interval of CGLT at magnetic local times ranging from 1800 to 0000 CGLT. Images are grouped according to prevailing K_p . Triangles mark the latitude of the Feldstein statistical auroral oval at the indicated local time for various Q -index values [Whalen, 1970]. Q -index values 1, 3, and 5 (and 7 for $K_p = 3$) correspond to triangles going from highest to lowest latitude on each histogram.

tively directed toward the sun. At 0000 CGLT, for $0 \leq K_p \leq 5$, the range of the McIlwain boundary in the nightside equatorial plane is $4.3 R_E \leq R_s \leq 6.7 R_E$, which falls mainly into the field model's most accurate range. It is evident from Figure 6 that there is good agreement between the average DMSP auroral boundary location and the mapping of R_s by the empirical Mead-Fairfield magnetic field model. The undistorted dipole mapping of R_s also compares quite well at all K_p values. It should be noted that the formula for the McIlwain injection boundary defines a curve at the instant of injection. After injection the boundary position shifts in response to electric fields and particle drift motions. If a DMSP image is taken some time after an injection event occurs, the auroral boundary position should reflect this change. Thus to the extent that the auroral boundary is related to the injection boundary the scatter depicted in Figure 6 could result from two sources: (1) statistical variations in the initial injection boundary location and (2) modifications of the boundary location after the injection event. Naturally, one would expect to see larger modifications in the boundary as the time lag between an injection event and a subsequent DMSP image increases. For a large number of cases under given conditions

the average time lag would depend on the relative frequency of DMSP images and injection events. Our observations show that in spite of these factors the average equatorward auroral boundary relates well to the empirical boundary found by McIlwain.

A study by Kamide and Winningham [1977] on the low-latitude boundary of ~ 100 -eV electrons compared the shape and location of these boundaries projected onto the equatorial plane with boundaries of calculated Alfvén layers. An Alfvén layer delineates the closest approach to earth of plasma moving earthward from the tail and depends on the impressed and corotation electric fields as well as particle energy and magnetic moment. The low-energy electron boundaries tracked well with the Alfvén layer for the appropriate electric fields that were estimated from hourly averaged B_z of the interplanetary magnetic field. This fact is in accord with our results using the empirical boundary that depends on K_p . The above authors also commented that their findings compared favorably with those of Liu *et al.* [1975a, b] cited earlier, except that the particle boundaries were distributed somewhat lower in latitude than the optical boundaries seen by Isis.

DMSP AURORAL BOUNDARY AND THE McILWAIN INJECTION BOUNDARY: PREMIDNIGHT

Because the known injection boundary extends from dusk to midnight, a comparison with the auroral equatorward boundary can also be made in that region to see whether the agreement found above extends into the evening sector. Histograms of the DMSP equatorward auroral boundary latitude, as functions of both K_p and local times ranging from 1800 to 2400 CGLT, are given in Figure 7. A DMSP satellite in a dawn-dusk orbital plane provided images during the same time period as was used above (November 14 to December 15, 1972). Its orbit allows nearly daylong coverage of the evening local time sector from 2000 to 2300 CGLT. Triangles at decreasing latitudes in Figure 7 locate the equatorial boundary of the statistical Feldstein oval as given by Whalen [1970] for Q .

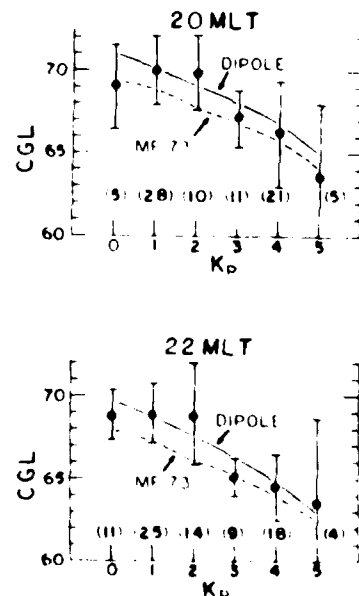


Fig. 8. Same as Figure 6 except showing average auroral and McIlwain boundaries at 2000 and 2200 CGLT.

1, 3, and 5. $Q = 7$ is also included for $Kp \geq 3$. The Q index is a 15-min auroral zone magnetic index employed by Russian workers and is roughly equivalent to Kp , especially during quiet conditions [Eather and Mende, 1971]. Although the Q index does not correspond exactly to Kp , it is obvious that the DMSP boundary distributions have a local time dependence similar to that of the auroral oval.

Figure 8 gives the latitude of the auroral and Mellwain injection boundaries at 2000 and 2200 CGLT in the same format as was used in Figure 6. In Figure 8 the small kink seen in the Mead-Fairfield 73 (MF 73) field mapping results from the transition from the MF 73Q to the MF 73D model at $Kp = 2$. For $Kp \geq 3$ the DMSP auroral boundary agrees well with the field-mapped Mellwain boundary. When data from the two DMSP satellites are combined, we conclude from Figures 6 and 8 that for moderate and high Kp values the average equatorward auroral boundary maps closely onto the statistical Mellwain injection boundary.

We also observe in Figure 8 that agreement between the statistical injection and auroral boundaries worsens toward low Kp values ($Kp = 0-2$). Aside from purely statistical errors, there are two possible explanations for this trend. (1) Some of the low Kp images represented in Figure 8 (about 20%) have a reduced sensitivity, as evidenced by faintness of city lights and background illumination. Such images would miss faint auroras from precipitation occurring several hours after the last injection and therefore would create a bias under low Kp conditions. (2) During intervals of low Kp , injections are rare, therefore only a few DMSP images may show auroral conditions directly connected with an injection. To compare DMSP results with the Mellwain boundary under quiet conditions, we should select only those images taken soon after the infrequent injections that do occur. In fact, this procedure should be used under all conditions, but because high Kp is generally associated with substorms and injections, most of the images at such times will automatically be within several hours of the most recent injection event.

COMPARISONS WITH GROUND-BASED PHOTOMETER STUDIES

Observations relating the injection boundary to auroral precipitation have been carried out previously. For example, ground-based photometric measurements, made from the foot of the ATS 5 field line by Eather et al. [1976], have been compared with particle fluxes observed by ATS 5 at synchronous orbit. Their auroral observations span latitudes above and below the ATS 5 field line projection and provide information about magnetospheric regions remote from the ATS satellite. They observe that injections occurring at ATS 5 correspond to auroral enhancements at the foot of the ATS 5 field line and auroral enhancements at other latitudes are injections which can be inferred from the dispersion in particle arrivals. Steady, weak auroras correspond to electron precipitation from the inner edge of the plasma sheet. On the 3 quiet days in their study period, Eather et al. observed a pre-midnight auroral boundary ranging from 66° to 69° at 2000-2200 CGLT. Figure 7 shows that DMSP images exhibited many cases of boundaries in this area when $Kp = 0$ or 1, although there are also cases where poleward. Those auroral boundaries which occur at latitudes greater than 70° CGL are substantially poleward of the Mellwain injection boundary, regardless of the field model used. Such auroras would fall outside of, or near to, the limits of the latitude range of the ground-based photometer located at 73° CGL.

The DMSP uses some DMSP images to detect auroras corre-

sponding to steady plasma sheet precipitation could result from the exposure problems discussed earlier. However, an explanation is still needed for the presence of intense arcs (by DMSP standards) observed poleward of the projected Mellwain boundary. If such instances are related to injections, then they may be examples of the so-called 'contracted oval substorms' [Kamide et al., 1975; Akasofu, 1975] suggested to originate well back in the plasma sheet. This proposed type of substorm occurs well poleward of most auroral zone observatories and is reported to coincide with a northward pointing interplanetary magnetic field. Poleward injections giving rise to contracted oval substorms do not contradict the observations of Eather et al. [1976], because they are presumed to occur within the preexisting plasma sheet, although further down the tail than usual.

SUMMARY

Measurements of the equatorward auroral boundary latitude near local midnight from 162 DMSP images show that the average latitude varies linearly with Kp or AE , decreasing from 67° CGL to about 61° CGL for $Kp \leq 5$ or $AE \leq 600$. The rather large scatter around the average positions indicates that the auroral boundary is only roughly related to ground magnetic conditions. However, a mapping of the appropriate Mellwain injection boundary from the equatorial plane to auroral latitudes produces a curve that coincides fairly well with average auroral boundaries at local midnight for Kp ranging from 1 to 5. At 2000 and 2200 CGLT the agreement is good for $Kp = 3-5$, but the auroral boundary averages about 2° poleward of the Mellwain boundary during quieter conditions ($Kp = 0-2$).

Acknowledgments. This research was supported in part by contracts AT 19(628)-5543 and 119628-77C-0085 and by the Atmospheric Research Section, National Science Foundation.

The Editor thanks R. H. Holzworth and A. T. Y. Lui for their assistance in evaluating this paper.

REFERENCES

- Akasofu, S.-I., A study of auroral displays photographed from the DMSP-2 satellite and from the Alaska meridian chain of stations, *Space Sci. Rev.*, **16**, 617, 1974.
- Akasofu, S.-I., The role of the north-south component of the interplanetary magnetic field on large scale auroral dynamics observed by the DMSP satellite, *Planet. Space Sci.*, **23**, 1349, 1975.
- Berkey, F. T., and Y. Kamide, On the distribution of global auroras during intervals of magnetospheric quiet, *J. Geophys. Res.*, **81**, 4701, 1976.
- Carovillano, R. L., Unified model of auroral substorm development, *Rep. AFRL-TR-0559*, Air Force Cambridge Res. Lab., Bedford, Mass., Aug. 31, 1975.
- Carovillano, R. L., M. S. Gussenhoven, R. E. Sheehan, and G. L. Siscoe, Study of auroral activity from Dapp photographs (abstract), *Eos Trans. AGU*, **55**, 1171, 1974.
- DeForest, S. E., and C. E. Mellwain, Plasma clouds in the magnetosphere, *J. Geophys. Res.*, **76**, 3587, 1971.
- Eather, R. H., and S. B. Mende, Airborne observations of auroral precipitation patterns, *J. Geophys. Res.*, **76**, 1746, 1971.
- Eather, R. H., S. B. Mende, and R. J. R. Judge, Plasma injection at synchronous orbit and spatial and temporal auroral morphology, *J. Geophys. Res.*, **81**, 2805, 1976.
- Fairfield, D. H., and G. D. Mead, Magnetospheric mapping with a quantitative geomagnetic field model, *J. Geophys. Res.*, **80**, 535, 1975.
- Holzworth, R. H., and C. E. Meng, Mathematical representation of the auroral oval, *Geophys. Res. Lett.*, **2**, 377, 1975.
- Kamide, Y., and J. D. Winningham, A statistical study of the instantaneous nightside auroral oval. The equatorward boundary of electron precipitation is observed by the ISEE 1 and 2 satellites, *J. Geophys. Res.*, **82**, 5571, 1977.

- Kamide, Y., S.-I. Akasofu, S. E. DeForest, and J. L. Kisabeth, Weak and intense substorms. *Planet. Space Sci.*, **23**, 579, 1975.
- Lui, A. T. Y., C. D. Anger, D. Venkatesan, W. Sawchuk, and S.-I. Akasofu, The topology of the auroral oval as seen by the Isis 2 scanning auroral photometer, *J. Geophys. Res.*, **80**, 1795, 1975a.
- Lui, A. T. Y., C. D. Anger, and S.-I. Akasofu, The equatorward boundary of the diffuse aurora and auroral substorms as seen by the Isis 2 auroral scanning photometer, *J. Geophys. Res.*, **80**, 3603, 1975b.
- Mauk, B. H., and C. E. Mellwin, Correlation of K_p with the substorm-injected plasma boundary, *J. Geophys. Res.*, **79**, 3193, 1974.
- Mellwin, C. E., Substorm injection boundaries, in *Magnetospheric Physics*, edited by B. M. McCormac, D. Reidel, Hingham, Mass., 1974.
- Nagata, T., T. Hirasawa, and M. Ayukawa, Discrete and diffuse auroral belts in Antarctica. *Rep. Ionos. Space Res. Jap.*, **29**, 149, 1975.
- Pike, C. P., and J. A. Whalen, Satellite observations of auroral substorms, *J. Geophys. Res.*, **79**, 985, 1974.
- Snyder, A. L., S.-I. Akasofu, and T. N. Davis, Auroral substorms observed from above the north polar region by a satellite, *J. Geophys. Res.*, **79**, 1393, 1974.
- Starkov, G. V., Analytical representation of the equatorial boundary of the oval auroral zone, *Geomagn. Aeron.*, **9**, 614, 1969.
- Walker, R. J., An evaluation of recent quantitative magnetospheric magnetic field models, *Rev. Geophys. Space Phys.*, **14**, 411, 1976.
- Whalen, J. A., Auroral oval plotter and nomograph for determining corrected geomagnetic local time, latitude and longitude for high latitudes in the northern hemisphere, *AFCRL Environ. Res. Pap. 327*, Air Force Cambridge Res. Lab., Bedford, Mass., July 27, 1970.

(Received March 17, 1978;
revised May 19, 1978;
accepted May 19, 1978.)

DMSP POLEWARD AURORAL BOUNDARIES AND
MOVEMENTS WITH MAGNETIC ACTIVITY

M. S. Gussenhoven, M. D'Anton, R. L. Carovillano (all at:
Department of Physics, Boston College, Chestnut Hill, MA
02167)

The DMSP images for October, 1974, are used to study the variation of the poleward edge of auroral displays and their latitudinal extent with a variety of ground magnetic indices. The variation with Dst relates to the influence of the ring current on high latitude accessibility of auroral particles. Consecutive DMSP images for this period (which includes a magnetic storm and several disturbed days) are gridded in corrected geomagnetic coordinates and local time. Two DMSP satellites (8531 and 9532) were recording at this time. The most poleward and the most equatorward edge of the aurora shown for each hourly interval of local time from 1800 to 0600 hours through the midnight sector are recorded. The well-established equatorward motion of the equatorward edge of the aurora near midnight, as magnetic activity increases, is shown also to be the case at other local times studied. The poleward motion is somewhat more complex and less regular; however, a significant movement of the auroral boundary towards higher latitude with increasing Dst is found at all local times.

References

- Eather, R.H., DMSP calibration, J. Geophys. Res., 84, 4134, 1979.
- Gussenhoven, M.S., M. D'Anton, and R.L. Carovillano, DMSP poleward auroral boundaries and movements with magnetic activity, FOS Trans. AGU, 12, 1168, 1978.
- Lui, A.T.Y., C.D. Anger, and S.-I. Akasofu, The equatorward boundary of the diffuse aurora and auroral substorms as seen by the Isis 2 auroral photometer, J. Geophys. Res., 80, 3603, 1975.
- McIlwain, C.E., Substorm injection boundaries, in Magnetospheric Physics, edited by B.M. McCormac, D. Reidel, Hingham, Mass., 1974.
- Nagata, T., T. Hirasawa, and M. Ayukawa, Discrete and diffuse auroral belts in Antarctica, Rep. Ionos. Space Res. Jap., 29, 149, 1975.
- Sheehan, R.E. and R.L. Carovillano, Characteristics of the equatorward auroral boundary near midnight determined from DMSP images, J. Geophys. Res., 83, 4749, 1978.

7. MAGNETOSPHERIC DETERMINANTS OF THE GLOBAL DISTRIBUTION OF PARTICLE PRECIPITATION

A. Introduction

The goal of this research has been to identify and quantify the magnetospheric factors that determine where the particle precipitation characteristics of the auroral zone occur at any given time. New observational characteristics of the auroral zone were presented in Chapter 6. In addition, the statistical or average auroral zone location is well known, as is the fact that displacements from the average are common. The magnetospheric processes that govern the displacements are the subjects of concern here.

In the simplest descriptions, the geometrical (convertible to geographical) quantities of interest are: 1) the opening angle of the poleward limit of the precipitation band, 2) the opening angle of the equatorward limit of the precipitation band, and 3) the displacement of the center of the band (in the sense of the center of a circle) from the dipole axis. These are essentially latitudinal variations. Variations in longitude were not included in this first (three part) phase of the investigation except as they arise from the displacements of the centers of the auroral bands from the geographical poles.

The first two quantities listed are believed to be controlled by the orientation and strength of the interplanetary magnetic field and by the magnetospheric ring current. The ring current contribution is particularly important in accounting for the largest displacements of the auroral precipitation from its average location.

A model describing how the ring current controls the opening angle of the poleward edge of the precipitation band has been proposed under this contract.

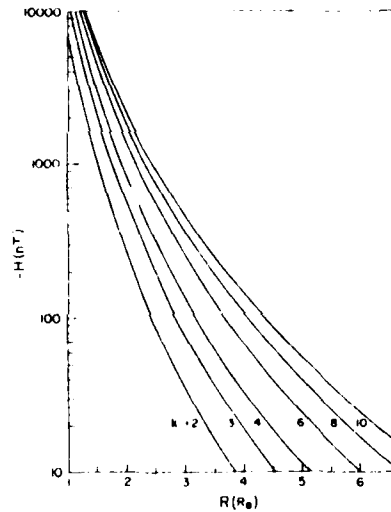
It requires for its use knowledge of the magnetic moment of the ring current (M_R). In this model, the location of the equatorward edge of the auroral zone is identified with the inner edge of the ring current (R_r).

Existing ring current models are not of much use for our purposes, because they require that the entire ring current particle distribution be specified as an input function. That function must be found empirically, by in situ spacecraft measurements, or by other means that are extraneous to the models themselves. It was necessary, therefore, as a first stage of this investigation to develop a ring current model in which the ring current evolved self-consistently to a given (presumably storm-time) state from a prior (presumably prestorm) state.

4. Quasi-Self-Consistent Ring Current Model

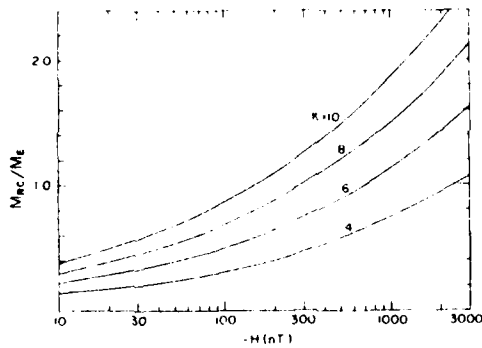
In this section, we summarize the quasi-self-consistent, high beta, injection model for the storm-time ring current that has been successfully developed by Siscoe (1979a). It has the advantage over previous models of completely determining all ring current parameters in terms of two observables: 1) the geomagnetic Dst index, and 2) the beta of the ring current plasma at a single (and arbitrary) distance. The ring current beta can be determined at any time prior to the ring current decay phase—even prior to the development of the storm. If this parameter (beta) is the same for all storms, then only Dst is needed to specify all ring current parameters. This possibility can be investigated empirically.

Some results obtained from the model are shown in Figures 7.1 to 7.3. Figure 7.1 shows the calculated relationship between Dst and the geocentric distance to the inner edge of the ring current (R_r) in units of earth radii (R_e). The family parameter, R , is the second of the two model parameters. It



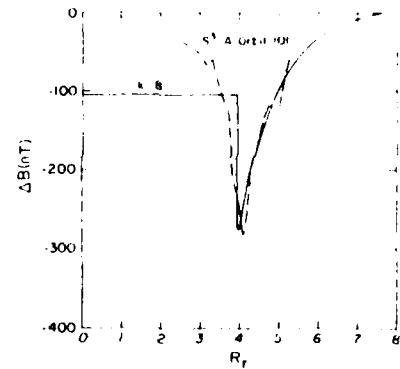
The dependence of the ring current disturbance field at earth (H) on the distance to the inner edge of the ring current (R) for different "entropy" plasmas characterized by k , the distance at which the beta of the plasma is unity.

Figure 7.1



The magnetic moment of the ring current (M_{RC}) in units of the geomagnetic dipole moment (M_E) as a function of the disturbance field (H) for different values of k .

Figure 7.2



A comparison between the model-predicted ($R = 4, k = 8$) disturbance field profile and storm-time disturbance field data from the S^3-A satellite for the storm of 17 December 1971 (Cahill, 1973).

Figure 7.3

is given by $k^2 = \mu R^2$, which is a constant of the model. Figure 7.1 indicates that when R_r moves into the range of 3 to 4 (R_e), storm-time Dst values result, in accord with available observations. Figure 7.2 shows the dependence of the ring-current magnetic moment (normalized to units of the earth's dipole moment) on Dst and the parameter k . Figure 7.3 gives a comparison between the ring current magnetic field calculated from the model and the only published example for which the values of k and R_r can be empirically and simultaneously determined (Hoffman, 1973). The agreement is quite good. The deviations seen at $r < 3.5$ (R_e) can be attributed to time variations, which were not taken into account in the calculated curve.

As these figures show, given observed values of Dst and k (or in the case of k perhaps a standard value will be adequate), values of M_R and R_r can be determined. These are the quantities which then govern the values of the first of the listed geometrical features of the particle precipitation.

C. Ring Current Effect on Polar Cap Size

The Dst versus M_R relationship displayed in Figure 7.2 has been used to assess the ring current contribution to the equatorward expansion of the auroral oval during geomagnetic storms (Siscoe, 1979b). The principle upon which the contribution is determined is simply stated. The ring current magnetic moment is a vector which points in the same direction as the geomagnetic dipole moment M_E . The solar wind interacts with the coupled earth-ring current system, which as a combined dipole moment $M_R + M_E > M_E$. Now we simply scale up the size of the magnetosphere from its size when there is no storm and when $M_R \ll M_E$, using the well-known dipole scaling relations. A larger magnetosphere necessarily has a larger amount of magnetic flux forming its tail. The magnetic

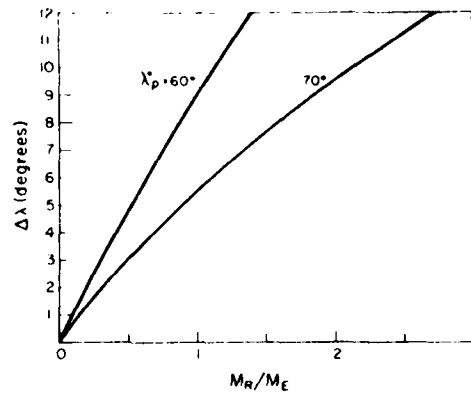
flux in the tail maps into the polar caps of the earth, which demarcate the polar boundaries of the auroral ovals. Thus, the poleward border of the ovals move equatorward as M_R increases. The formula expressing this relationship (Siscoe, 1979b) is:

$$\cos \lambda_p = (\cos \lambda_p^*) \left(1 + \frac{M_R}{M_E}\right)^{1/3} \left(\frac{p_{st}}{p_{st}^*}\right)^{1/12}$$

where λ_p is the magnetic latitude of the poleward edge of the oval, p_{st} is the solar wind stagnation pressure, and $\lambda_p^* = 70^\circ$ and $p_{st}^* = 1.2 \times 10^{-8}$ dyne cm^{-2} are fiducial (actually about average) values. Since we are interested here in the contribution from M_R , we set $p_{st} = p_{st}^*$, i.e., we assume an average solar wind stagnation pressure. Then we can plot the equatorward displacement $\Delta\lambda = \lambda_p^* - \lambda$ as a function of M_R/M_E . This is shown here as Figure 7.4. We see from this figure that a displacement of 5° requires a magnetic moment ratio near unity, and a displacement of 10° , a ratio of approximately two.

The curve in Figure 7.4 and the curves in Figure 7.2 can be combined to provide a plot of the displacement, $\Delta\lambda$, as a function of H ($\approx \frac{2}{3} \text{Dst}$) for different assumed values of the parameter k . This is shown here as Figure 7.5. We see, as expected, $\Delta\lambda$ increases with increasing $|\text{Dst}|$ and with increasing k .

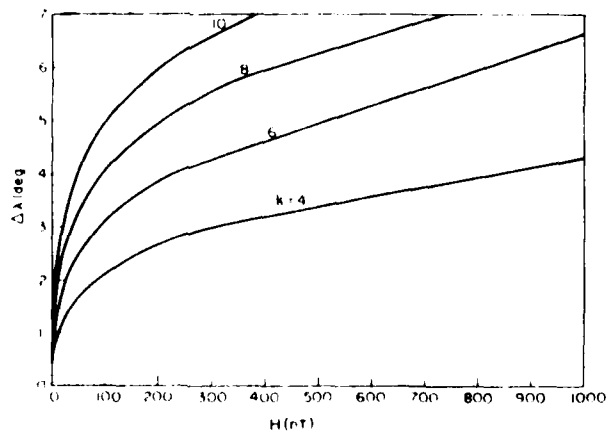
As an example, consider the curve for which $k = 8$ and for the purpose of illustration let $\text{Dst} = \frac{3}{2} H$. The actual proportionality factor between Dst and H depends on the strength of the currents induced in the earth by the storm and can vary from a minimum of unity to a maximum of $3/2$, the value assumed. Thus, in the case of a large storm that achieved a disturbance level given by $\text{Dst} = -500$ nT, the corresponding value of H would be -333 nT. Using the $k = 8$ curve, we then find $\Delta\lambda = 5.75^\circ$, or that the poleward edge of the auroral oval would be located at a geomagnetic latitude near 64° .



The dependence of the latitudinal shift of the poleward border of the auroral oval on the magnetic moment of the ring current, M_R (measured here in units of the geomagnetic dipole moment, M_E).

The two cases shown correspond to initial ($M_R = 0$) locations of the border at $\lambda_p^* = 60^\circ$ and 70° geomagnetic latitudes.

Figure 7.4



The dependence of the latitudinal shift of the poleward border of the auroral oval on the ring current magnetic field ($Dst \approx 1.5 H$), as determined from the $\lambda_p^* = 70^\circ$ curve of Fig. 7.4 and the previous derived relation between M_R and H (Siscoe, 1979a) in Fig. 7.2.

Figure 7.5

Against the prediction given here, we can compare the observations relating to the storm of 11 February 1958 published by Akasofu and Chapman (1962). This particular storm was characterized by a large negative value of Dst, which reached -500 nT, and by a large equatorward motion of the auroral zone. All sky camera observations stations located in the mainland United States, Canada and Alaska revealed that during one interval of about 20 minutes duration, the northern edge of the auroral oval was located at approximately 55° geomagnetic latitude.

Clearly it would be desirable to perform similar comparisons for other storms. However, the important conclusion to be drawn from this one storm for which the comparison can be readily made is that the effect of the ring current magnetic moment can account for about 30 percent of the maximum achieved equatorward displacement of the poleward edge of the oval.

We know already that the size of the oval is modulated by the direction and magnitude of the north-south component of the interplanetary magnetic field (IMF). The IMF control is independent of the ring current control discussed here. The study by Holzworth and Meng (1975) shows that the oval expands by about 0.9° for every 1 nT increase in the southward component of the IMF. Thus a 10° displacement requires a southward component of only 11 nT, which is not a very large value to be associated with a major geomagnetic storm. It is, therefore, not unreasonable to conclude that in the case of the 11 February 1958 storm the combined effects of the ring current and the IMF could have brought the poleward edge of the auroral oval southward of the Canadian border.

D. Polar Cap Off-Set

The radius of the auroral circle varies typically between 15 and 23 degrees in response primarily to changes in the orientation of the interplanetary magnetic field (Holzworth and Meng, 1975). The auroral circle is displaced on the average about 4 degrees in the anti-solar direction from the geomagnetic pole, but at any time the offset varies typically within 3 degrees from the average value (Meng et al., 1977).

The geometry is shown in Figure 7.6. The equations on the figure give the variation in both the radius θ_p and the offset δ as a function of solar wind dynamic pressure p_{st} , as predicted by the standard magnetospheric scaling relations. The weak dependence of θ_p and δ on p_{st} implies that the commonly observed variations in θ_p and δ cannot be caused by corresponding variations in p_{st} .

In the course of this work, we have demonstrated that the interplanetary magnetic field does not exert its main control over the polar cap size through the modulation of the magnetospheric ring current. We determined that the ring current required to produce a change in polar cap size comparable to that which is commonly observed would also produce a large geomagnetic storm ($Dst \approx -200\gamma$), which is not commonly observed. (In fact, the calculation was performed to show that the ring current effect can be important during magnetic storms.) This result, not unexpectedly, supports the general belief that the variation in polar cap size results from a net transfer of magnetic flux into the tail from the dayside, with an associated change in the shape of the magnetosphere. We note here that the presently existing magnetospheric scaling relations, which can be used to investigate the effect of the ring current on the polar cap size, are not able to treat phenomena that entail a change in magnetospheric

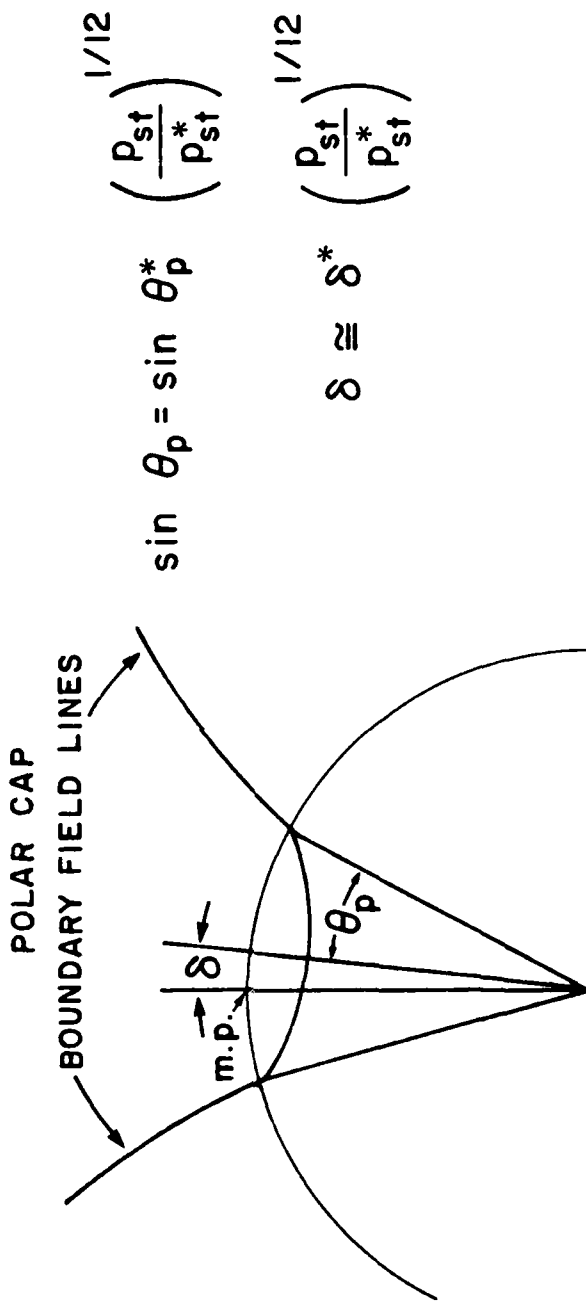


Figure 7.6. Geometry of the polar cap in terms of an auroral circle of size θ_p and offset angle, δ , from the magnetic pole (m.p.). P_{st} is the solar wind dynamic pressure, starred quantities are reference values.

shape. This result motivated the investigation into two-parameter scaling relations, which can handle such problems, as is described below.

The anti-sunward displacement of the center of the polar cap with respect to the geomagnetic pole evidently has its ultimate cause in the sunward-tailward asymmetry in the magnetosphere itself, which is imposed by the sense of the solar wind flow.

In thinking of magnetic field lines in mechanical terms, field lines are given the attribute of tension. The force by which the solar wind drags out the magnetosphere to form the geomagnetic tail is then envisioned to be communicated to the earth by the tension in the field lines that connect the earth and the tail. These are the polar cap field lines. In light of this conception, which has its basis in the theory of elastic media, it is natural to suggest that the tailward displacement in question is a direct consequence of the tension operating through the polar cap field lines.

The mathematical statement of the hypothesis that the tailward offset of the polar cap results from the force acting between the earth and the tail was treated analytically for the case of a two-dimensional interaction. An offset of the order of 0.4 degrees was obtained this way. The calculated two-dimensional offset is too small to account for the observations, but the differences between the two and three-dimensional cases were sufficient to offer hope that the three dimensional offset could be substantially larger.

The three-dimensional case was then integrated numerically. The result did not differ materially from the previous two-dimensional case. If the tail force only is considered, the offset is an order of magnitude too small. Interestingly, if the dayside force (the Chapman-Ferraro force) is used, the resulting offset is slightly over 2 degrees, or about 50 percent of the observed displacement. Since the dayside force is dominated by the dynamic pressure of

the solar wind, there is here a justification for ascertaining the degree of correlation between the polar cap offset and the solar wind dynamic pressure.

Even should the total solar wind force on the boundary account for roughly half of the polar cap offset, we would conclude the magnetospheric distortion not directly related to communicating the solar wind force to the earth must contribute substantially, if not predominantly, to the offset. This result, like the one relating to the polar cap size, indicates that the magnetosphere regularly changes its shape (i.e., degree of distortion) and not merely its size, in response to change in solar wind conditions. The need to generate magnetospheric scaling relations to account for changes in shape is thus once again emphasized.

E. Two-Parameter Scaling Relations

The analysis described above provided the motivation for proceeding to a specific extension of the magnetospheric scaling relations. We will here briefly outline the progression this problem made under this contract. We will illustrate that progress by means of an example which shows that the new approach is well chosen and that it provides answers to a new class of problems.

When the set of independent variables is restricted to the solar wind stagnation pressure (i.e., only the normal component of the solar wind force on the magnetopause) and the planetary magnetic moment (including the ring current contribution), there is only one combination of independent parameters that has the dimension of length. The length can be chosen to be the planetocentric distance to the subsolar stagnation point, R_m . It is evident that if a geometry is described by a single scale length, then change in size but not shape will occur as R_m changes. This is the underlying basis for the "constant shape" assumption of the existing scaling relations.

Many previous studies support the principle that the amount of flux in the tail is determined primarily by the tangential component of the solar wind force on the magnetopause, a neglected component in the prior scaling formalism. Whereas in the prior formalism the independent variable could be taken to be the solar wind stagnation pressure or the scale size R_m , since one is uniquely given in terms of the other, in the present formalism one may choose a solar wind pair of independent variables, namely: the normal and tangential drags on the magnetopause, or an internal pair of variables, that, in principle, may be derived from the solar wind pair. We choose R_m and the magnetic flux in the tail, F_T , to be the pair of independent variables. This choice will serve to extend the previous one-parameter set of scaling relations to a two-parameter set. The method proceeds as before, only now there are more parameters out of which to construct the dimensions of the magnetospheric quantities of interest.

A detailed dimensional argument, the final realization of which permits the easy application of the method, shows that the new scaling relations take the same form as the old ones, except that the old scaling constants become functions of the dimensionless ratio $F_T R_m / \mu_0 M_p$, where M_p is the effective magnetic moment of the planet.

To illustrate the result, consider the magnetospheric quantity B_{st} , which is the magnetic field strength inside the magnetopause at the subsolar stagnation point. In the old formalism B_{st} was fixed simply by $B_{st}^2 / 2\mu_0 = p_{st}$, the stagnation pressure. Or in terms of R_m , it was given by $B_{st} = a_0 / R_m^3$, where a_0 is known from theoretical calculations performed in the early 1960's by Mead and Beard and by Midgley and Davis. In the new formalism B_{st} must be expressed in the form $B_{st} = \frac{a(F_T R_m / \mu_0 M_p)}{R_m^3}$, where $a(x)$ is some as yet unspecified

function of x . Now, typical values of the independent parameters for the case of earth give $F_{Tm}R_m/\mu_o M_E \approx \frac{1}{2}$. Thus, in the spirit of going from a prior formulation characterized, in effect, by the condition $F_{Tm}R_m/\mu_o M_E = 0$ to one for which the ratio is non-zero but small, we are justified in claiming improvement if we merely make a Taylor series expansion of the function $a(x)$ and terminate the series at the linear term. That is, we take

$$a = a_o + a_1 \frac{F_{Tm}R_m}{\mu_o M_E}$$

where a_o is the old constant and a_1 is a constant that must be determined by theory or experiment, but once it is fixed it applies to all values of the independent parameters. From available observations, we estimate the new term to be about 30 percent of the old one, and with opposite sign. For example,

$$B_{st} = \frac{a_o}{R_m^3} + \frac{a_1 F_{Tm} R_m}{\mu_o M_E R_m^3} \cong 70 \gamma - 20 \gamma = 50 \gamma$$

One of the goals of the present investigation is to improve the determination of the value of the new constant, both by appropriately tailored data analysis and by specific model calculations. In the latter, the computer model of Olson and Pfitzer will be especially valuable.

The result just obtained can be used to answer one of the new class of questions involving changes in magnetospheric shape: for constant solar wind stagnation pressure (hence $B_{st} = \text{const.}$), in a flux transfer event, by how much does R_m change for unit flux transferred to the tail? Mathematically the answer is

$$\left. \frac{\partial R_m}{\partial F_T} \right|_{B_{st} = \text{const}} = \frac{a_1 R_m^2}{3\mu_o M_E a_o + 2a_1 F_{Tm} R_m}$$

For the estimated value of a_1 and typical values of the other parameters, this equation predicts

$$\frac{\Delta F}{F} \approx - 8.5 \frac{\Delta R_m}{R_m}$$

This result is very different from that obtained by merely equating the flux missing from the dayside as a result of a decrease in R_m to the increase in the flux in the tail. The proportionality factor derived based on this purely kinematical principle is less than 2. The dynamical forces that are in fact determining the constitution of the tail require a much larger increase in tail flux for a given decrease in R_m . The additional flux comes from the nightside of the magnetosphere and is associated with the observable phenomenon of the earthward movement of the plasma sheet when the tail flux increases. This aspect of the total tail phenomenology was explicitly incorporated in the model of Coroniti and Kennel (1972). We have here tied down the many model parameters that result if one tries to construct the various pieces of the dynamical picture independently and then assemble them.

The observed typical range in $\frac{\Delta R_m}{R_m}$ that results from flux transfer has been shown by Maezawa (1974) and by Holzer and Slavin (1978) to be 0.1. The above formula then predicts a typical range for $\Delta F_T/F_T$ of 0.85, which corresponds to a polar cap angular radius range from 18° to 25° , as is observed.

The method of the two-parameter scaling analysis is now ready for general exploitation to address questions concerning the energy input rate into the magnetosphere, and for replacing the old ad hoc electric field scaling relations by equations properly derived according to the principles described above. The result will be a set of relations connecting magnetospheric features and processes to the independent solar wind parameters that determine the normal and tangential drags on the magnetopause.

References

- Akasofu, S.-I., and S. Chapman, The lower limit of latitude (US sector) of northern quiet auroral arcs, and its relation to Dst (H), J. Atmos. Terr. Phys., 25, 9, 1963.
- Cahill, L. J., Jr., Magnetic storm inflation in the evening sector, J. Geophys. Res., 78, 4724-4730, 1973.
- Coroniti, F. V., and C. F. Kennel, Changes in magnetospheric configuration during substorm growth phase, J. Geophys. Res., 77, 3361-3370, 1972.
- Hoffman, R. A., Particle and field observations from Explorer 45 during the December 1971 magnetic storm period, J. Geophys. Res., 78, 4771-4777, 1973.
- Holzer, Robert E., and James A. Slavin, Magnetic flux transfer associated with expansions and contractions of the dayside magnetosphere, J. Geophys. Res., 83, 3831, 1978.
- Holzworth, R. H., and C.-I. Meng, Mathematical representation of the auroral oval, Geophys. Res. Lett., 2, 377-380, 1975.
- Maezawa, K., Dependence of the magnetopause position on the southward interplanetary magnetic field, Planet. Space Sci., 22, 1443, 1974.
- Meng, C.-I., R. H. Holzworth, and S.-I. Akasofu, Auroral circle-delineating the poleward boundary of the quiet auroral belt, J. Geophys. Res., 82, 164-172, 1977.
- Siscoe, G. L., A quasi-self-consistent axially symmetric model for the growth of a ring current through earthward motion from a pre-storm configuration, Planet. Space Sci., 27, 285-295, 1979a.
- Siscoe, G. L., A Dst contribution to the equatorward shift of the aurora, Planet. Space Sci., 27, 997-1000, 1979b.

DA
FILM
O —